NOS Inhibition of Novel Fluorescent Polycyclic Ligands

Jacques Joubert, B.Pharm

Dissertation submitted in partial fulfillment of the requirements for the degree

Magister Scientiae

in
Pharmaceutical Chemistry, School of Pharmacy
at the North-West University (Potchefstroom Campus)

Supervisor: Prof. S.F Malan
Co-supervisor: Dr. S. van Dyk

Potchefstroom
December 2007

To my parents, Andre and Lina Joubert

TABLE OF CONTENTS

ABSTRACT

In recent years polycyclic compounds have been shown to exhibit pharmacological profiles of importance in the symptomatic and proposed curative treatment of neurodegenerative diseases (e.g. Parkinson's and Alzheimer's disease). These structures also show modification and improvement of the pharmacokinetic and pharmacodynamic properties of drugs in current use. The use of fluorescent techniques have found widespread applicability in receptor pharmacology and offers an attractive alternative to the use of radioligand studies such as multicolor detection, stability, sensitivity, low hazard and lower cost. Fluorescent ligands can be used to determine receptor properties like receptor internalization and sub-cellular localization, the thermodynamics and kinetics of ligand binding and to assess the nature of the microenvironment of the ligand binding sites.

Nitric oxide (NO) is a molecular messenger involved in a number of physiological processes in mammalians. It is synthesised by nitric oxide synthase (NOS) from L-arginine and its overproduction could lead to a number of neurological disorders. The aim of this study was to synthesise a series of novel indazole, indole and other fluorescent derivatives conjugated to polycyclic structures for evaluation in NOS assays. NOS is a target system where fluorescent techniques and fluorescently labelled NOS inhibitors, such as 7-nitroindazole (7-NI), can be used for detecting the biophysical properties of enzyme-ligand interactions and thus facilitate development of novel inhibitors of neurodegeneration. This could lead to a greater insight into the neuroprotective mechanism and a possible cure/treatment for neurodegenerative diseases.

A series of compounds incorporating polycyclic structures such as 3-hydroxy-4-aza-8-oxoheptacyclo[9.4.1.$0^{2,10}$.$0^{3,14}$.$0^{4,9}$.$0^{9,13}$.$0^{12,15}$]tetradecane and amantadine as well as suitable fluorescent moieties were selected for synthesis. The polycyclic structures were conjugated to the fluorescent moieties by amination and esterfication or amidation using activation chemistry with the carbodiimides, CDI and DCC. The fluorescent groups were selected on the basis of their spectroscopic properties, ease of synthesis and

structure-activity relationship requirements for NOS inhibition. The groups included *N*-methylanthranilic acid, indazole-3-carboxylic acid, 1-fluoro-2,4-dinitrobenzene, 1-cyanoisoindole, 1-thiocyanatisoindole and 1-nitroisoindole.

In the biological evaluation the oxyhemoglobin (oxyHb) assay was employed to determine the activity of the novel compounds at an enzymatic level of NOS. This assay is principally based on the reaction of NO with oxyHb and the formation of methemoglobin (metHb). The slope of the absorption difference between 401 nm and 421 nm versus time is an indication of NOS activity. From this inhibition data the IC_{50} values were calculated and compared.

The compounds showed inhibition of the NOS enzyme at a micro molar range. Of the compounds that were tested, only the isoindole and indazole compounds showed significant inhibition at low concentrations. 100 % enzyme inhibition could not be achieved, because of solubility problems. The polycyclic structures conjugated to the indazole moiety increased the NOS activities, when compared to the unconjugated indazole-3-carboxylic acid. The anthranilic and dinitrobenzene derivitaves only showed low or no inhibition of the NOS enzyme.

3-{4-aza-8-oxo-heptacyclo[0.4.1.$0^{2,10}$.$0^{3,14}$.$0^{4,9}$.^{09,13}.$0^{12,15}$]tetradecyl}-1*H*-indazole-3-carboxylate and *N*-(1-cyano-2*H*-isoindol-2yl)adamantan-1-amine gave the best inhibition at a concentration of 250 μM, inhibiting the enzyme 83.7 % and 89.9 %, respectively. The compounds containing indole and indazole systems clearly have higher affinity for the NOS enzyme than other structures evaluated in this study.

We have thus identified a series of fluorescent structures with moderately high affinity for the NOS enzyme, which may be utilized for further *in vitro* and *in vivo* studies using modern imaging techniques. In view of the increase in lipophilicity originating from the pentacycloundecyl cage structure, it is expected that the new structures will display an increase in blood brain barrier permeability when compared to 7-NI. The novel compounds also represent a new class of NOS inhibitors and provide the foundation for potential therapeutic agents. These compounds thus have potential as useful pharmacological tools to investigate enzyme-ligand interactions in the quest for effective neuroprotective strategies.

UITTREKSEL

Dit is die afgelope aantal jaar aangetoon dat polisikliese verbindings farmakologiese eienskappe van belang vir die simptomatiese en moontlik genesende behandeling van neurodegeneratiewe siektes (bv. Parkinson en Alzheimer se siektes) het. Hierdie strukture verander en verbeter ook die farmakokinetiese en farmakodinamiese eienskappe van geneesmiddels wat tans gebruik word. Fluoressensietegnieke word wyd in reseptorfarmakologie gebruik en bied 'n aantreklike alternatief vir radioligandstudies. Van die voordele van die tegniek is veelkleurige deteksie, stabiliteit, sensitiwiteit, groter veiligheid en laer koste. Fluoresserende ligande word ook gebruik om sekere reseptoreienskappe, soos reseptorinternallisasie, sub-sellulêre lokalisasie, die termodinamika en kinetika van ligandbinding, en die aard van die mikro-omgewing van ligand-bindingsplekke, te bepaal.

Stikstofoksied (NO) is 'n molekulêre boodskapper wat 'n rol in verskeie neurologiese toestande in soogdiere speel. NO word deur stikstofoksiedsintetase (NOS) vanaf L-arginien gesintetiseer, en oorproduksie kan tot verskeie neurologiese toestande lei. Die doel van hierdie studie was om 'n reeks nuwe indasool-, indool- en ander fluoresserende derivate, gekonjugeerd aan polisikliese strukture, vir verdere evaluering in NOS-studies te sintetiseer. NOS is 'n teikenstelsel waar fluoressensietegnieke en fluoresserende NOS-inhibeerders, soos 7-nitroindasool (7-NI), gebruik kan word om die biofisiese eienskappe van ensiem-ligandinteraksies te bepaal en om dan ook die ontwikkeling van nuwe inhibeerders vir neurodegenerasie te fasiliteer. Dit kan tot 'n groter begrip van neurobeskermde meganismes en die ontwikkeling van geneesmiddels vir neurodegeneratiewe toestande lei.

'n Reeks verbindings bestaande uit polisikliese strukture soos 3-hidroksi-4-asa-8-oksoheptasiklo[9.4.1.$0^{2,10}$.$0^{3,14}$.$0^{4,9}$.$0^{9,13}$.$0^{12,15}$]tetradekaan en amantadien, asook geskikte fluoresserende strukture is vir sintese geselekteer. Die polisikliese verbindings is deur aminering en esterfikasie of aminering na aktivering met die karbodiimiede, karbonieldiimidasool (KDI) en disikloheksielkarbidiimied (DSK), met die fluoresserende strukture gekonjugeer. Die fluoresserende groepe is op grond van hul spektroskopiese eienskappe, gemak van sintese en struktuur-aktiwiteitsverwantskappe vir NOS-inhibisie geselekteer. Die fluorofore sluit *N*-metielantranielsuur, indasool-3-karboksielsuur, 1-fluoor-2,4-dinitrobenseen, 1-sianoisoindool, 1-tiosianoisoindool en 1-nitroisoindool in.

Die oksihemoglobienmetode (oksiHb) is in die biologiese studie gebruik om die aktiwiteit van die nuwe verbindings op ensimatiese vlak van NOS te bepaal. Die toets is hoofsaaklik op die reaksie van NO met oksiHb en die vorming van methemoglobien (metHb) gebaseer. Die helling van die absorpsieverskille tussen 401 en 421 nm teenoor tyd is 'n aanduiding van NOS-aktiwiteit. Die IC_{50}-waardes is vanaf die inhibisiewaardes bereken en met mekaar vergelyk.

Die verbindings toon by mikromolêre konsentrasies inhibisie van die NOS-ensiem. Volledige ensieminhibisie kon as gevolg van oplosbaarheidsprobleme nie bereik word nie. Die polisikliese indasoolkonjugaat het sterker NOS-inhibisie as die ongekonjugeerde indasool-3-karboksielsuur getoon. Die antranielsuur- en dinitrobenseenderivate het slegs geringe of geen inhibisie van die NOS-ensiem getoon.

3-{4-Asa-8-okso-heptasiklo[0.4.1.$0^{2,10}$.$0^{3,14}$.$0^{4,9}$.^{09,13}.$0^{12,15}$]tetradekiel}-1*H*-indasool-3-karboksilaat en *N*-(1-siano-2*H*-isoindool-2-iel)adamantaan-1-amien het by 'n konsentrasie van 250 µM die beste inhibisie getoon en die ensiem is onderskeidelik met 83.7 % en 88.1 % geïnhibeer. Die verbindings in die reeks wat indasool- of indoolstrukture bevat toon dus die beste affiniteit vir die NOS-ensiem.

Die gesintetiseerde verbindings verteenwoordig 'n nuwe klas NOS-inhibeerders met relatief hoë affiniteit vir die NOS-ensiem, wat verder gebruik kan word vir *in vitro*- en *in vivo*-studies deur moderne fluoresserende tegnieke te gebruik. Hierdie verbindings het vanweë die hoër lipofilisiteit van die pentasikloundekielstrukture potensieel ook hoër deurlaatbaarheid deur die bloedbreinskans

CHAPTER 1
INTRODUCTION

1.1 BACKGROUND

Neurodegeneration and the development of neuroprotective agents have in recent years become an increasingly important focus of research. Much time and effort have gone into establishing the cause of disorders like Parkinson's disease (PD) and Alzheimer's disease (AD) as they negatively influence the quality of life of millions of people around the world. Neurodegeneration can be described as the process by which certain neurons in the central nervous system (CNS), and especially the brain, are damaged by a variety of mechanisms. There are three key mechanisms of neuronal cell death, which may act separately, or co-operatively to cause neurodegeneration. This "lethal triplet" of metabolic compromise, excitotoxicity and oxidative stress causes neuronal cell death that is both necrotic and apoptotic in nature (figure 1.1). Aspects of these three mechanisms are believed to play a role in the neurodegeneration that occurs in both acute conditions, such as stroke and epilepsy, and in chronic neurodegenaritive disorders like Parkinson's disease, Alzheimer's disease and Huntington's disease (Alexi *et al.*, 2000; Greene & Greenamyre, 1996).

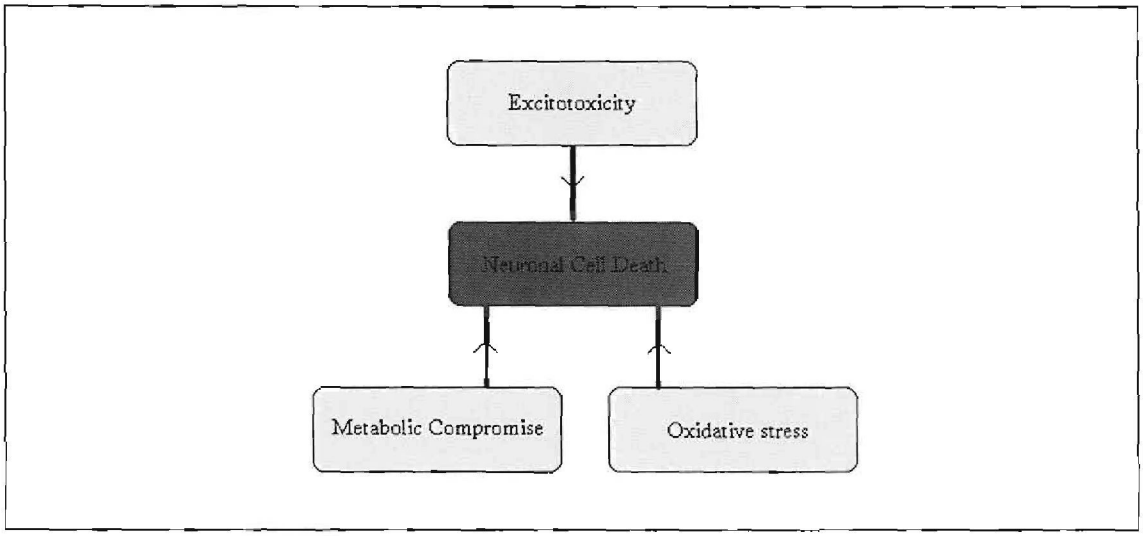

Figure 1.1: Lethal triplet in neuronal cell death.

1.2 RATIONALE

1.2.1 POLYCYCLIC STRUCTURES

Investigations into the synthesis and chemistry of novel saturated polycyclic hydrocarbon 'cage' compounds have been the aim of several research groups. The medicinal potential of these compounds was realised with the discovery that amantadine exhibits antiviral activity. Subsequent to this discovery, it was found that amantadine could be benificial to patients with Parkinson's disease. It expresses its anti–Parkinsonian activity by increasing extracellular dopamine (DA) levels *via* DA re-uptake inhibition (Mizoguchi *et al.*, 1994) or DA release and NMDA receptor antagonism (Danysz *et al.*, 1997). Interest in the pharmacology of polycyclic cage amines was further stimulated when the dimethyl derivative of amantadine, memantine, was found to be a clinically well tolerated NMDA receptor antagonist (Parsons *et al.*, 1999). Considering the antiviral activity of amantadine, further studies into related polycyclic cage compounds led to the discovery of other compounds with antiviral properties. A structural similarity exists between the policyclic cage structure of adamantane amines and that of the pentacycloundecane amines (Oliver *et al.*, 1991). Pentacycloundecylamines are derived from Cookson's diketone (Pentacyclo[5.4.$0^{2,6}$.$0^{3,10}$.$0^{5,9}$]undecane-8,11-dione), the so called "bird cage" compound, obtained from the intramolecular photocyclisation of the Diels Alder adduct of *p*-benzoquinone and cyclopentadiene (Cooksen *et al.*, 1958).

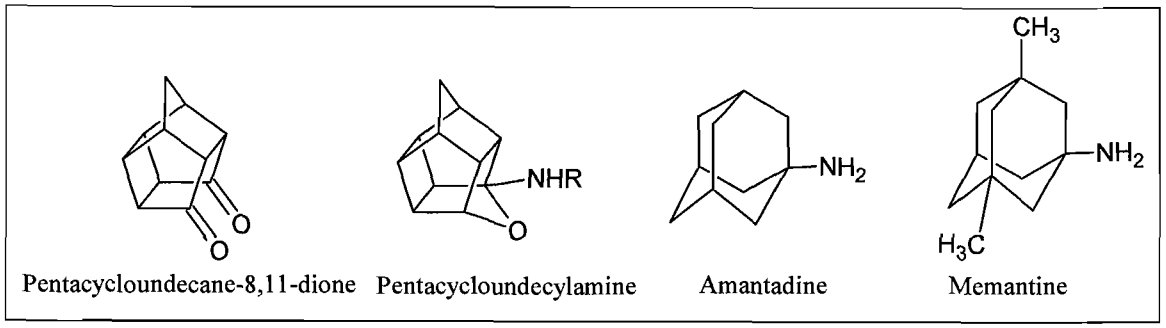

Pentacycloundecane-8,11-dione Pentacycloundecylamine Amantadine Memantine

Figure 1.2: Structural similarities of the pentacycloundecane derivatives with amantadine and memantine (Oliver *et al.*, 1991).

The observed anti-parkinsonian activity of amantadine led to the evaluation of the pentacycloundecylamines as possible therapeutic agents for parkinson's disease (Oliver *et*

al., 1991). Another benefit of the pentacycloundecylamines is their ability to enter the CNS. For drugs to exert meaningful effects in the CNS they have to cross the blood brain barrier (BBB) and it was found that the pentacycloundecylamines penetrate the CNS in sufficient concentration to exert pharmacological effects. (Zah *et al.*, 2003).

The polycyclic cage thus appears to be a useful scaffold to explore the design of potential pharmacological active compounds in the field of neurodegeneration.

1.2.2 ENZYME INHIBITION

The selective inhibition of MAO-B has been shown to have neuroprotective effects in MPTP animal models (Langston *et al.*, 1994). MAO-B inhibition prevents the formation of the toxic MPP^+ species by inhibiting the bioactivation of MPTP. There is also evidence that the inhibition of nNOS protects against MPTP mediated neurotoxicity in animals (Matthews *et al.*, 1997). The potential roles of MAO–B and NOS in neurodegenerative prosesses and their selective inhibition are thus areas of intense investigation. 7-Nitroindazole (7-NI) is a selective inhibitor of nNOS (Babbedge *et al.*, 1993) and treatment of animals with 7-NI provides protection against MPTP neurotoxicity (Hantraye *et al.*, 1996. & Schulz *et al.*, 1995).

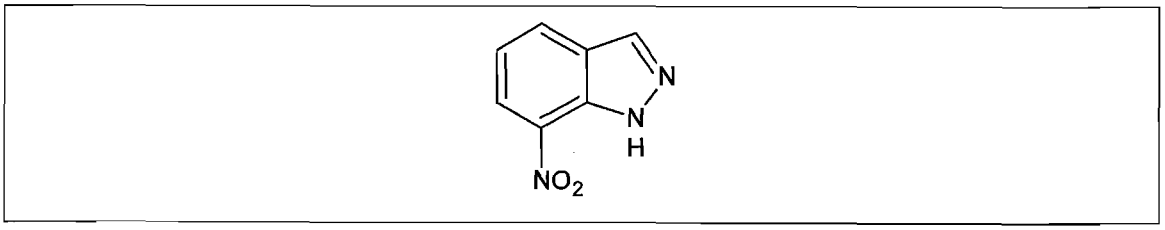

Figure 1.3: 7-Nitroindazole

These neuroprotective effects are thought not associated with decreased MPP^+ production since 7-NI did not inhibit the MAO-B catalysed oxidation of benzylamine by mouse brain mitochondrial preparations. In another study, striatal levels of MPP^+ in MPTP-treated mice were compared between 7-NI injected and control mice (Przedborski *et al.*, 1996) and the striatal MPP^+ levels were unaffected by neuroprotective doses of 7-NI. This lead to the conclusion that the neuroprotective effect of 7-NI was mainly due to nNOS inhibition. However, several studies show that planar, heterocyclic compounds (Ooms *et al.*, 2000) are inhibitors of MAO-B (Kneubuehler *et al.*, 1995), suggesting that 7-NI, also

a planar heterocyclic compound, could inhibit MAO-B. This led Castagnoli's group to investigate the MAO-B inhibiting properties of 7-NI (Castagnoli *et al.*, 1998). The effect of different 7-NI concentrations on the MAO-B catalysed oxidation of MPTP to its metabolite $MPDP^+$ was studied *in vitro*. In this study 7-NI was found to be a competitive inhibitor of MAO-B.

7-NI was also found to protect against the MPTP induced depletion of nigrostriatal DA in mice (Di Monte *et al.*, 1997). This effect was accompanied by a significant decrease in the striatal levels of MPP^+ showing that the neuroprotective effect of 7-NI is at least partly mediated through the inhibition of MAO-B. Similar striatal MPP^+ levels were obtained for both 7-NI together with MPTP and MPTP only treated mice by injecting a higher dose of MPTP in the 7-NI treated mice. In this case a modest (20 %) protection of DA depletion was observed suggesting that the inhibition of MAO-B may not be the only mechanism mediating the protection against MPTP induced neurotoxicity. According to these results, the neuroprotective effects of 7-NI may therefore be due to MAO-B inhibition, nNOS inhibition or inhibition of both enzymes. Recently, Royland *et al.* (1997) described the effect of 7-NI and *N*-nitro-*L*-arginine, another NOS inhibitor, on MPTP-induced striatal ATP depletion. The results showed that 7-NI prevented the striatal ATP loss in mice after MPTP administration. However, *N*-nitro-*L*-arginine didn't have any effect on MPTP induced ATP loss suggesting the importance of MAO-B inhibition rather than NOS inhibition in 7-NI mediated neuroprotection. The effect of 7-NI on 3-nitrotyrosine immunoreactivity in the substantia nigra, which is considered as a marker for peroxynitrite mediated neurotoxicity (Ischiropoulos *et al.*, 1992) was also evaluated. An increase in 3-nitrotyrosine immunoreactivity was reported in MPTP treated baboons which were blocked by 7-NI providing evidence for the involvement of nNOS inhibition in protection against MPTP induced neurotoxicity (Ferrante *et al.*, 1999).

1.2.3 FLUORESCENT PROBES

Fluorophores currently used as fluorescent probes offer sufficient permutations of wavelength range, Strokes shift and spectral bandwidth to meet requirements imposed by fluorescent instrumentation. The fluorescent output of a given fluorophore depends on the efficiency with which it absorbs and emits photons, and its ability to undergo repeated

excitation/emission cycles (Haugland *et al.*, 2002). A large number of fluorescent probes are available for studies of various cell components and metabolic processes. Fluorescent probes are one of the cornerstones of real-time imaging of live cells and a powerful tool for cell biologists. They can be used to detect specific cellular components, environmental conditions like pH and Ca^{2+} concentration, or be used as enzyme substrates. They provide high sensitivity, great versatility while perturbing the cell under investigation minimally and offer an attractive alternative to the application of radioligands. The following fluorescent probes were chosen for this study.

Table 1.1: Excitation and emmision values of fluorophores selected for this study (Haugland *et al.*, 2002).

Fluorophore	λ_{ex} (nm)	λ_{em} (nm)
Indazole-3-carboxylic acid	330	410
N-methylanthranilic acid	330	446
1-cyanoisoindole	419	493
1-tiocyanoisoindole	360	455
1-fluoro-2,4-dinitrobenzene	397	527

1.3 AIM OF STUDY

From the information above, it was decided to synthesise a series of fluorescent polycyclic derivatives structurally related to 7-NI and to explore their neuroprotective ability/potential. The fluorescent compounds for this study were selected on the basis of their spectroscopic properties, ease of synthesis and structural similarities to 7-nitroindazole to exhibit NOS inhibition. The compounds planned for synthesis include *N*-methylanthranilic acid, indazole-3-carboxylic acid, 1-fluoro-2,4-dinitrobenzene, 1-cyanoisoindole, 1-thiocyanoisoindole and 1-nitroisoindole conjugated to 3-hydroxy-4-aza-8-oxoheptacyclo[9.4.1.$0^{2,10}$.$0^{3,14}$.$0^{4,9}$.$0^{9,13}$.$0^{12,15}$]tetradecane and amantadine (Table 1.1). For this study we thus attempted to identify a series of fluorescent structures with

high affinity for the NOS enzyme, which may be utilised for further *in vitro* and *in vivo* studies using modern imaging techniques. These compounds could have potential as useful pharmacological tools to investigate enzyme-ligand interactions in the quest for more effective neuroprotective strategies.

To reach the aim the following was done:

- Synthesis of selected fluorophores, and conjugation thereof to polycyclic structures.
- *In vitro* evaluation of NOS inhibition utilising the oxyhemoglobin assay.

Table 1.2 Compounds evaluated and synthesised in this study

Compound	Structure
3-{4-Aza-8-oxo-heptacyclo[0.4.1.$0^{2,10}$.$0^{3,14}$.$0^{4,9}$.^{09,13}.$0^{12,15}$]tetradecyl}-1*H*-indazole-3-carboxylate (1)	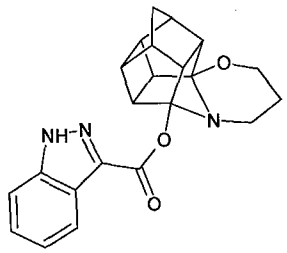 **(1)**
3-{4-Aza-8-oxo-heptacyclo[0.4.1.$0^{2,10}$.$0^{3,14}$.$0^{4,9}$.^{09,13}.$0^{12,15}$]tetradecyl}-2-(methylamino)benzoate (2)	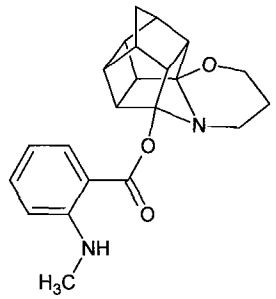 **(2)**
8-Benzylamino-8,11-oxapentacyclo[5.4.$0^{2,6}$. $0^{3,10}$.$0^{5,9}$]undecane (3)	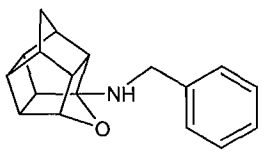 **(3)**

***N*-Adamantan-1-yl-1*H*-indazole-3-carboxamide (4)**	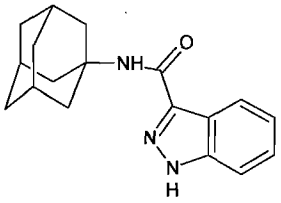 (4)
***N*-Adamantan-1-yl-2(methylamino)benzamide (5)**	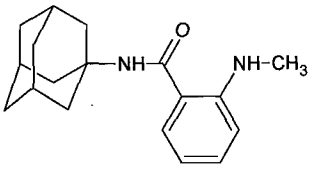 (5)
***N*-(2,4-Dinitrophenyl)adamantan-1-amine (6)**	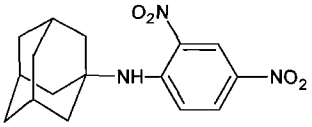 (6)
***N*-(1-Cyano-2*H*-isoindol-2yl)adamantan-1-amine (7)**	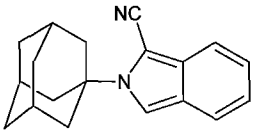 (7)
***N*-(1-Thiocyano-2*H*-isoindol-2yl)adamantan-1-amine (8)**	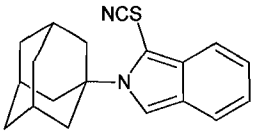 (8)
***N*-(1-Nitro-2*H*-isoindol-2yl)adamantan-1-amine (9)**	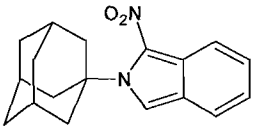 (9)

It is expected that the indazole and isoindole moieties will have moderate to high NOS activity as they have greater structural similarity to 7-NI than the anthranilic and dinitrobenzene compounds. These structures should also provide adequate fluorescent properties to be used for further studies.

CHAPTER 2
LITERATURE REVIEW

The purpose of this chapter is to give insight into drug targets of neurodegenerative disorders and to give an overview of fluorescence and fluorescent techniques which could be utilised as potentially useful pharmacological tools to investigate enzyme-ligand or receptor-ligand interactions in the quest for effective neuroprotective strategies.

2.1 NEURODEGENERATIVE DISORDERS

Because of its potential clinical application, neuroprotection is an intensively studied area. There are numerous neurodegenerative diseases, among which are Parkinson's disease (PD), Alzheimer disease (AD), Huntington's disease (HD) and Machado-Joseph disease (MJD).

PD is an age-dependent (strikes 1-2 % of the "over 50" population), neurodegenerative disorder involving the selective loss of dopaminergic nigostratial neurons (Castagnoli *et al.*, 2000). It is now clear that PD can be defined in biochemical terms primarily as a dopamine deficiency state resulting from degeneration or injury to dopaminergic neurons (Marsden, 1990). Even in patients with mild symptoms, dopaminergic neuron loss of 50 % (Jelliger, 1997; Fearnley & Lees, 1999) and stratial dopamine loss of 70 % - 80 % are observed. Another pathological, but not unique, characteristic of PD is the presence of intracellular inclusion bodies called Lewy bodies in the surviving nerve cells (Forno, 1996; Gibb, 1999). In clinical terms PD is characterised by three cardinal features; rest tremors in the 3 – 5 Hz range, muscle rigidity and bradykinesia. Postural instability (sometimes judged a cardinal feature) is usually absent in early disease (Samil *et al.*, 2004).

Insights into the pathophysiology of PD and other neurodegenerative disorders from exogenous sources have been derived from biochemical, neuroprophysiological and anatomical studies of the MPTP animal model of the disease (Speciale, 2002). The

molecular mechanism by which MPTP selectively damages nigrostratial neurons has been the subject of extensive research (Castagnoli *et al.*, 2000). MPTP was first synthesised by illicit drug dealers in an attempt to produce MPPP, a synthetic heroin. MPTP is metabolised by MAO-B to $MPDP^+$ (figure 2.1), which is then further oxidised to the corresponding pyridinium species MPP^+ (Smeyne *et al.*, 2004), the ultimate human neurotoxin (Castagnoli *et al.*, 2000).

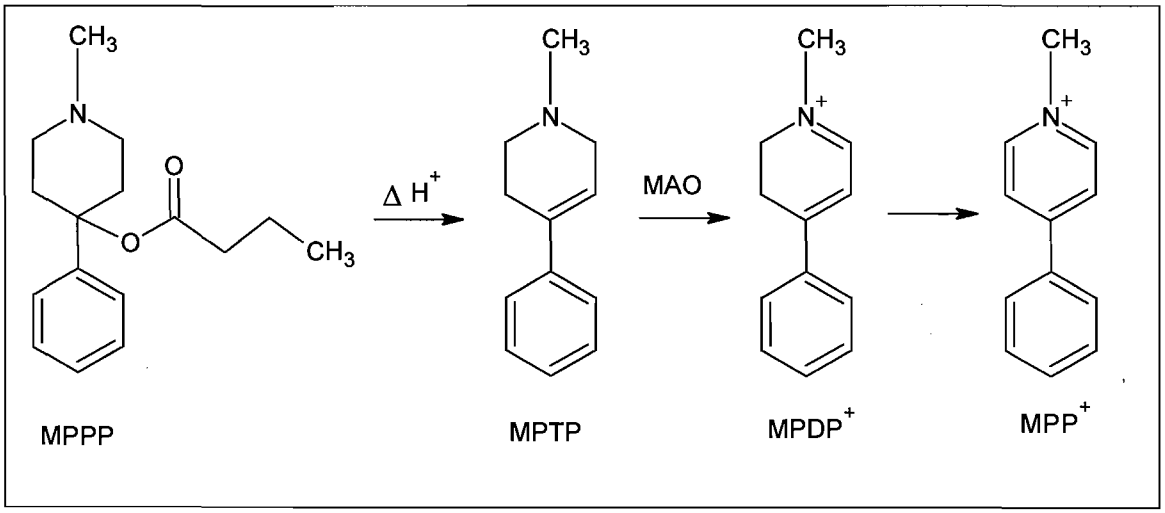

Figure 2.1: MAO-B catalyzed oxidation of MPTP (Smeyne *et al.*, 2004).

MPP^+ is transported into the nigrostratial nerve terminals by the DA transporter where it subsequently localises within inner mitochondrial membranes and inhibits complex I of the mitochondrial respiratory chain (Cleeter *et al.*, 1992). The inhibition leads to cell death, causing DA depletion in the brain. The damage is initially seen at the nerve terminal, probably because MPP^+ is taken up into nigral neurons via the high affinity DA reuptake system at the terminal level. The exact mechanism leading to cell death is not clear but it is thought to take place through a complicated pathway (Lanson *et al.*, 1994). One possibility is the increased free radical production due to complex I inhibition. However, there is not enough evidence to support this mechanism.

Alzheimer disease (AD) is a progressive form of dementia occurring in middle age or later, characterised by loss of short-term memory, deterioration in behaviour and intellectual performance, and slowness of thought. These impairments are associated with

neuronal loss, synaptic changes and the accumulation of proteinaceous lesions in certain vulnerable areas of the brain (Standaert & Young, 2000).

Huntington's disease (HD) is a hereditary disease caused by a defect in a single gene that is inherited as an autosomal dominant characteristic, tending to appear in half of the children of parents with this condition. The symptoms which begin to appear in early middle age, include unsteady gait, jerky involuntary movements accompanied later by behavioural changes, progressive dementia and ultimately severely demented patients die after 15-25 years of illness. HD post mortem brains show substantial general atrophy, but most prevalent is the selective loss of GABAergic, medium spiny, neurons of the caudate and putamen (Difiglia & Vonsattel, 1998); interneuron's (mostly NADPH- and ChAT-postive) are spared. In the cortex, degeneration of neurons projecting to the basal ganglia is observed in the deeper layers. Other less affected areas include the globus pallidus, subthalamic nucleus, and amygdala. Pathology outside the CNS is thought to be minimal.

Machado-Joseph disease (MJD) is an autosomal dominant neurodegenerative disorder caused by an expansion of CAG trinucleotide repeats in the MJD gene (Takiyama *et al.*, 1993; Kawaguchi *et al.*, 1994). Normal alleles vary from 12 to 43 repeats, whereas expanded alleles vary between 56 and 86 repeats (Takiyama *et al.*, 1993). The CAG repeat size exhibits an inverse correlation with age at onset and is also partially correlated with several clinical manifestations, although the causative chain of events at cellular level is not yet understood (Stevanin *et al.*, 2000). The wide range of clinical manifestations include: gait and limb ataxia; dysarthria and dysphagia; pyramidal syndrome, supranuclear, progressive external ophthalmoplegia; extrapyramidal signs, including dystonia, rigidity and bradykinesia; a lower motor neuron disease, amyotrophy; loss of tactile, algesic and vibration senses; eyelid retraction, loss of weight and a sleep disorder (Jardim *et al.*, 2001). Patients become confined to a wheelchair and are later bedridden. The median survival time after onset is 17 years. Neuropathologic lesions are widespread in MJD. There is extensive neuronal cell loss and gliosis in Clarke's columns, dentate nucleus, pontine nuclei, and vestibular nuclei. There is moderate to severe involvement of substantia nigra, anterior horn cells, and motor cranial nerve nuclei (Rosenberg, 1992). Variable degrees of involvement of the striatum, subthalamic nucleus, and globus pallidus have also been reported (Sequeiros *et al.*, 1993).

A variety of symptoms and causes of neurodegeneration thus exist. For the causes of these diseases only a few treatments have been identified, but no cure so far.

2.2 NITRIC OXIDE SYNTHASE (NOS)

The role of nitric oxide (NO) as a biological signalling molecule is well established. NO is produced by the nitric oxide synthases (NOS), a class of heme proteins capable of converting L-arginine to NO and L-citrulline. Despite the large body of knowledge associated with the NOSs, mechanistic details relating to the unique oxidative chemistry performed by these enzymes remain to be fully eludicated (Martin *et al.*, 2007).

The NOSs are a family of enzymes in the body that contributes to transmission from one neuron to another, to the immune system and to dilating blood vessels. It does so by synthesis of nitric oxide from the terminal nitrogen atom of L-arginine in the presence of NADPH and oxygen (O_2) (figure 2.2) (Dawson *et al.*, 1991) to L-citruline and NO via the intermediate N^G-hydroxy-L-arginine (Martin *et al.*, 2007). NOS is the only known enzyme that has several cofactors including NADPH, flavin adenine dinucleotide (FAD), flavin mononucleotide (FMN), heme, tetrahydrobiopterin (BH_4) and calmodulin (Kerwin. *et al.*, 1995). Although NO mediates several physiological functions (table 2.1), a number of disease states are associated with either the overproduction or underproduction of NO, making the NOS pathway an attractive target for the development of therapeutics (Martin *et al.*, 2007). Overproduction by NOS has been implicated in a number of clinical disorders, including acute (stroke) and chronic (Alzheimer's, Parkinson's and Huntington's disease) neurodegenerative diseases, convulsions and pain (Moncada *et al.*, 1991).

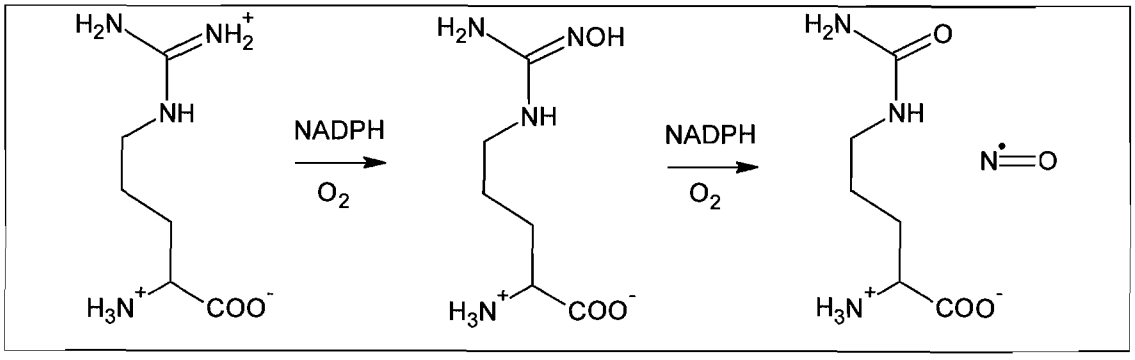

Figure 2.2: NOS catalysed conversion of *L*-arginine to *L*-citrulline and NO (Kerwin *et al.*, 1995).

For these reasons molecular tools capable of providing mechanistic insights into the production of NO and/or the inhibition of the NOS enzymes remain of interest. The developement of neuroprotective agents is orientated towards the synthesis of novel structures that interfere with some step of the complex chemical signalling system involving NOS and the inhibition of the enzyme itself.

2.2.1 NOS ISOFORMS

Three distinct NOS enzymes have been identified and characterised, products of different genes, with different subcellular localisation, regulation, catalytic properties, and inhibitor sensitivity; neuronal NOS (nNOS) and endothelial NOS (eNOS), which are constitutively expressed, and inducible NOS (iNOS) (Steuhr, 1999 & Martin *et al.*, 2007). nNOS and eNOS are physiologically activated by steroid hormones or neurotransmitters such as NO, dopamine, glutamate and glycine that increase the intracellular calcium concentrations. In contrast iNOS is Ca^{2+} independent and is expressed in a broad range of cell types. This form of NOS is induced after stimulation with cytokines and exposure to microbial products. After permanent activation, it continuously produces high concentrations NO (Knowles *et al.*, 1994).

Since these isoforms possess a distinct cellular localisation and are differently regulated, they represent specific targets for potential therapeutic approaches (table 2.1).

2.2.2 NOS STRUCTURE

All three isoforms are active as the homodimer with each subunit containing a C-terminal reductase domain (with binding sites for NADPH, FAD and FMN) and a N-terminal oxygenase domain containing the heme prostetic group (Roman *et al.*, 2002). The carboxyl-terminal reductase domain homologous to the cytochrome P450 reductase has binding sites for L-arginine and H_4B. They also share an amino-terminal oxygenase domain, containing a heme prosthetic group, which is linked in the middle of the protein to a calmodulin-binding domain. Binding of calmodulin appears to act as a "molecular switch" to enable electron flow from flavin prosthetic groups in the reductase domain to heme. This facilitates the conversion of O_2 and L-arginine to NO and L-citrulline (Haugland *et al.*, 2002). The oxygenase domain of each NOS isoform also contains an

BH_4 prosthetic group, which is required for the efficient generation of NO. Unlike other enzymes where BH_4 is used as a source of reducing equivalents and is recycled by dihydrobiopterin reductase, BH_4 activates heme-bound O_2 by donating a single electron, which is then recaptured to enable nitric oxide release (Steur *et al.*, 1999).

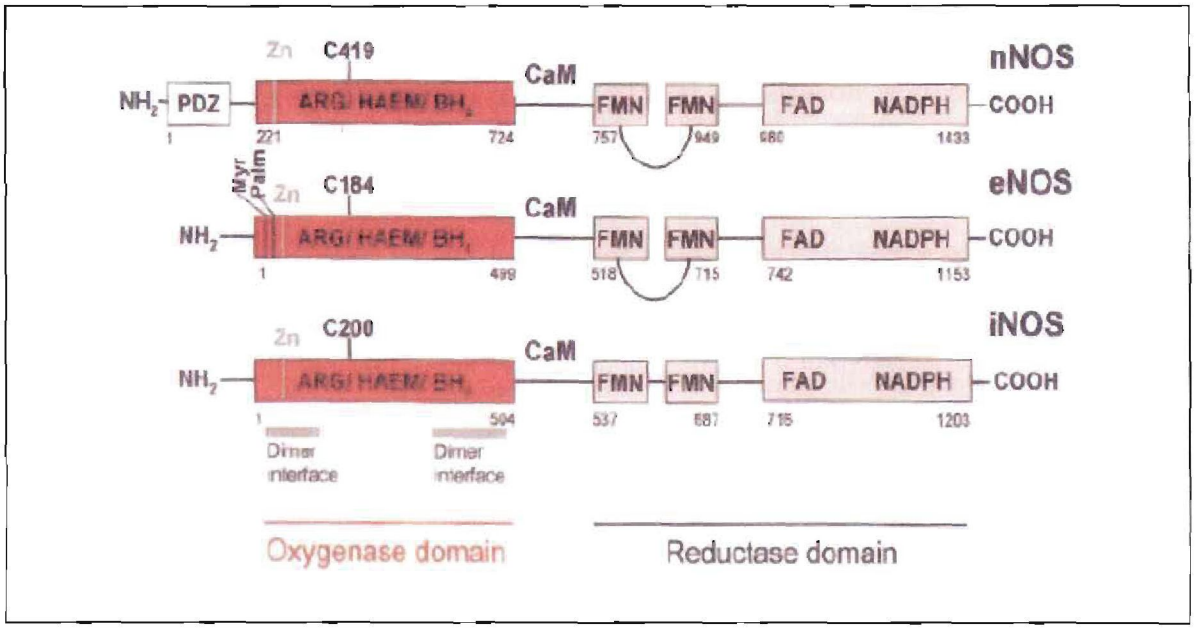

Figure 2.3: Domain structure of human nNOS, eNOS and iNOS. Oxygenase, reductase and PDZ domains are denoted by solid boxes and the amino acid residue number at the start/end of each domain is shown. The cysteine residue which ligates the heme and the CaM-binding site is indicated for each isoform, as is the location of the zinc-ligating cysteines (Zn in grey). The auto-inhibitory loop within the FMN regions of nNOS and eNOS are also shown and the grey bars indicate the dimer interface in the oxygenase domain (Taken from Alderton *et al.*, 2001).

The first nitric oxide synthase to be identified was found in neuronal tissue (nNOS) and the endothelial NOS (eNOS) was the third to be identified. They were originally classified as "constituitvely expressed" and "Ca^{2+} sensitive" but it is now known that they are present in many different cell types and that expression is regulated under specific physiological conditions.

Table 2.1: Postulated roles for NO synthesised by three NOS isosformes (Adapted from: Moncada et al., 1991; Stuer, D.J. 1999; Martin *et al.*, 2007)

Isoform	Category	Roles
Neuronal NOS (nNOS or NOS1)	Ca^{2+} dependant	Produces NO in neuronal tissue in both the central and peripheral nervous system. It is involved in neurotransmission and long-term potentiation. Neuronal NOS also performs a role in cell communication and is associated with plasma membranes.
Inducible NOS (iNOS or NOS2)	Ca^{2+} independant	Can be found in the immune system, but is also found in the cardiovascular system. It uses the oxidative stress of NO (a free radical) by macrophages in immune defence against pathogens and tumor cells.
Endothelial NOS (eNOS or NOS3)	Ca^{2+} dependant	Generates NO in blood vessels and is involved with regulating vascular function. It is a constitutive Ca^{2+} dependent NOS and provides a basal release of NO. It is involved in the regulation of smooth muscle relaxation and vascular tone. eNOS is associated with plasma membranes surrounding cells and the membranes of Golgi bodies within cells.

In nNOS and eNOS, physiological concentrations of Ca^{2+} in cells regulate the binding of calmodulin to the "latch domains", thereby initiating electron transfer from the flavins to the heme moieties. In contrast, calmodulin remains tightly bound to the inducible and Ca^{2+}-insensitive isoform (iNOS) even at a low intracellular Ca^{2+} concentration, acting essentially as a subunit of this isoform.

Nitric oxide may itself regulate NOS expression and activity. Specifically, NO has been shown to play an important negative feedback regulatory role on eNOS, and therefore

vascular endothelial cell function. This process, known formally as *S*-nitrosation (and referred to by many in the field as *S*-nitrosylation), has been shown to reversibly inhibit eNOS activity in vascular endothelial cells. This process may be important because it is regulated by cellular redox conditions and may thereby provide a mechanism for the association between "oxidative stress" and endothelial dysfunction.

In addition to eNOS, both nNOS and iNOS have been found to be *S*-nitrosated, but the evidence for dynamic regulation of those NOS isoforms by this process is less complete. In addition, both nNOS and eNOS have been shown to form ferrous-nitrosyl complexes in their heme prosthetic groups that may act partially to self-inactivate these enzymes under certain conditions. The rate-limiting step for the production of nitric oxide may well be the availability of L-arginine in some cell types. This may be particularly important after the induction of iNOS (Rosen *et al.*, 2002; Alderton *et al.*, 2001).

2.2.3 NOS INHIBITORS

The NOS isoforms are responsible for forming NO under many physiological and pathological conditions. Since aberrant generation of NO is associated with severe pathological conditions, drugs for the pharmacological modulation of NO have been sought (Alderton *et al.*, 2001). The therapeutic benefit of agents that decrease NO levels is however controversial as NO may exert both positive and negative effects on physiological condition and pathophysiological progressions (Muscara *et al.*, 1999). Because free NO is a transient species with a half life of about five seconds, many investigations of this gaseous molecule have relied largely on studies of NOS (Haugland *et al.*, 2002). NO has also been connected to long-term potentiation, guanile cyclase activation, neurotransmitter release and reuptake as well as glutamate (NMDA) mediated neurotoxicity (Hoffman & Taylor, 2001).

NOS is thus an important drug target, and isoform selective inhibitors are needed to block uncontrolled production of NO in disease states. It is critical for these inhibitors not to affect eNOS as it would severely perturb blood pressure homeostasis. A common pharmacological approach to study the role of a biological mediator is to investigate how processes related to it are affected by the administration of specific inhibitors. Thus, guanidines such as L-NAME and aminoguanidine are NOS inhibitors extensively used in

pharmacological tests, where it is believed that their pharmacological effects are exerted by inhibition of NOS isoforms and a presumed lowered NO content in tissues (Ogden *et al.*, 1995. & Griffith *et al.*, 1996). In addition, the clinically used antihypertensive guanidine compound, guanabenz has been shown to have inactivating effects on nNOS (Nakatsuka *et al.*, 1998). Although there is evidence from *in vitro* studies for the inhibitory effects of this guanidine, it has however not been clearly demonstrated to affect NO levels *in vivo*.

Table 2.2: List of common NOS inhibitors (Nishihira, 2000. & Okabe, 1994. & Barlas, 2002).

Compound.	NOS activity.	Structure.
1400W.	Highly selective inhibitor of inducible nitric oxide synthase (iNOS) in vitro.	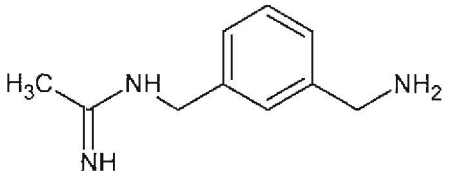
Nitro-L-arginine.	Potent inhibitor of all three NOS isoforms.	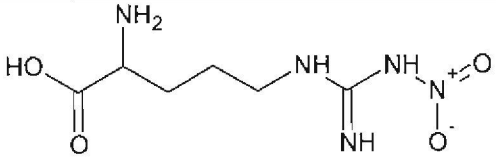
L-N6-(1-iminoethyl)-lysine.	A selective iNOS inhibitor.	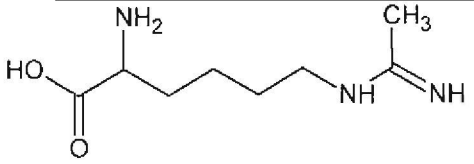
NG-methyl-L-arginine, acetate salt.	Competitive, irreversible inhibitor of all three NOS isoforms.	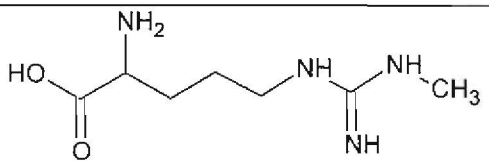
7-Nitroindazole.	Reversible, competitive and selective nNOS inhibitor and selective MAO-B inhibitor.	

Methylene blue.	Methylene blue is a direct inhibitor of al three NOS isoforms	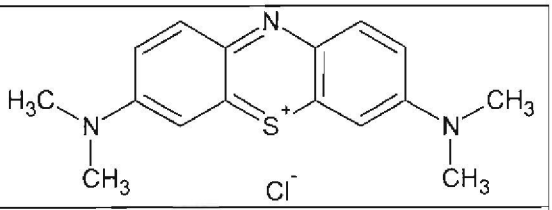
Aminoguanidine.	Inhibits both constitutive and inducible nitric oxide synthetase, but has a relative slectivity towards iNOS	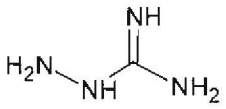
L-NAME.	A non-selective inhibitor of NOS that has been used experimentally to induce hypertension.	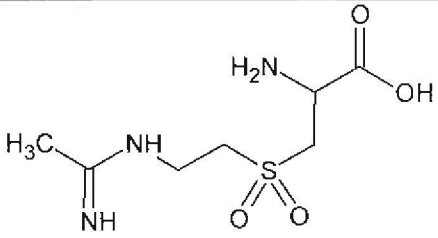
Guanabenz	Guanabenz has been shown to have inactivating effects on nNOS	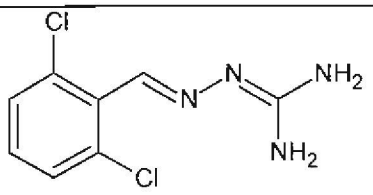

The majority of known NOS inhibitors are nonselective or iNOS selective and only a few compounds are able to selectively inhibit nNOS, among which 7-nitroindazole (Moore *et al.*, 1993), 1-(2-trifluoromethyl-phenyl)-imidazole (TRIM) (Handy *et al.*, 1995), some aromatic amidines (Reif *et al.*, 1999) and amino acid derivatives (for example, aminoguanidines) (Huang *et al.*, 1999). TRIM has been reported to be relatively selective for nNOS, but with low potency. The nitroindazole family are more potent nNOS inhibitors but their selectivity between isoforms remain low, at least *in vitro* (Moore *et al.*, 1993. & Handy *et al.*, 1995).

2.2.4 INDICATORS FOR NITRIC OXIDE

Studies on the physiological roles of NO have been hampered by the difficulty in obtaining direct *in vivo* measurements of this compound due to its extremely short half-life and low concentrations.

Probably the most successful indicator for nitric oxide has been 4,5-diaminofluorescein diacetate (DAF-2 DA), which was developed by Kojima and collaborators (1998). 4,5-Diaminofluorescein (DAF-2) demonstrates high sensitivity and specificity to NO and has been widely applied for NO detection and imaging. DAF-2 DA is membrane permeable and is deacetylated by intracellular esterases to 4,5-diaminofluorescein (DAF-2). DAF-2 is in itself non-fluorescent, but reacts with NO in the presence of oxygen to form the highly fuorescent triazolofuorescein (DAF-2T) which has excitation and emission maxima at 495 nm and 515 nm respectively (Kojima *et al.*, 1998). It has been used to identify individual nitric oxide producing neurons in brain slices, mitochondria (Lopez-Figueroa *et al.*, 2000), and in living plant cells (Foissner *et al.*, 2000). The conversion of DAF-2 to DAF-2T, (figure 2.4) by reaction with NO increases quantum efficiency by over 180-fold. It is likely that DAF-2 does not react directly with NO but with N_2O_3 formed in the course of NO oxidation, yielding the product DAF-2T. DAF-2 does not react in neutral solutions with other oxidised species such as NO_2 and NO_3, and other reactive oxygen spesies such as O_2, H_2O_2, and $ONOO^-$ in neutral solutions providing specificity for NO detection (Kojima *et al.*, 1998).

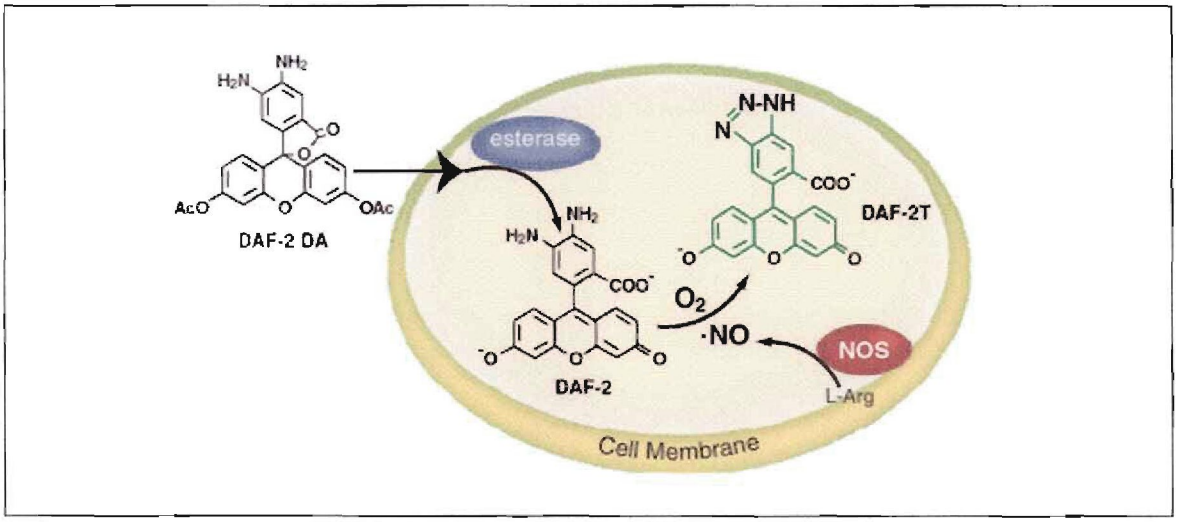

Figure 2.4: The principle of nitric oxide detection by DAF-2 DA (Kojima *et al.*, 1998).

Another successful indicator for nitric oxide has been the Griess reagent. The Griess test is a chemical analysis test which detects the presence of organic nitrite compounds. The Griess diazotization reaction on which the Griess reagent relies was first described in

1858 by Peter Griess. Under physiological conditions, NO is readily oxidised to nitate or is trapped by thiols as an *S*-nitroso adduct. The Griess reagent provides a simple and well characterised colorimetric assay for nitriles and nitrates that have been reduced to nitrites, with a detection limit of about 100 nM. Nitrites react with sulfanilic acid in acidic solution to form an intermediate diazonium salt that couples to N-(1-naphthyl)ethylenediamine to yield a purple azo derivative that can be monitored by absorbance at 548 nm. A typical commercial Griess reagent contains 0.2 % N-(1-naphthyl)ethylenediamine dihydrochloride, and 2 % sulphanilamide in 5 % phosphoric acid. Sample pretreatment with nitrate reductase and glucose 6-phosphate dehydrogenase is reported to reduce nitrate without producing excess NADPH, which can interfere with the Griess reaction. The Griess reagent can also be used to analyse NO that has been trapped as an S-nitroso derivate by a modification that uses mercuric chloride or copper (II) acetate to release NO from its complex (Haugland *et al.*, 2002).

The oxyhemoglobin assay is another well established assay for the detection of nitric oxide (NO) under aerobic conditions. Its popularity in very different areas of research is based primarily on its sensitivity and specificity for NO under aerobic conditions, inexpensiveness, ease of implementation and for the most part, rather modest technical requirements (Feelisch *et al.*, 1996). The major drawback of the oxyhemoglobin assay is that the oxyhemoglobin is not commercially available and the preperation of oxyhemoglobin involves oxygenation of the dithionite reduced heme protein followed by de-salting with a seperation funnel (Dacres *et al.*, 2005).

The oxyhemoglobin assay was first described by Feelisch and Noack 1987, to quantify NO release by chemical NO donors, then modified by Salter and Knowles 1989, to apply it to measure NOS activity and increase sensitivity. The method is based on the stoichiometric conversion of oxyhemoglobin to methemoglobin and nitrate (equation 1) by nitric oxide (NO), which can be followed spectrophotometrically and has been widely validated and used in several experimental systems. This reaction accounts largely for the inhibitory effect of hemoglobin on the biological effects of endogenously formed or exogenously applied NO (Feelisch *et al.*, 1996).

$$\mathbf{HbO_2 + NO \longrightarrow metHb + NO_3^-} \quad (1)$$

Under aerobic conditions in aqueous solution NO is highly unstable, as it is prone to rapid reactions with oxygen (O_2), superoxide anions (O_2^-), thiols (RSH) and a variety of metal containing proteins. As holds true for any method of NO quantification, the reaction of the detector molecule with NO should ideally be more rapid than that of other competing reactants. For the oxyHb assay, this prerequisite is met by the high rate of reaction between NO and oxyHb, which has been estimated to be at least 26 times faster than the autoxidation of NO in aqueous solution. The quenching and scavenging effect of superoxides may be limited by the addition of superoxide dismutase (SOD), both to increase the trapping efficiency of oxyHb for NO and to prevent the potential oxidation of oxyHb to metHb. Thiols will also not interfere with NO measurement since the reaction rate of NO/oxyHb is much faster than that of the reaction rate of NO/O_2 (Wink *et al.*, 1994). The rapid reaction between NO and oxyHb has the advantage of almost stoichiometrically trapping NO under the most experimental conditions. The oxyHb assay is therefore somewhat unique among methods for NO determination in that it is less subjected to constraints imposed by competing with oxygen, superoxide or thiols (Feelisch *et al.*, 1996).

The transformation to the tri-valent form of the central iron atom of hemoglobin is linked to a change in its absorption characteristics in the visible range (Privat *et al.*, 1997). The formation of NO can be continuously monitored by time-dependant recording of the absorbance changes in the Soret band associated with oxyHb oxidation (Kelm *et al.*, 1997). At pH 7.4, the absolute UV spectra of oxyHb is charactarised by an intense absorption Soret- or γ-band with a maximum at 415 nm and two weaker β- and α-bands with absoption maxima at 542 nm and 577 nm (Feelisch *et al.*, 1996). Methemoglobin's γ-band has an absorption maximum at 405 nm and 540 nm, respectively. The differences between oxyHb and metHb's spectral characteristicts become evident when the spectra are superimposed (figure 2.5). The absorbance intensities of both species are only equal at a few discrete wavelengths equal. Such spectral points of identical absorbance intensity are the so called isosbestic points and they do not change during the conversion of oxyHb to metHb. The absorbance difference at a given isosbestic point will stay zero throughout the entire reaction.

During this procedure, an absolute spectrum is recorded with the sample and reference cuvettes containing oxyHb and vehicle, respectively. After the reaction is started, NO reacts with oxyHb to form metHb. The new spectra recorded over time will present the absolute spectra of varying mixtures of oxyHb and metHb (figure 2.6). The original assay used the absorbance difference between 401 nm (maximum point) and 411 nm (isosbestic point) however, greater sensitivity is achieved by monitoring the absorption difference between the wavelengths 401 nm and 421 nm (minimum point), this gives close to maximal sensitivity (Privat *et al.*, 1997).

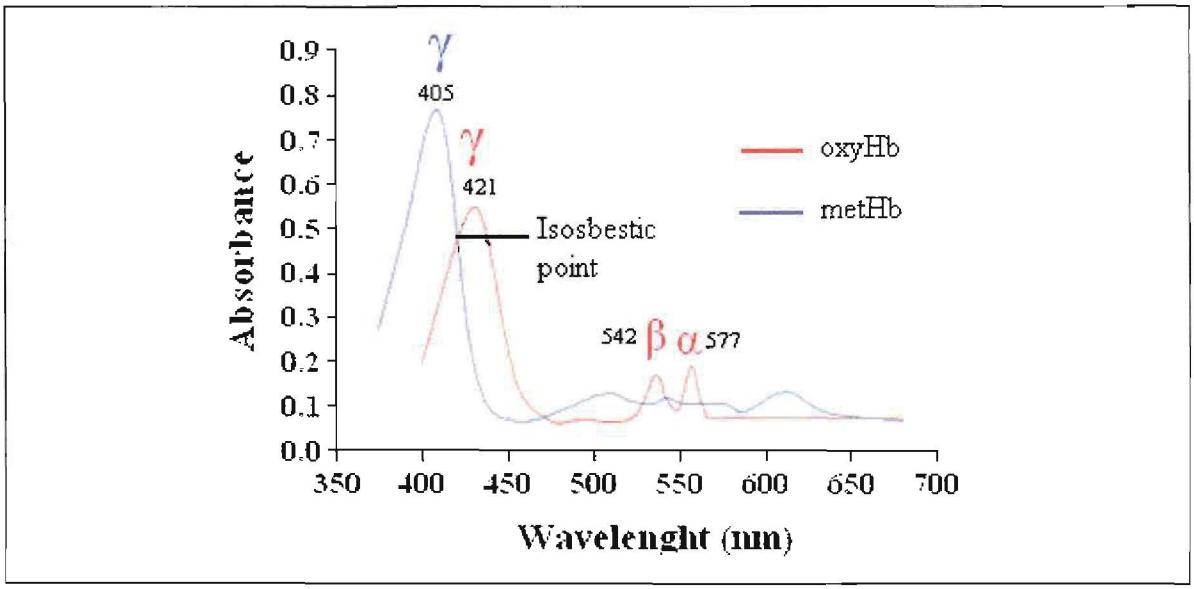

Figure 2.5: Superimposed absolute spectra of oxyhemoglobin (oxyHb) and methemoglobin (metHb). Intersection points represent the isosbestic wavelengths at which the absolute absorbance of both species are identical (adapted from Feelisch *et al.*, 1996).

The disadvantage of this procedure however, is that the actual concentrations of the individual hemoglobin derivatives can only be read from the absolute absorbance when complete convertion of oxyHb to metHb has occurred (Feelisch et al., 1996). In order to obtain information about the extent of conversion and thus the amount of NO generated, the vehicle is no longer used as a reference, but only the oxyHb containing solution is employed. Instead of using the contents of a second cuvette, the absorbance of the same cuvette at a second wavelength is chosen as a reference.

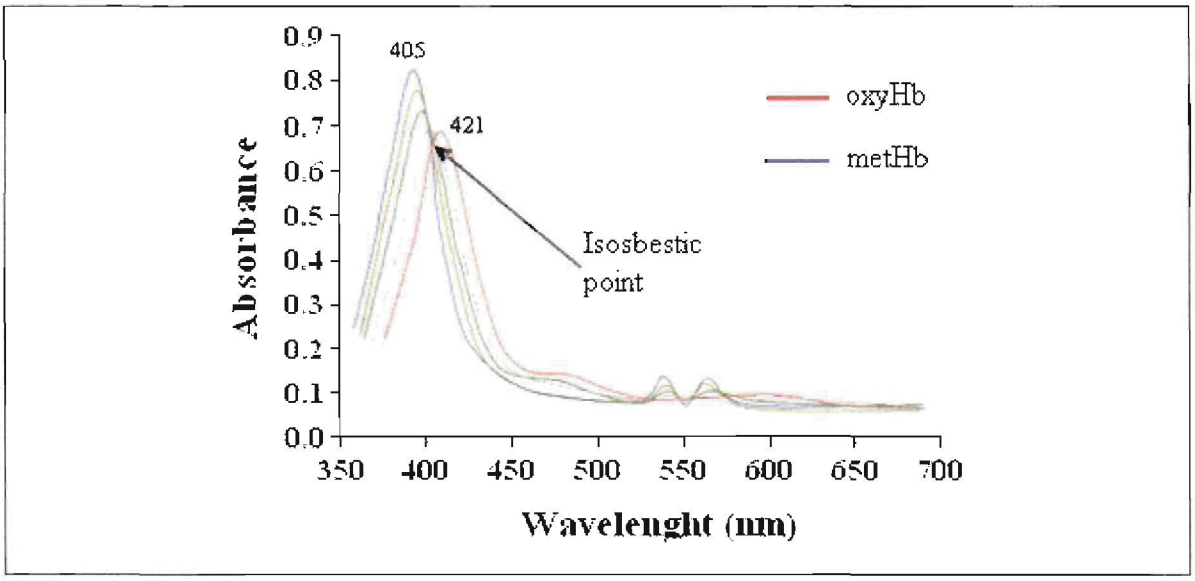

Figure 2.6: Changes in the absolute spectrum of an oxyHb containing solution upon NO-mediated conversion to metHb. Although the total concentration of hemoglobin remains constant, the spectroscopic features change as oxyHb is converted to metHb (adapted from Feelisch *et al.*, 1996).

If the light absorbance properties of the sample at a specific wavelength are recorded against the reference spectrum in a repetitive manner, difference spectra, the changes in absorbance will reflect the loss of oxyHb and the simultaneous formation of metHb (figure 2.7). In addition to the *isosbestic* points, there are certain regions corresponding to the formation of metHb where the absorbance increases (between 370 nm and 410.5 nm with a maximum at 401 nm) and regions corresponding to the loss of oxyHb where absorbance decreases (e.g. between 410.5 nm and 472 nm, with a minimum at 421 nm). From the difference spectra, the wavelength at which maximum change in absorbance occurs and a nearby isosbestic wavelength in usually subtracted from each other to determine metHb formation (Feelisch *et al.*, 1996).

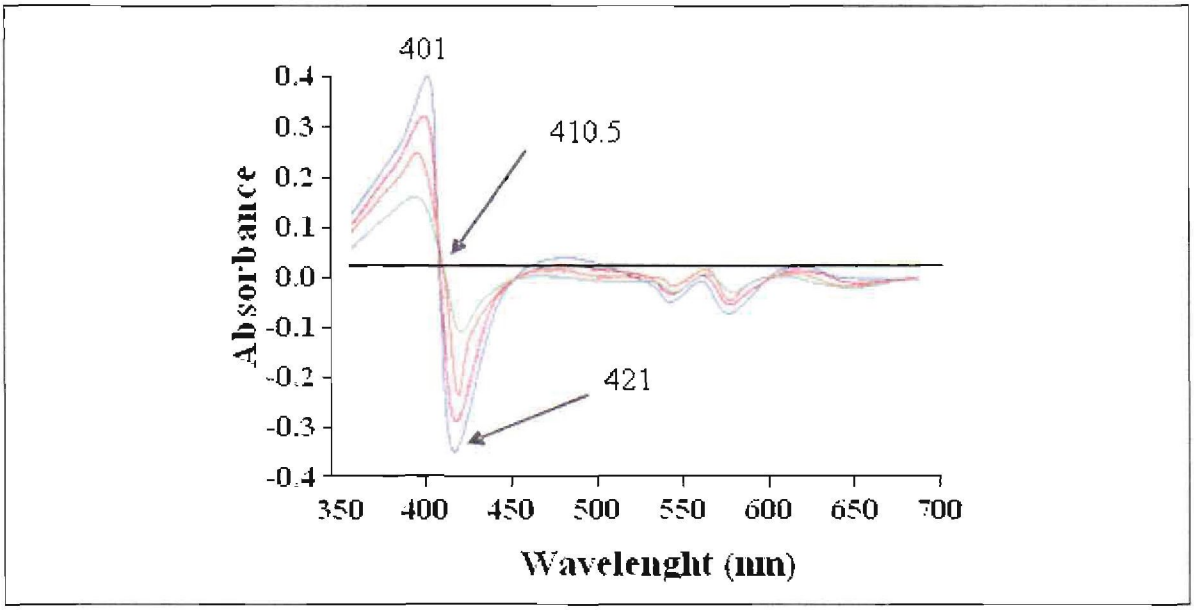

Figure 2.7: Representative difference spectral scans of the redox conversion of oxyHb to metHb. The spectra were recorded during the gradual convertion of oxyHb (5 μm) to metHb of NO from spermicide NONOate (40 μm). 410.5 nm is the isosbestic point used as the internal reference in the classical oxyHb assay, and 401 nm represents one of the wavelengths at which the absorbance is maximal, and 421 nm represents the wavelength at which the absorbance is minimal. Repeated scans were performed at 10 second intervals (adapted from Kelm et al., 1996).

The more NO is generated the larger the absorbance difference (ΔA) will be. This linear relationship between the absorbance difference (ΔA) and the amount of metHb formed is used to calculate the change in methb concentration. In order to calculate the time dependant increase of metHb concentration, the absorbance difference between a wavelength of maximal absorbance change (e.g. 401 nm) and an internal reference wavelength (e.g. 410 nm or 421 nm) are measured as a function of time. The slope of the resulting curve is a measure of increase in metHb concentration and thus NO formation of enzyme activity.

The oxyhemoglobin assay will be used in this study because of its popularity in very different areas of research, which is based primarily on its sensitivity and specificity for NO under aerobic conditions, inexpensiveness, ease of implementation and for the most part, rather modest technical requirements.

2.3 THE USE OF FLUORESCENT TECHNIQUES IN DRUG DESIGN.

Fluorescent techniques enable researchers to detect particular components of complex biomolecular assemblies, including live cells, with exquisite sensitivity and selectivity (Haugland *et al.*, 2002). The fluorescent imaging of living cells and tissues allows dynamic processes such as signalling, excitability, transport, apoptosis and development to be investigated in more biologically realistic contexts than the disassembled model systems employed in traditional biochemical analysis (Wells, 2003). The use of these techniques have found widespread applicability in receptor pharmacology (Malan *et al.*, 2004), and offer an attractive alternative to the application of radioligands (Li *et al.*, 2003). Fluorescence techniques offer a number of important advantages over other methods (table 2.3)

Table 2.3: Advantages of fluorescent techniques (Wells, 2003).

Advantage	Description
Sensitivity and selectivity	Fluorescent probes permit sensitive and selective detection of many biological molecules.
Multicolour detection	This allows the detection and resolution of multiple targets using fluorescent labels that can be spectrally removed.
Stability	Fluorescently labelled molecules offer several distinct advantages over radio labelled molecules with respect to stability.
Low hazard	Most fluorophores are easy to handle, and in the majority of cases, the simple use of gloves affords adequate protection.
Lower cost	Long shelf life and lower costs for transportation and disposal of fluorophores make fluorescent labelling less expensive than radiolabelling
Environmental sensitivity	Sensitive to the environment

Like any technique there are some (not insurmountable) problems (table 2.4).

Table 2.4: The general problems and solutions in fluorescence imaging (taken from Haugland *et al.*, 2002).

Problem	Possible solution.
Noise (grainy image).	Stronger illumination; better arc lamp; longer exposures; optimising filters and camera; wide-field microscopy; image processing.
Bleaching.	Shorter exposures; weaker illumination; better fluorophores; anti-fading reagents (when appropriate).
Image blurring / background (due to out-of-focus light).	Deconvolution (for weak fluorescence); confocal and two-photon (due to out-of-focus light) microscopy (for imaging thick samples); other special imaging techniques.
Imaging thick samples.	Deconvolution (40 μm); confocal (150 μm), two-photon (500 μm); special low-magnification imaging techniques.

2.3.1 THE FLUORESCENT PROCESS

Fluorescence is a luminescence that is mostly found as an optical phenomenon in cold bodies, where the molecular absorption of a photon triggers the emission of another photon with a longer wavelength. It is the result of a three-stage process that occurs in certain molecules (generally polyaromatic hydrocarbons or heterocycles) called fluorophores, fluorochromes or fluorescent dyes (Haugland *et al.*, 2002 & Evanko, 2005). The process responsible for fluorescence is illustrated by a single electronic state Jablonski diagram (figure 2.9). The energy difference between the absorbed and emitted photons ends up as molecular vibrations or heat. Usually the absorbed photon is in the ultraviolet range, and the emitted light is in the visible range, but this depends on the absorbance curve and Stokes shift (figure 2.10) of the particular fluorophore. Stokes shift is the difference (in wavelength or frequency units) between positions of the band maxima of the absorption and luminescence spectra (or fluorescence) of the same electronic transition.

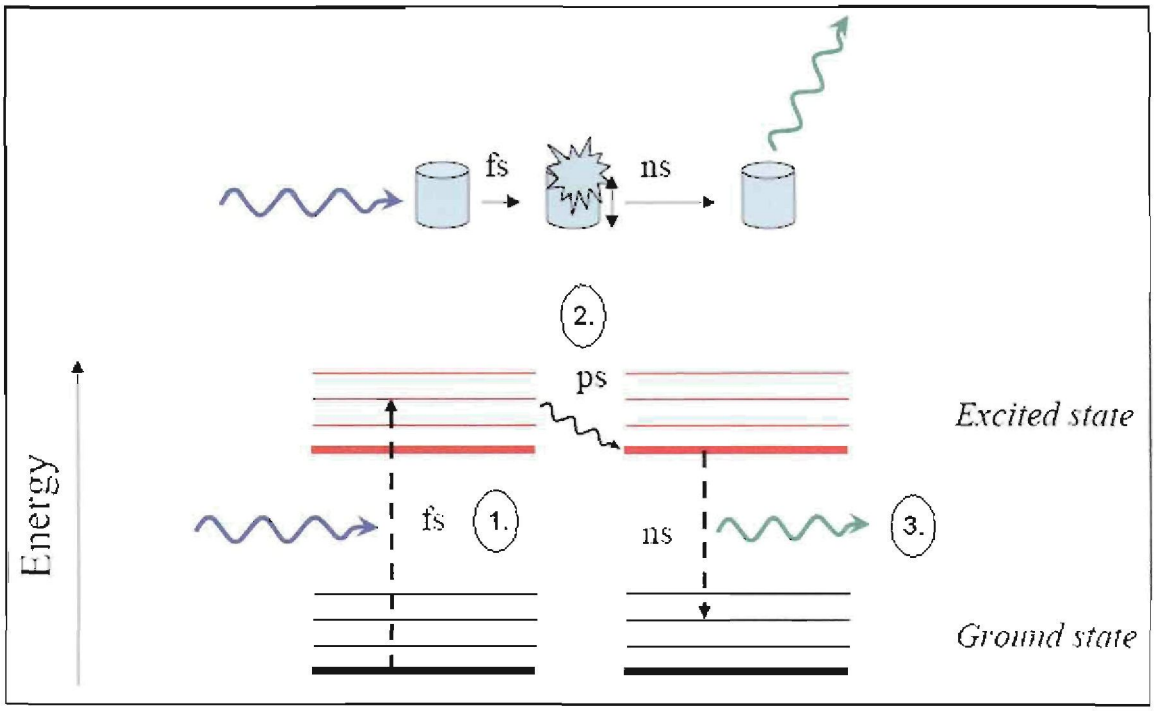

Figure 2.9: The Jablonski diagram: illustrares the processes involved in creating an excited electronic single state by optical absorption and subsequent emission of fluorescence. The three-stage fluorescence process consists of; Stage 1: Excitation; when a photon with a frequency of f and an energy of fs (Berkley, 2005), is supplied by an external source such as a lamp or a laser (Haugland *et al.*, 2002), and absorbed by a fluorophore, it creates a short lived excited electronic single state. Stage 2: Excited-state lifetime; this is a brief period where the excited molecules undergoes an intersystem crossing to the longer lived lowest vibrational energy level. It is from this relaxed single excited state that fluorescence emission originates (Haugland *et al.*, 2002). Stage 3: Fluorescence emission; the fluorophore then returns to the ground state by emission of a photon with energy ns, which varies, depending on what ground state level it returns to (Berkley, 2005).

The Stokes shift occurs because the molecule loses a small amount of the absorbed energy before re-releasing the rest of the energy as luminescence or fluorescence (the so-called Stokes fluorescence), depending on the time between the absorption and the reemission. This energy is often lost as thermal energy (Berkley, 2005).

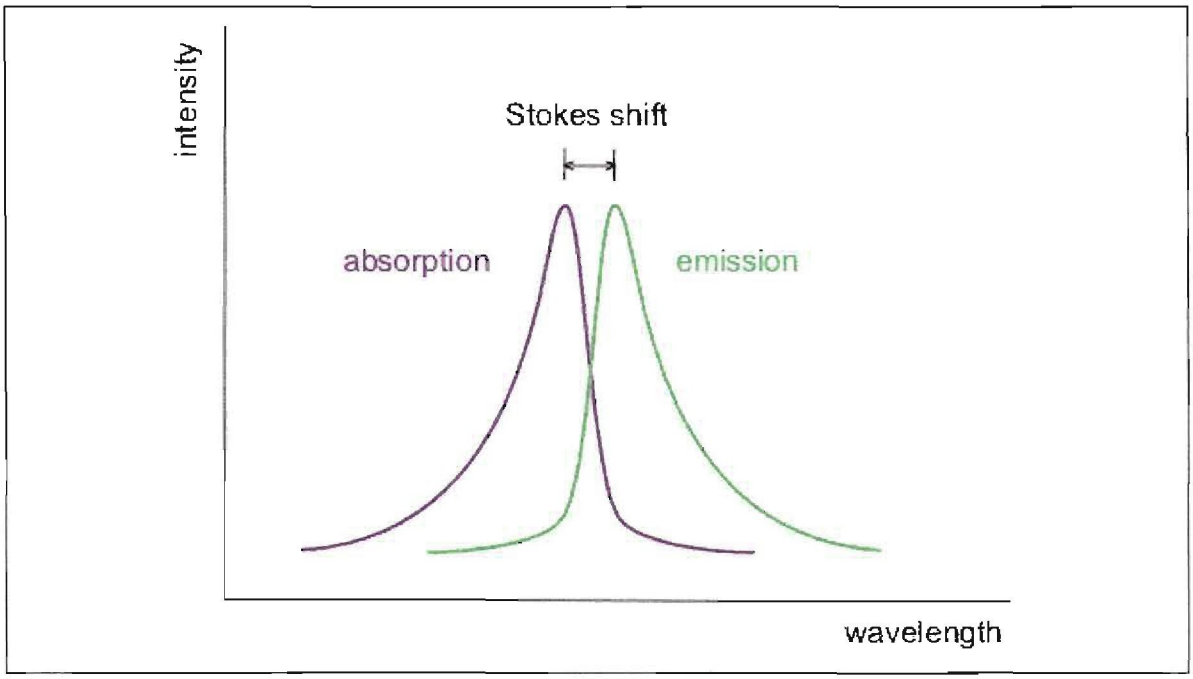

Figure 2.10: Stokes Shift: Stokes shift is the difference (in wavelength or frequency units) between positions of the band maxima of the absorption and luminescence spectra (or fluorescence) of the same electronic transition (Berkley, 2005).

2.4 CHOICE OF FLUORESCENT PROBES

A fluorophore, in analogy to a chromophore, is a component of a molecule which causes a molecule to be fluorescent. It is a functional group in a molecule which will absorb energy of a specific wavelength and re-emit energy at a different (but equally specific) wavelength. The amount and wavelength of the emitted energy depend on both the fluorophore and the chemical environment of the fluorophore (Haugland *et al.*, 2002). Fluorophores currently used as fluorescent probes offer sufficient permutations of wavelength range, Strokes shift and spectral bandwidth to meet requirements imposed by fluorescent instrumentation. A large number of fluorescent probes are available for studies of various cell components and metabolic processes. Fluorescent probes are one of the cornerstones of real-time imaging of live cells and a powerful tool for cell biologists. They can be used to detect specific cellular components, react with environmental conditions, like pH and Ca^{2+} concentration, or be used as enzyme

substrates. They provide high sensitivity and great versatility while perturbing the cell under investigation minimally.

In this study it was decided to incorporate fluorescent structures directly on polycyclic moieties. A series of fluorescent compounds were selected as possible NOS inhibitors to be used as molecular tools capable of providing mechanistic insights into the production of NO. These compounds have structural similarities to 7-NI and it is hypothesised that they could exert NOS inhibitory activity because of this structural correlations and give sufficient fluorescent intensities to study the kinetics of ligand enzyme or ligand receptor interactions by using modern fluorescent techniques.

The indazole, isoindole, anthranilic and dinitrobenzene compounds were selected on the basis of their spectroscopic properties, ease of synthesis and structure activity requirements for NOS activity (table 2.5). Bodipy, dansyl chloride and the indolizine compounds were also considered, but because of structural bulkiness, mainly bodipy, and difficulties in synthesis the idea was excluded, but not discarded for future studies. These compounds could be used as an alternative to radioligand binding studies in nonradioactive assays as it will have a lower cost, lower hazard and better sensitivity.

2.5 FLUORESCENT DETECTION METHODS

Fluorescence illumination and observation is the most rapidly expanding microscopy technique employed today, both in the medical and biological sciences, a fact which has spurred the development of more sophisticated fluorescent microscopes and numerous fluorescence accessories. Although these fluorescent detection methods were not used in this study, it is important to know what imaging techniques are available to detect various cellular components by means of fluorescent imaging for further studies.

Many biological objects are large enough to be seen through a microscope but their optical properties are so similar to the surrounding environment that the optical microscope cannot detect them. When such objects are made fluorescent, they can be readily detected with a fluorescence microscope (Dobrucki, 2003). By using fluorescence microscopy, the precise location of intracellular components labelled with specific fluorophores can be monitored, as well as their associated diffusion coefficients, transport

characteristics, and interactions with other biomolecules. In addition, the dramatic response in fluorescence to localised environmental variables enables the investigation of pH, viscosity, refractive index, ionic concentrations, membrane potential, and solvent polarity in living cells and tissues (Axzelrod *et al.*, 2005).

Table 2.5: Fluorescent compounds as possible NOS inhibitors.

Indazole-3-carboxylic acid 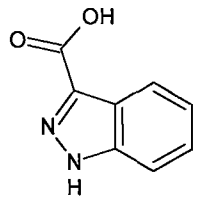	N-methylantranilic acid 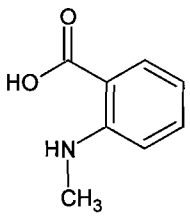	1-cyanoisoindole 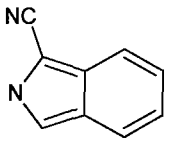
1-tiocyanoisoindole 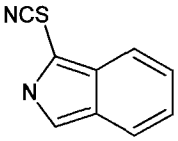	1-nitrocyanoisoindole 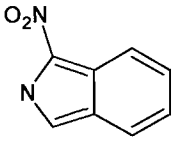	indolizine carboxilic acid 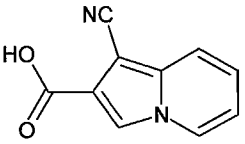
indolizine carboxilic acid 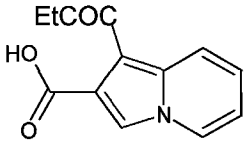	Dansyl chloride 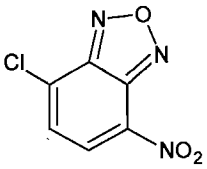	Bodipy 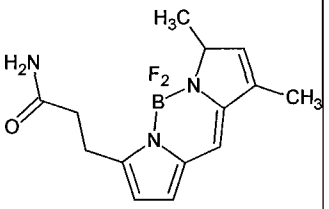

Flow cytometry is a technology that has impacted both basic cell biology and clinical medicine in a very significant manner. The most common detection system in flow cytometry uses fluorescent molecules that are attached to the particle of interest (Gunsekera *et al.*, 2003) or which bind specifically to cellular constituents. Flow cytometry is a means of measuring certain physical and chemical characteristics of cells or particles as they flow in a fluid stream through a beam of light, usually a laser (Robinson, 1993). Flow cytometers can be considered to be specialized fluorescence

microscopes and flow cytometer is made up of three main systems: fluidics, optics, and electronics. The key advantage of flow cytometry is that a very large number of particles can be evaluated on each and every cell.

The confocal laser scanning microscope (CLSM) has contributed to many fields of contemporary biomedical research and enhanced the display of biological information in a most aesthetically pleasing manner (Paddock, 2002). Confocal microscopes are capable of observing selected thin layers of a thick specimen placed under the microscope. As a result, confocal images have significantly less fluorescence blur and out-of-focus light and resolution as well as contrast is improved. The CLSM produces optical sections by using a focused laser beam to scan the specimen (Paddock, 2002) and series of confocal sections can be combined into a three-dimensional image (Dobrucki, 2003). In CLSM a laser beam or an arc-discharge serves as light source and is then focused by an objective lens into a small focal volume within a fluorescent specimen. A mixture of emitted fluorescent light as well as reflected laser light from the illuminated spot is the recollected by then objective lens. A beam splitter separates the light mixture by allowing only the laser light to pass through and reflecting the fluorescent light into the detection apparatus. After passing a pinhole the fluorescent light is detected by a photo-detection device transforming the light into an electrical signal which is recorded by a computer (Dobrucki, 2003).

Multi-photon fluorescent microscopy (MPFM) is probably the most important development in fluorescence microscopy since the introduction of confocal imaging in the mid-1980's. It provides researchers with unique possibilities when imaging deep into live tissues and carrying out experiments over extended periods of time (Gu *et al.*, 1994). In 1-photon fluorescence excitation, a single photon has sufficient energy to excite the fluorescence molecule from ground state to an excited state. The excited molecule then relaxes to a state from which it decays back to ground state with the emission of a longer wavelength photon. In MPFM excitation, 2 or more photons, which individually have insufficient energy to excite the fluorescence molecule, interact co-operatively to achieve excitation (Gu *et al.*, 1994; Abdulatif *et al.*, 1998). MPFM operates with a different principle from the conventional single photon confocal microscopy in that conventional confocal microscope uses pinholes to achieve optical sectioning capability. In a two-

photon fuorescence microscope, owing to the quadratic dependence of the intensity of two photon induced fuorescence on the excitation input, the fuorescence emission drops off rapidly on either side of the focal point, thereby generating an optical sectional view at that point. The localisation of the fuorescence around the focal point gives two-photon fluorescence microscopy its intrinsic depth resolution (Gu *et al.*, 1994). A laser beam is raster scanned across a focal plane within the labelled specimen, and fluorescence is detected by a photomultiplier tube to produce a digital image on a computer.

The fluorescent microscope have become an important instrument in the field of biology and medicine, opening the doors for more advanced microscope designs, such as the confocal laser scanning microscope (CLSM) and the multi-photon fluorescent microscope. CLSM is a valuable tool for obtaining high resolution images and three-dimentional reconstructions. The key feature of confocal microscopy is its ability to produce blur-free images of thick specimens at various depths, but photobleaching and photodamage are unfortunate drawbacks. Multiphoton microscopy is still in its early stages but it is set to become a major new technique in biological microscopy. It features attractive advantages over confocal microscopy for imaging living cells and tissues. Multiphoton microscopy seems to be the fluorescent imaging technique of choice but costs, expensiveness, commercial unavailability and complexity of use limits its application. Confocal microscopy became a standard technique toward the end of the 1980s and is still the fluorescent imaging technique of choice for most researches.

2.6 CONCLUSION

Nitric oxide synthase (NOS) is a target system where fluorescent techniques and fluorescently labelled NOS inhibitors can be used as molecular tools capable of providing mechanistic insights into the production of NO. For this study we thus attempted to identify a series of fluorescent structures with high affinity for the NOS enzyme that may be utilised for further *in vitro* and *in vivo* studies using modern imaging techniques. The fluorescent compounds selected has structural similarities to 7-nitroindazole (a relatively selective nNOS inhibitor) and include indazole-3-carboxylic acid, N-methylanthranilic acid, 1-fluoro-2,4-dintirobenzene and various isoindoles, that will be conjugated to polycyclic structures. These compounds, especially the indazole and isoindole

compounds could have potential as useful pharmacological tools to investigate enzyme-ligand interactions in the quest for more effective neuroprotective strategies.

This could also lead to a greater insight into the neuroprotective mechanism and a possible cure/treatment for neurodegenerative disorders.

CHAPTER 3
SYNTHETIC PROCEDURES

3.1 STANDARD EXPERIMENTAL PROCEDURES

3.1.1 INSTRUMENTATION

NUCLEAR MAGNETIC RESONANCE SPECTROSCOPY (NMR): ^{1}H and ^{13}C NMR spectra were obtained using a Varian Gemini 300 spectrometer at a frequency of 300.075 MHz and 75.462 MHz, respectively. This was done in a 7 Tesla magnetic field and tetramethylsilane (TMS) was used as internal standard. A bandwidth of 1000 MHz at 24 kG was applied for ^{1}H-^{13}C-decoupling. All chemical shifts are reported in parts per million (ppm) relative to the signal from TMS ($\delta = 0$) added to an appropriate deuterated solvent. The following abbreviations are used to describe the multiplicity of the respective signals: s – singulet, bs – broad singulet, d – doublet, dd – doublet of doublets, t – triplet, q – quartet and m – multiplet. Spectra of selected compounds are included in annexure 1.

MASS SPECTROSCOPY (MS): The MS spectra were recorded on an analytical VG 70-70E mass spectrometer using electron ionisation (EI) at 70 eV techniques. Relevant spectra are included in annexure 1.

INFRARED SPECTROSCOPY (IR): IR spectra were recorded on a Nicolet Magna – IR 550 spectrometer. Samples were applied either as film or incorporated in KBr pellets. Relevant spectra are included in annexure 1.

MELTING POINT (MP) DETERMINATION: Melting points were determined using a Stuart SMP-10 melting point apparatus and capillary tubes. The melting points are uncorrected.

3.1.2 CHROMATOGRAPHIC TECHNIQUES

THIN LAYER CHROMATOGRAPHY (TLC): Analytical TLC was performed on 0.20 mm thick aluminium silica gel sheets (Alugram® SIL G/UV_{254}, Kieselgel 60, Macherey-Nagel, Düren, Germany). Visualisation was achieved using UV light (254 nm and 366 nm), an ethanol solution of ninhydrin or iodine vapours, with mobile phases prepared on a volume-to-volume basis using the Prism model of Nyiredy *et al.* (1985).

COLUMN CHROMATOGRAPHY: Product mixtures were purified using standard glass columns varying in size. Flash column chromatography was applied to some of the mixtures. The stationary phase used was silica gel (0.063 – 0.200 mm/70 – 230 mesh ASTM, Macherey-Nagel, Düren, Germany) with mobile phases as indicated for each compound.

3.2 SYNTHESIS OF SELECTED COMPOUNDS

The well-described Cookson's diketone, pentacyclo[5.4.0.$0^{2,6}$.$0^{3,10}$.$0^{5,9}$]undecane-8,11-dione, was synthesised according to the published method (Cookson *et al.*, 1958, 1964). The reaction involved Diels-Alder adduct formation and subsequent photocyclisation to yield the polycyclic cage structure. Figure 3.1 gives a schematic representation of the synthetic route that was followed. This structure served as primary basis in all further synthetic preparations.

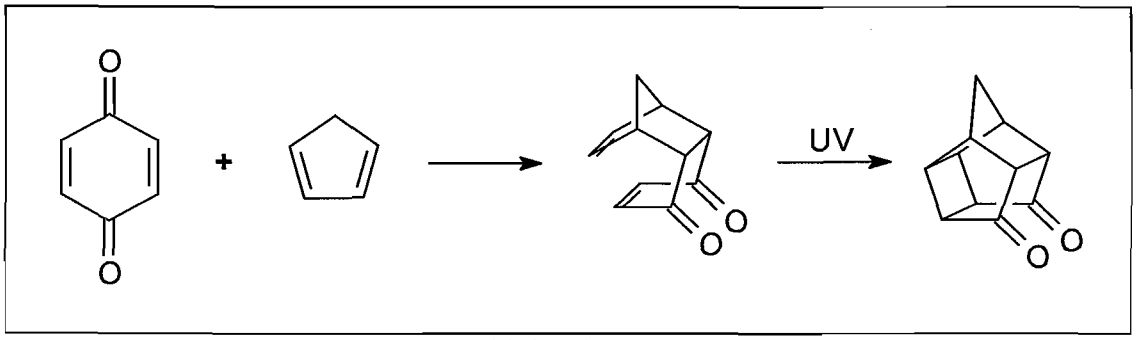

Figure 3.1: Synthesis of pentacyclo[5.4.0.$0^{2,6}$.$0^{3,10}$.$0^{5,9}$]undecane-8,11-dione.

3.2.1 GENERAL APPROACH – ESTERIFICATION AND ETHERFICATION

3-Amino-1-propanol was to be applied as a linker between pentacyclo[5.4.0.$0^{2,6}$.$0^{3,10}$.$0^{5,9}$] undecane-8,11-dione and the relevant drug conjugated to it. Instead of the intermediate imine forming following Dean-Stark dehydration, a rearranged cage structure was obtained where an oxyginane ring had formed on C-8 (figure 3.2). The OH group of this structure was used to react the rearranged cage compound with the carboxylic acid groups of indazole-3-carboxylic acid and *N*-methylanthranilic acid, respectively. This was achieved by activating the carboxylic acid groups of *N*-methylanthranillic acid with *N,N'*-carbodiimidazole (CDI) and indazole-3-carboxylic acid with *N,N'*-dicyclohexylcarbodiimide (DCC). These activated structures reacted with the OH group on the "cage" compound to form the respective esters. NGP-101 was synthesised by reductive amination. It is included in this series because of the polycyclic structure.

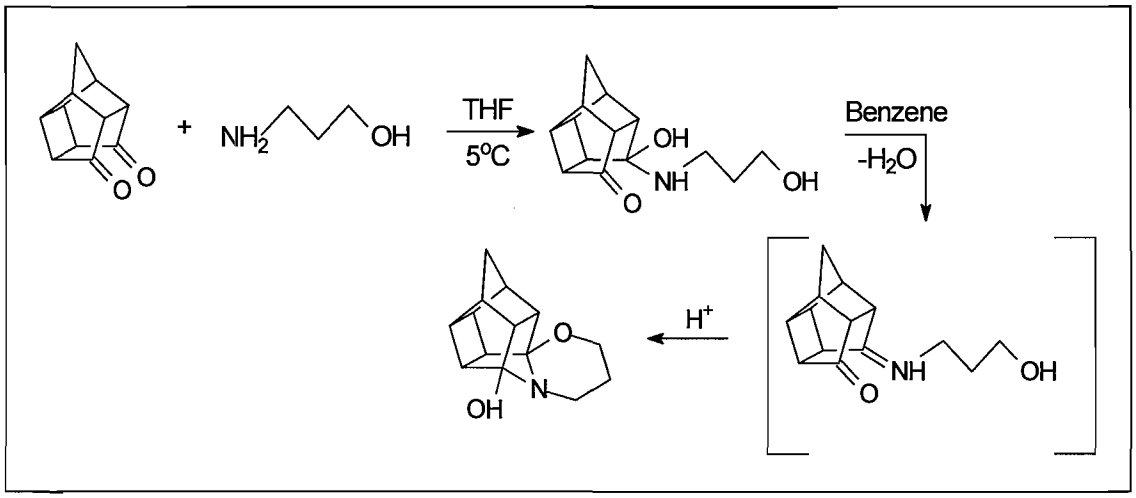

Figure 3.2: Synthetic route of the rearranged cage structure.

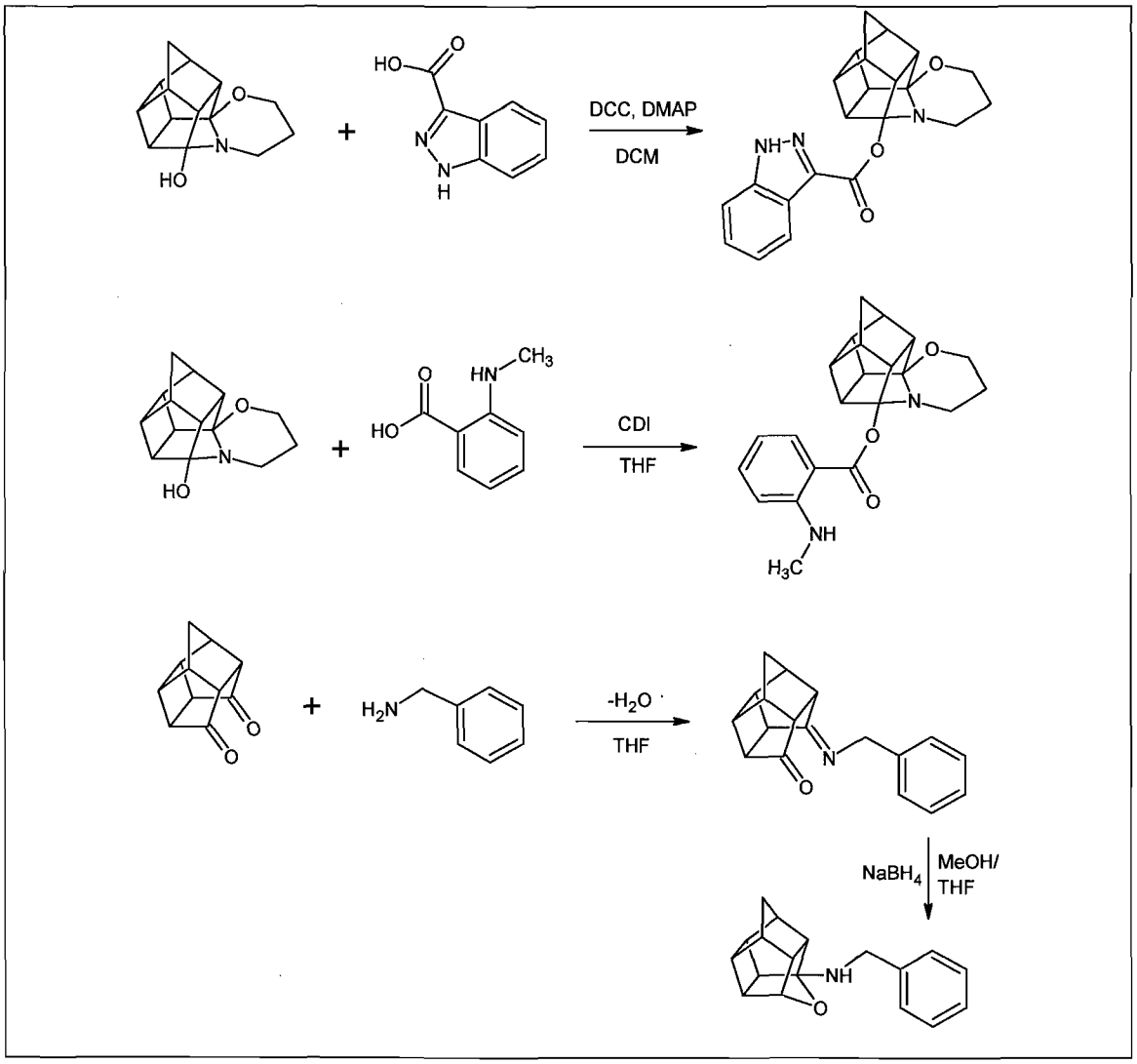

Figure 3.3: Synthetic pathway for the ester compounds of the selected fluorescent derivatives and NGP-101.

3.2.2 GENERAL APPROACH – AMINATION OF AMANTADINE

The amine group of amantadine.HCl was reacted with the activated carboxylic acid groups of indazole-3-carboxylic acid and *N*-methylanthranilic acid using activation chemistry. *N,N'*-dicyclohexylcarbodiimide (DCC) was used as activating agent for indazole-3-carboxylic acid and *N,N'*-carbodiimidazole (CDI) for *N*-methylanthranilic acid. 1-fluoro-2,4-dinitrobenzene was reacted with the amine of amantadine.HCl to afford the secondary amine compound. Furthermore, the three indole structures were

conjugated to the amine group of amantadine.HCl by reacting *o*-phtaldialdehyde in the presence of a catalytic amount of sodiumcyanide, sodiumtiocyanide or sodiumnitrate. This formed the three isoindole compounds.

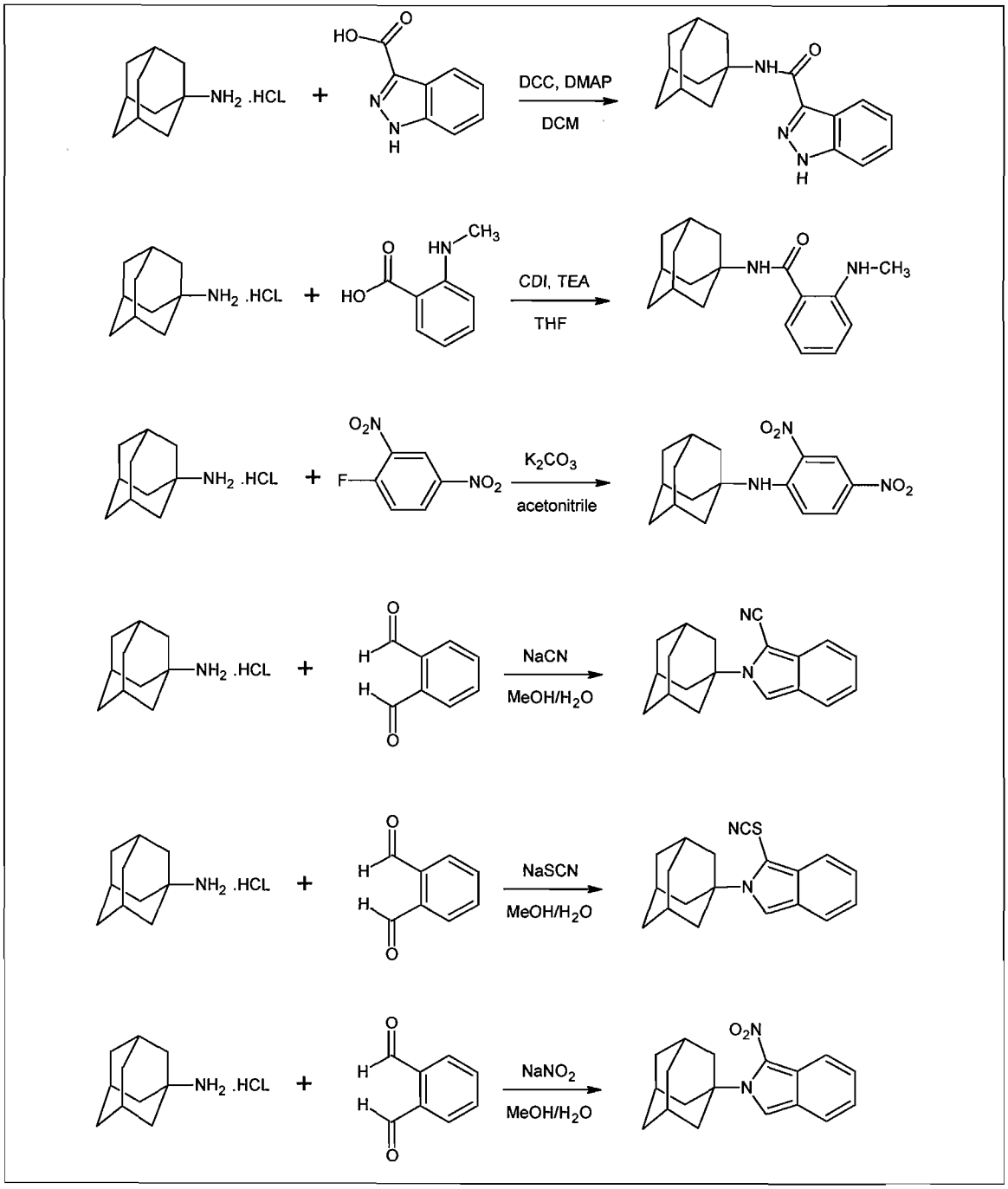

Figure 3.4: Synthesis of the amide and amine fluorescent compounds using amantadine.HCl. (TEA = Triethylamine).

3.2.3 PENTACYCLO[5.4.0.0^{2,6}.0^{3,10}.0^{5,9}]UNDECANE-8,11-DIONE

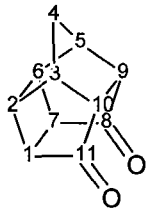

Synthesis: *p*-Benzoquinone (10 g, 9.25 mmol) was dissolved in dried benzene (400 ml) and oxidised with MnO_2 (50 mg) by refluxing the mixture for 20 minutes. The reaction mixture was protected from light by means of aluminium foil. Activated charcoal was added and the mixture allowed to reflux for a further 5 minutes. This was done in order for fine impurities to be absorbed from the reaction mixture. The hot mixture was vacuum-filtered through Celite® to produce a clear yellow solution. Recrystallisation of the freshly oxidised *p*-benzoquinone was suppressed by flushing the same filtering system with dried methanol (100 ml). This solution was cooled down to 5 °C by placing it on an external ice bath. Freshly monomerised cyclopentadiene (12.23 g, 9.25 mmol) was slowly and stoichiometrically added keeping the reaction temperature between 5 °C and 18 °C. The reaction was monitored by means of TLC and presumed complete as soon as the *p*-benzoquinone spot was no longer visible on the TLC plate. The photolabile reaction mixture was removed from the external ice bath, protected from light and stirred for 1 hour at room temperature. Thereafter activated charcoal was added and the mixture stirred at room temperature for a further 30 minutes. Removal of the activated charcoal, followed by *in vacuo* evaporation of benzene resulted in the formation of an intensely coloured amber oil. Excess solvent was allowed to fully evaporate in a dark fume hood to afford the yellow Diels-Alder adduct crystals. The crystals were dissolved in ethyl acetate (4 g per 100 ml) and irradiated with UV light for 6 hours, using a photochemical reactor. Decolouration of the solution indicated that cyclisation of the adduct was complete. Evaporation of the solution afforded a light yellow residue, which was purified by Soxhlett extraction in cyclohexane to produce the cage compound as fine white crystals (Yield: 13 g, 7.471 mmol, 80.80 %). The physical characteristics of these crystals correlated with that in Cookson *et al.* (1958, 1964).

3.2.4 3-HYDROXY-4-AZA-8-OXOHEPTACYCLO[9.4.1.$0^{2,10}$.$0^{3,14}$.$0^{4,9}$.$0^{9,13}$.$0^{12,15}$] TETRADECANE

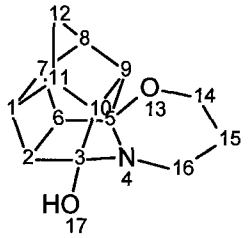

Synthesis: Pentacyclo[5.4.$0^{2,6}$.$0^{3,10}$.$0^{5,9}$]undecane-8,11-dione (3 g, 17.24 mmol) was dissolved in 30 ml of tetrahydrofuran and cooled down to 5 °C while stirring in an ice bath. 3-amino-1-propanol (1.105 ml, 17.22 mmol) dissolved in 6 ml THF, was added slowly with continued stirring of the reaction mixture at 5 °C. The carbinolamine started precipitating after approximately 15 min, but the reaction was allowed to reach completion for an additional 30 min. Water was removed from the reaction mixture azeotropically by refluxing it in 60 ml dry benzene using a Dean-Stark apparatus for 1 h or until no water was collected in the trap. The benzene was removed under reduced pressure and the rearranged cage structure, a yellow oil, was crystallised from THF to render the final product as a colorless crystalline solid (Yield: 3 g, 12.99 mmol, 75.33 %).

Physical data: $C_{14}H_{17}NO_2$; **mp:** 170-172 °C; **^{1}H NMR** (300 MHz, $CDCl_3$) δ_H (Spectrum 1): 4.97-3.94 (bs, 1H, H-17), 3.85-3.74 (m, 2H, H-14a, 14b), 3.73-3.67 (m, 2H, H-16a, 16b), 3.02-2.53 (3 x m, 8H, H-1, 2, 6, 7, 8, 9, 10, 11), 1.80:1.52 (AB-q, 2H, *J* = 10.58 Hz, H-12a, 12b), 1.75-1.55 (m, 2H, H-15a, 15b); **^{13}C NMR** (75 MHz, $CDCl_3$) δ_C (Spectrum 2): 101.45 (2 x s, C-3, 5), 62.69 (t, C-14), 54.97 (d, C-6), 53.14 (d, C-2), 45.73 (d, 1C), 44.63 (d, 1C), 44.00 (d, 1C), 42.92 (d, 1C), 42.41 (t, C-16), 41.67 (t, C-12), 41.48 (d, 1C), 41.01 (d, 1C), 24.33 (t, C-15); **MS** (EI, 70 eV) *m/z* (Spectrum 3): 231 (M^+), 174, 151, 139, 91, 41, 28; **IR** (KBr) ν_{max} (Spectrum 4): 3446, 1484, 1346, 1320, 1166 cm^{-1}.

3.2.5 3-{4-AZA-8-OXO-HEPTACYCLO[0.4.1.$0^{2,10}$.$0^{3,14}$.$0^{4,9}$.^{09,13}.$0^{12,15}$] TETRADECYL}-1*H*-INDAZOLE-3-CARBOXYLATE (1)

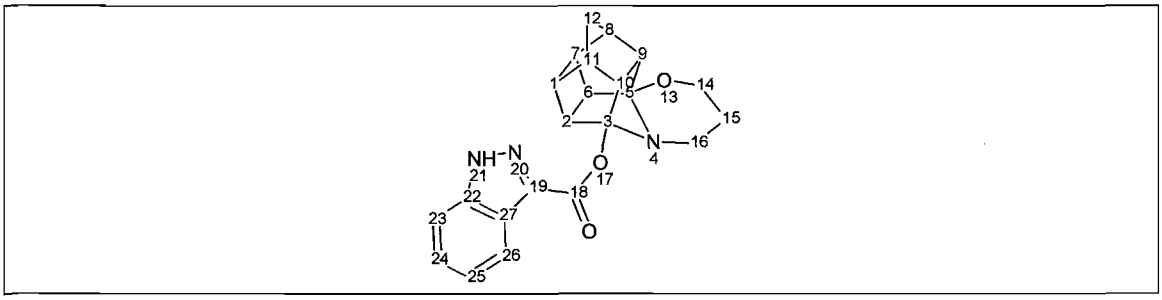

Synthesis: 1*H*-indazole-3-carboxylic acid (0.702 g, 4.323 mmol), 3-hydroxy-4-aza-8-oxoheptacyclo[9.4.1.$0^{2,10}$.$0^{3,14}$.$0^{4,9}$.$0^{9,13}$.$0^{12,15}$]tetradecane (0.702 g, 4.32 mmol) and dimethylaminopyridine (0.09 g, 0.737 mmol) was dissolved in dried dichloromethane (40 ml). The mixture was cooled down to 5 °C using an external ice bath. *N,N'*- dicyclohexylcarbodiimide (DCC; 1.5 g, 7.27 mmol) was added in molar excess and stirred for an additional 5 min at 5 °C. Thereafter the mixture was stirred for 48 hours at room temperature. After 48 hours the solvents were removed *in vacuo* and the residue suspended in 50 ml water, extracted with DCM (3 x 25 ml) and dried over $MgSO_4$. The solvents were removed and yielded a colourless oil. Resolution of the product mixture was accomplished by three column chromatography steps, two of those with (EtOAc:DCM:PE, 1:1:1), and one with (EtOH:THF, 1:1, Rf = 0.69), yielding the product as a white powder (Yield: 255 mg, 0.68 mmol, 16 %).

Physical data: $C_{22}H_{21}N_3O_3$; **mp:** 190 °C; **^{1}H NMR** (300 MHz, $CDCl_3$) δ_H (Spectrum 5): 8.14-8.11 (dd, 2H, J = 8.19, 0.89 Hz, H-23), 7.70-7.67 (dd, 2H, J = 8.38, 0.94 Hz, H-26), 7.42-7.36 (m, 3H, H-24), 7.26-7.21 (m, 3H, H-25) 3.89-3.09 (2 x m, 4H, H-14a, 14b, 16a, 16b), 2.95-2.62 (3 x m, 8H, H-1, 2, 6, 7, 8, 9, 10, 11), 2.89-2.87 (d, 2H, H-26a, 26b), 1.89-1.12 (2 x m, 4H, H-12a, 12b, 15a, 15b); **^{13}C NMR** (75 MHz, $CDCl_3$) δ_C (Spectrum 6): 163.47 (s, C-18), 140.97 (s, C-19), 139.37 (m, C-25), 127.06 (s, C-27), 123.93 (m, C-26), 122.64 (m, C-24), 121.66 (d, C-23), 110.74 (s, C-3,5), 56.14 (t, C-14), 49.96 (2 x d, C-2, C-6), 49.12 (t, C-16), 49.12 (d, 2C), 33.89 (s, C-20), 30.94 (q, C-8), 24.90 (t, C-15); **MS** (EI, 70 eV) *m/z* (Spectrum 7): 375 (M^+), 243, 224, 145, 98, 56, 41, 28; **IR** (KBr) ν_{max} (Spectrum 8): 3277, 2931, 2851, 2360, 1625, 1448, 1242cm^{-1}.

3.2.6 3-{4-AZA-8-OXO-HEPTACYCLO[0.4.1.$0^{2,10}$.$0^{3,14}$.$0^{4,9}$.$0^{09,13}$.$0^{12,15}$]TETRA DECYL}-2-(METHYLAMINO)BENZOATE (2)

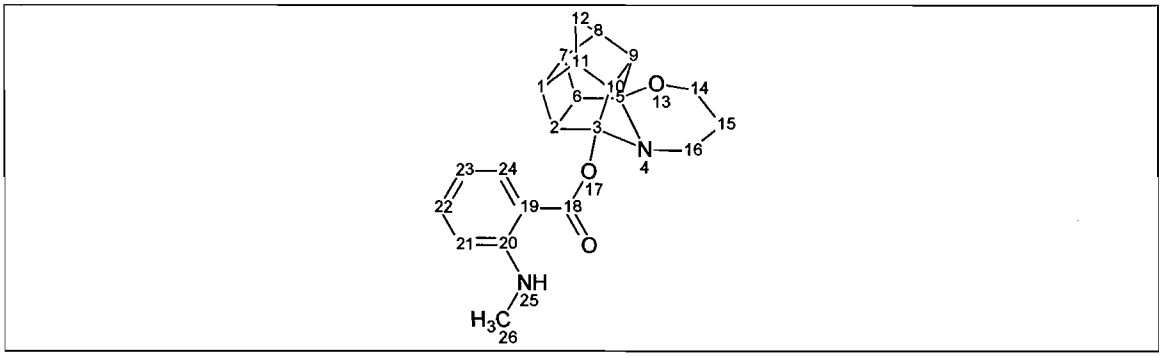

Synthesis: *N*-Methylanthranilic acid (0.390 g, 2.583 mmol) was added to a stirred solution of *N,N'*-carbonyldiimidazole (0.421 g, 2.583 mmol) in anhydrous tetrahydrofuran (25 ml). After 24 hours 3-Hydroxy-4-aza-8-oxoheptacyclo[9.4.1.$0^{2,10}$.$0^{3,14}$.$0^{4,9}$.$0^{9,13}$.$0^{12,15}$]tetradecane (0.6 g, 2.583 mmol) in tetrahydrofuran (10 ml) was added and the mixture was allowed to react for 72 hours at room temperature. The precipitate was filtered and washed with cold THF (2 x 15 ml) yielding the product as a light yellow powder (Yield: 336 mg, 0.82 mmol, 36 %).

Physical data: $C_{22}H_{24}N_2O_2$; **mp:** 213 °C; **^{1}H NMR** (300 MHz, $CDCl_3$) δ_H (Spectrum 9): 7.91-7.90 (dd, 2H, J = 9.58, 1.14 Hz, H-24), 7.38–7.24 (m, 3H, H-22), 6.64-6.61 (dd, 2H, J = 8.27, 0.79 Hz, H-21), 6.57–6.51 (m, 3H, H-23), 3.89–3.094 (2 x m, 4 H, H-14a, 14b, 16a, 16b), 2.95 -2.62 (3 x m, 8H, H-1,2,6,7,8,9,10,11), 2.89 -2.87 (d, 2H, J = 5.99 HZ H-26a, 26b), 1.81 – 1.50 (2 x m, 4H, H-12a, 12b, 15a, 15b); **^{13}C NMR** (75 MHz, $CDCl_3$) δ_C (Spectrum 10): 166.60 (s, C-18), 152.23 (s, C20), 134,75 (d, C-22), 131.93 (d, C-24), 114.29 (d, C-23), 110.68 (d, C-21), 109.74 (s, C-3,5), 63.05 (t, C-14), 55.52 (2 x d, C-2, C-6), 43.93 (d, 2C), 43.91 (t, C-16), 43.88 (t, C-12), 29.46 (q, C8), 24.00 (t, C-15); **MS** (EI, 70 eV) *m/z* (Spectrum 11): 364 (M^+), 231, 230, 214, 134, 69, 43; **IR** (KBr) ν_{max} (Spectrum 12): 3377, 2957, 2360, 1687, 1520, 1343, 1226, 1180 cm^{-1}.

3.2.7 8-BENZYLAMINO-8,11-OXAPENTACYCLO[5.4.0^{2,6}.0^{3,10}.0^{5,9}] UNDECANE (3)

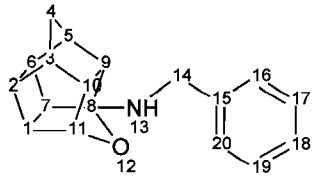

Synthesis: Pentacyclo[5.4.0^{2,6}.0^{3,10}.0^{5,9}]undecane-8,11-dione (5 g, 21.64 mmol) was dissolved tetrahydrofuran (50 ml) and cooled down to 5 °C while stirring in an ice bath. Benzylamine (3.2 g, 29.9 mmol) was added slowly, with continued stirring of the reaction mixture at 5 °C. The carbinolamine started precipitating after approximately 10 min, but the reaction was allowed to reach completion for an additional 20 min. The carbinolamine was isolated by filtration. Water was removed from the reaction mixture azeotropically by refluxing it in 60 ml dry benzene using a Dean-Stark apparatus for 1 h or until no water collected in the trap. The benzene was removed under reduced pressure and the Schiff base, 8-benzyliminopentacyclo[5.4.0^{2,6}.0^{3,10}.0^{5,9}]undecane-11-one, a yellow oil, was dissolved in a mixture of anhydrous methanol (30 ml) and anhydrous THF (150 ml). Without any purification a reduction was carried out by adding sodium borohydride (2 g, 52.8 mmol) in excess and stirring the mixture overnight (18 hours) at room temperature. The solvents were removed in vacuo, the residue was suspended in water (100 ml) and extracted with dichloromethane. The combined organic fractions were washed with water (2 x 100ml), dried over anhydrous magnesium sulphate and evaporated in *vacuo* to yield a yellowish oil. Resolution of the product mixture was accomplished by flash column chromatography (PE: EtOAc: DCM, 1:1:1, R_f = 0.63). Crystallisation from absolute ethanol rendered the final product as a colourless crystalline solid (Yield: 3.00 g, 11.32 mmol, 39.02 %).

Physical data: $C_{18}H_{19}NO$; **mp:** 78 °C; **^{1}H NMR** (300 MHz, $CDCl_3$) δ_H (Spectrum 13): 7.34–7.188 (m, 5H, H – 16, 17, 18, 19, 20), 4.67 (t, 1H, J = 5,20 Hz, H–11), 4.034 (ABq, 2H, J_{AB} = 16.72 Hz, H–14a, 14b), 2.86–2.40 (3 x m, 8H, H–1, 2, 3, 4, 5, 6, 7, 9, 10), 2.27 (bs, 1H, NH), 1.90–1,518 (Abq, 2H, J = 10.65 Hz, H–4a,b) **^{13}C NMR** (75 MHz, $CDCl_3$) δ_C (Spectrum 14): 140.82 (s, C-15), 128,37 (c, C-16, 20), 127.89 (d, C-17,19), 126.83 (d, C-18), 82.47 (d, C-11), 55.24 (d, C-7/9), 54.82 (d, C-7/9), 47.68 (t, C-14), 44.89 (d, 1C),

44.86 (d, 1C), 44.607 (d, 1C), 43.26 (t, C-4), 43, 19 (d, 1C), 42.02 (d, 1C), 41,57 (d, 1C); **MS** (EI, 70 eV) *m/z* (Spectrum 15): 265 (M^+), 237, 186, 131, 91, 65, 28. **IR** (KBr) ν_{max} (Spectrum 16): 3313, 2971, 2858, 1451, 1299, 1010, 731 cm^{-1}.

3.2.8*N*-ADAMANTAN-1-*YL*-1*H*-INDAZOLE-3-CARBOXAMIDE (4)

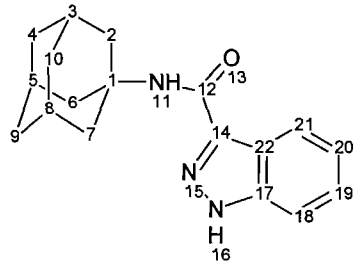

Synthesis: To a solution of 1H-indazole-3-carboxylic acid (0.3g, 1.85 mmol) in DMF (7 mL) was added in one portion *N,N'*-carbonyldiimidazole (0.33 g, 2.035 mmol). The resulting solution was warmed at 60 °C for 2 hours and then cooled to room temperature before adding a solution of amantadine.HCL (0.280 g, 1.85 mmol) in DMF (3 ml) and triethylamine (0.77 ml). The resulting solution was reacted for 24 hours at room temperature. Thereafter the precipitate was filtered and washed with cold THF (2 x 15 ml), yielding the product as a white amorphous solid. (Yield: 288 mg, 0.768 mmol, 41.5 %).

Physical data: $C_{18}H_{21}N_3O$; **mp:** 212 °C **^{1}H NMR** (300 MHz, $CDCl_3$) δ_H (Spectrum 17): 8.14-8.11 (dd, 2H, J = 8.39, 0.89 Hz, H-23), 7.70-7.67 (dd, 2H, J = 8.72, 0.92 Hz, H-26), 7.42-7.36 (m, 3H, H-24), 7.26-7.21 (m, 3H, H-25), 2.10 (s, 3H, H-3, 5, 7), 2.02-2.00 (d, 6H, J = 2.96 Hz, H-2a, 2b, 8a, 8b, 9a, 9b), 1.70-1.65 (m, 6H, H-4a, 4b, 6a, 6b, 10a, 10b); **^{13}C NMR** (75 MHz, $CDCl_3$) δ_C (Spectrum 18): 156.45 (s, C-12), 127.06 (s, C-22), 123.16 (m, C-21), 122.63 (s, C-19), 111.26 (d, C-18), 51.59 (s, C-1), 48.27 (3 x t, C-2, 8, 9), 34.75 (3 x t, C-3, 5, 7), 28.99 (3 x d, C-4, 6, 10); **MS** (EI, 70 eV) *m/z* (Spectrum 19): 295 (M^+), 238, 135, 91, 43, 28; **IR** (KBr) ν_{max} (Spectrum 20): 3459, 2911, 2854, 1672, 1493, 1197, 856 cm^{-1}.

3.2.9 *N*-ADAMANTAN-1-YL-2(METHYLAMINO)BENZAMIDE (5)

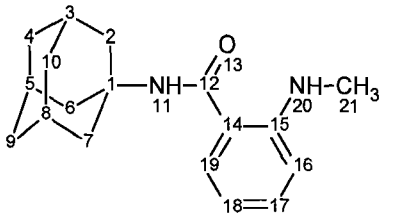

Synthesis: *N*-Methylanthranilic acid (0.5 g, 3.308 mmol) was added to a stirred solution of *N,N'*-carbonyldiimidazole (0.53 g 3.308 mmol) in anhydrous tetrahydrofuran (25 ml). After 24 hours amantadine.HCL (0.5 g, 3.308 mmol) in tetrahydrofuran (10 ml) was added and the pH was adjusted to 8-9 with triethylamine. The mixture was allowed to react overnight at room temperature. After 74 hours the reaction mixture was heated to ensure complete reaction. The precipitate was filtered and washed with cold THF (2 x 15 ml) yielding the product as a light yellow powder (Yield: 336 mg, 0.82 mmol, 25 %).

Physical data: $C_{18}H_{24}N_2O$; **mp:** 213 °C; **^{1}H NMR** (300 MHz, $CDCl_3$) δ_H (Spectrum 21): 7.98-7.96 (dd, 2H, J = 7.48, 0.821 Hz, H-19), 7.49 (bs, 1H, NH), 7.29-7.24 (m, 3H, H-17), 6.60-6.52 (m, 3H, H-18), 6.59-6.57 (dd, 2H, J = 8.43, 1.28 Hz, H-16), 2.85 (d, 3H, C-21), 2.00 (s, 3H, H-3, 5, 7), 1.87 – 1.60 (d, 6H, J = H-2a, 2b, 8a, 8b, 9a, 9b), 1.56-1.47 (m, 6H, H-4a, 4b, 6a, 6b, 10a, 10b); **^{13}C NMR** (75 MHz, $CDCl_3$) δ_C (Spectrum 22): 151.64 (s, C-14), 132.60 (d, C-16), 132.42 (d, C-18), 117.37 (s, C-15) 113.90 (d, C-17), 109.984 (d, C-13), 51.28 (s, C-1), 40.49 (3 x t, C-2, 8, 9), 35.65 (3 x t, C-3, 5, 7), 29.63 (s, C-21), 28.99 (3 x d, C-4, 6, 10); **MS** (EI, 70 eV) *m/z* (Spectrum 23): 284 (M^+), 151, 135, 94, 41, 28; **IR** (KBr) ν_{max} (Spectrum 24): 3338, 2924, 1635, 1454, 1172, 848, 755 cm^{-1}.

3.2.10*N*-(2,4-DINITROPHENYL)ADAMANTAN-1-AMINE (6)

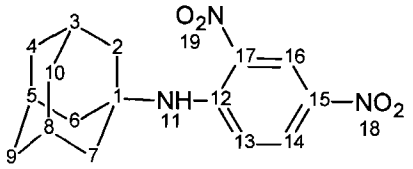

Synthesis: 1-Fluoro-2,4-dinitrobenzene (0.707 ml, 2.5 mmol), amantadine.HCl (0.378 g, 2.5 mmol) and K_2CO_3 (0.691 g, 5 mmol) was dissolved in 50 ml absolute acetonitrile. The pH was adjusted to 8-9 with triethylamine. The reaction mixture was stirred in the dark for 48 hours, where after the mixture was filtered, and the precipitate extracted with DCM (3 x 25 ml) and dried over $MgSO_4$. The solvent was removed *in vacuo* rendering the product as a bright yellow powder (Yield: 403 mg, 1.268 mmol, 50 %).

Physical data: $C_{16}H_{19}N_3O_4$; **mp:** 300 °C; **^{1}H NMR** (300 MHz, $CDCl_3$) δ_H (Spectrum 25): 9.13-9.12 (d, 2H, J = 2.77 Hz, H-16), 8.18-8.13 (dd, 3H, J = 3.40, 1.18 Hz, H-14), 7.25-7.23 (d, 2H, J = 9.80 Hz, H-13), 2.21 (s, 3H, H-3, 5, 7), 2.12-2.11 (d, 6H, J = 2.96 Hz, H-2a, 2b, 8a, 8b, 9a, 9b), 1.76-1.75 (m, 6H, H-4a, 4b, 6a, 6b, 10a, 10b), 1.55 (bs, 1H, NH); **^{13}C NMR** (75 MHz, $CDCl_3$) δ_C (Spectrum 26): 147.76 (s, C-13), 135.39 (s, C-15), 129.17 (d, C-16), 124.86 (d, C-17), 116.20 (s, C-12), 54.28 (s, C-1), 42.09 (3 x t, C-2, 8, 9), 36.04 (3 x t, C-3, 5, 7), 29.80 (3 x d, C-4, 6, 10); **MS** (EI, 70 eV) *m/z* (Spectrum 27): 317 (M^+), 196, 135, 93, 41, 28; **IR** (KBr) ν_{max} (Spectrum 28): 3439, 2926, 2855, 2360, 1541, 1338, 1146, 831 cm^{-1}.

3.2.11 *N*-(1-CYANO-2*H*-ISOINDOL-2*YL*)ADAMANTAN-1-AMINE (7)

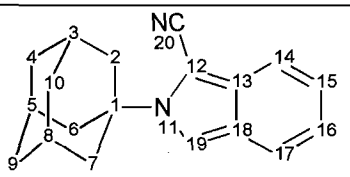

Synthesis: Amantadine hydrochloride (0.5 g, 3.301 mmol) and NaCN (0.162 g, 3.301 mmol) was dissolved in 20 ml methanol/water. To this was added *o*-phtaldialdehyde (0.442 g, 3.301 mmol) and the pH was adjusted to 8-9 with glacial acetic acid. The reaction mixture was protected from light and stirred at room

temperature for 24 hours. The mixture was filtered and resolution with flash column chromatography (EtOAc: PE 1:1, R_f = 0.65) yielded the product as a white amorphous solid (Yield: 338 mg, 1.223 mmol, 37 %).

Physical data: $C_{19}H_{20}N_2$; **mp:** 160 °C; **^{1}H NMR** (300 MHz, $CDCl_3$) δ_H (Spectrum 29): 7.67-7.61 (2 x m, 6H, H-15, 16), 7.48 (s, 1H, H-19), 7.24-7.03 (2 x dd, 4H, J = 7.84, 1.01 Hz; J = 8.64, 0.99 Hz, H-14, 17), 2.44-2.43 (d, 6H, J = 3.19 Hz, H-2a, 2b, 8a, 8b, 9a, 9b) 2.301 (s, 3H, H-3, 5, 7), 1.82-1.80 (m, 6H, H-4a, 4b, 6a, 6b, 10a, 10b); **^{13}C NMR** (75 MHz, $CDCl_3$) δ_C (Spectrum 30): 133.72 (s, C-12), 125.20 (m, C-15), 122.61 (s, C-19), 122.25 (d, C-14), 120.76 (m, C-16), 117.67 (d, C-17) 60.29 (s, C-1), 42.90 (s, C-20), 42.85 (3 x t, C-2, 8, 9), 35.83 (3 x t, C-3, 5, 7), 29.89 (3 x d, C-4, 6, 10); **MS** (EI, 70 eV) *m/z* (Spectrum 31): 276 (M^+), 135, 93, 41, 28; **IR** (KBr) ν_{max} (Spectrum 32): 3446, 2910, 2852, 2360, 1624, 1182, 783 cm^{-1}.

3.2.12 N-(1-THIOCYANO-2*H*-ISOINDOL-2YL)ADAMANTAN-1-AMINE (8)

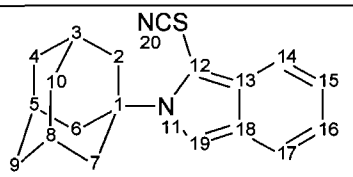

Synthesis: Amantadine hydrochloride (0.5 g, 3.301 mmol) and NaSCN (0.27 g, 3.301 mmol) was dissolved in 20 ml methanol/water. To this was added *o*-phtaldialdehyde (0.442 g, 3.301 mmol) and the pH was adjusted to 8-9 with glacial acetic acid. The reaction mixture was protected from light and stirred at room temperature for 48 hours. The reaction mixture was filtered and resolution with flash column chromatography (EtOAc: PE 1:1, R_f = 0.56) yielded the product as an orange amorphous solid (Yield: 210 mg, 0.68 mmol, 21 %).

Physical data: $C_{19}H_{20}N_2S$; **mp:** 210-215 °C; **^{1}H NMR** (300 MHz, $CDCl_3$) δ_H (Spectrum 33): 7.76 (s, 1H, H-19), 7.74-7.41 (2 x dd, 4H, J = 9.24, 1.88 Hz; J = 13.43, 6.80 Hz, H-14, 17), 7.39-7.24 (2 x m, 6H, H-15, 16), 2.29-2.28 (d, 6H, H-2a, 2b, 8a, 8b, 9a, 9b, J = 20.29, 2.89 Hz), 2.13 (s, 3H, H-3,5,7), 1.79-1.67 (m, 6H, H-4a, 4b, 6a, 6b, 10a, 10b);

^{13}C NMR (75 MHz, $CDCl_3$) δ_C (Spectrum 34): 140.86 (s, C-12), 134.69 (m, C-15), 130.71 (s, C-19), 127.72 (d, C-14), 123.11 (m, C-16), 122.24 (d, C-17), 55.47 (s, C-1), 47.43 (s, C-20), 40.06 (3 x t, C-2, 8, 9), 36.35 (3 x t, C-3, 5, 7), 32.62 (3 x d, C-4, 6, 10); **MS** (EI, 70 eV) *m/z* (Spectrum 35): 307 (M^+), 261, 163, 135, 91, 41, 28; **IR** (KBr) ν_{max} (Spectrum 36): 3139, 2910, 2851, 2190, 1421, 1182, 783 cm^{-1}.

3.2.13 N-(1-NITRO-2*H*-ISOINDOL-2YL)ADAMANTAN-1-AMINE (9)

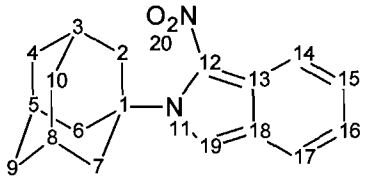

Synthetic method: Amantadine hydrochloride (0.5 g, 3.301 mmol) and $NaNO_2$ (0.27 g, 3.301 mmol) was dissolved in 20 ml methanol/water. To this was added *o*-phtaldialdehyde (0.442 g, 3.301 mmol) and the pH was adjusted to 8-9 with glacial acetic acid. The reaction mixture was protected from light and stirred at room temperature for 72 hours. The reaction mixture was filtered and resolution with flash column chromatography (EtOAc: PE 1:1, R_f = 0.73) yielded the product as a light yellow amorphous solid (Yield: 245 mg, 0.827 mmol, 25 %).

Physical data: $C_{18}H_{20}N_2O_2$; **mp:** 213 °C; **^{1}H NMR** (300 MHz, $CDCl_3$) δ_H (Spectrum 37): 7.82 (s, 1H, H-19), 7.75-7.60 (2 x dd, 4H, J = 8.32, 3.26 Hz; J = 8.24, 2.96, H-15, 16), 7.48-7.24 (2 x m, 6H, H-14, 17), 2.27-2.12 (d, 6H, J = 10.02 Hz, H-2a, 2b, 8a, 8b, 9a, 9b), 2.10 (s, 3H, H-3,5,7), 1.78-1.67 (m, 6H, H-4a, 4b, 6a, 6b, 10a, 10b); **^{13}C NMR** (75 MHz, $CDCl_3$) δ_C (Spectrum 38): 147.76 (s, C-12), 135.389 (m, C-15), 129.17 (s, C-19), 129.17 (d, C-14), 124.95 (m, C-16), 116.14 (d, C-17) 54.23 (s, C-1), 42.07 (3 x t, C-2, 8, 9), 36.08 (3 x t, C-3, 5, 7), 32.46 (3 x d, C-4, 6, 10); **MS** (EI, 70 eV) *m/z* (Spectrum 39): 297 (M^+), 163, 135, 91, 41, 28. **IR** (KBr) ν_{max} (Spectrum 40): 3446, 2906, 1666, 1453, 1221, 730 cm^{-1}.

3.3 CONCLUSION

The compounds were successfully synthesised, resulting in 9 novel fluorescent compounds. The yields of the synthetic procedures ranged from 16 % to 50 %. The lower yields were attributed to the formation of various possible by-products during the synthetic procedure as well as inadequate purification of product mixture during column chromatography. Yields could be improved through optimisation of synthetic procedures and purification techniques as well as further purification of remaining fractions of product mixture after completion of column chromatography. The structures were characterised using the analytical instrumentation and techniques described at the beginning of this chapter. Characteristic signals observed for each specific compound, gave confirmation of their structure. In order to meet the objective of this study, the synthesised compounds were subjected to NOS assays. The results of these studies are discussed in chapter 4.

CHAPTER 4
BIOLOGICAL EVALUATION AND RESULTS

The aim of this study was to design and synthesise a series of novel fluorescent polycyclic derivatives and to evaluate these compounds for neuroprotective activity. It is hypothesised that the novel fluorescent compounds may have the ability to inhibit nitric oxide synthase (NOS), as the compounds selected as fluorescent ligands have structural similarities to 7-nitroindazole, which is reported to be a selective neuronal NOS (nNOS) inhibitor (Handy *et al.*, 1999).

In the biological evaluation, the oxyhemoglobin assay was employed to determine the activity of the novel compounds at an enzymatic level of NOS. This assay is principally based on the reaction of nitric oxide with oxyhemoglobin and the formation of methemoglobin. The slope of the absorption difference between 401 nm and 421 nm versus time is an indication of NOS activity (see chapter 2, section 2.2.4). And from this inhibition data the IC_{50} values were calculated and compared.

4.1 NITRIC OXIDE SYNTHASE DETERMINATION

4.1.1 INTRODUCTION

The nitric oxide synthase (NOS) is an enzyme in the body that contributes to transmission from one neuron to another, to the immune system and to dilating blood vessels. It does so by synthesis of nitric oxide (NO) from the terminal nitrogen atom of L-arginine in the presence of NADPH and oxygen (O_2) (Dawson *et al.*, 1991). Although NO mediates several physiological functions, a number of disease states are associated with either the overproduction or underproduction of NO, making the NOS pathway an attractive target for the development of therapeutics (Martin *et al.*, 2007).

One of the most commonly used methods for detecting NO, is the oxyhemoglobin reaction assay that uses the shift in the optical absorption spectra when oxyhemoglobin reacts with NO in aqueous solution to form methemoglobin. An adapted method

described by Salter and Knowles (1998) was employed for the determination of NOS activity by measuring the conversion of oxyHb to metHb.

Its popularity in very different areas of research is based primarily on its sensitivity and specificity for NO under aerobic conditions, inexpensiveness, ease of implementation and for the most part, rather modest technical requirements.

The method is based on the principal reaction of oxyhemoglobin (oxyHb) with NO to form methemoglobin (metHb) and nitrate (equation 1), a reaction which also accounts largely for the inhibitory effect of hemoglobin on the biological effects of endogenously formed or exogenously applied NO (Feelisch *et al.*, 1996).

$$\mathbf{HbO_2 + NO \longrightarrow metHb + NO_3^-} \quad (1)$$

4.1.2 MATERIALS AND APPLICATIONS

All the materials were purchased from Sigma-Aldrich (UK) and Merck (St. Louis, MO, USA). Spectrophotometric scans were recorded using a Varian Cary-50 UV-Visible spectrophotometer. The slope values were calculated at specific wavelengths and calculated from the inhibition data. All data analysis, calculation and graphs were done using Prism 4.02® (GraphPhad, Sorrento Valley, CA).

4.1.3 ANIMALS

The study protocol was approved by the Ethics Committee for Research on Experimental Animals of the North-West University (Potchefstroom campus). Male Spraque-Dawley rats were sacrificed by decapitation and the brain tissue was removed and kept on ice for homogenation. After homogenation, the alliquoted brain homogenate was snapped freezed with liquid N_2 and stored at -70 °C.

4.1.4 METHODS

HEPES buffer (100 mM) was prepared by dissolving the HEPES in double-distilled or milliQ-grade water and brought to pH 7.4 by the addition of 4 N NaOH at 37 °C. This can be stored for several weeks at 4 °C.

The extraction buffer is firstly prepared by dissolving sucrose (320 mM), HEPES (20 mM), and ethylenediaminetetra-acetic acid (1 mM) in double-distilled or milliQ-grade water and adjusting its pH to 7.4 at room temperature by addition of 10 % HCl (Salter and Knowles, 1998). The following constituents are then added to the final concentrations indicated: 0.1 mM D/L dithiotherol (DTT), 0.5 μM leupeptin, soybean-trypsin inhibitor (10 μg/ml) and aprotin (2 μg/ml). The extraction buffer was then made up to its final volume with distilled water and distributed into aliquots (typically 50 ml per aliquot) and stored at -20 °C until required.

Phenylmethylsulphonyl fluoride (PMSF; 10 mg/ml) is unstable in aqueous solution and is not included in the buffer at this stage, but prepared as a solution in absolute ethanol, stored at -20 °C, and added to the extraction buffer during the extraction procedure. The composition of the extraction buffer is designed to permit extraction of NOS from tissues without breaking intracellular organelles and minimising proteolysis (Dawson and Knowles, 1999).

Extractions and storage of tissue samples prior to the assay were carried out at 0 °C – 4 °C to avoid loss of enzyme activity. Fresh rat brain was weighed in 50 ml pre-cooled Falcon tubes and placed on ice. After rinsing with ice cold extraction buffer, a measured volume of extraction buffer (5 ml/g tissue) was added to the tissue. The sample was then homogenised with a mechanical homogeniser while the temperature was maintained at 4 °C. After 10 seconds of homogenisation the PMSF (10 μM/ml of extraction buffer) was added to the mixture and it was homogenised for a further 30 seconds. The homogenate was then centrifuged at 12 000 x g for 10 minutes. Once the supernatant was collected, it was divided into 2 ml aliquots which were assayed immediately or snapped freezed and stored at -70 °C.

The oxyhemoglobin solution was prepared by carefully dissolving the hemoglobin crystals (25 mg) in 1000 μl of cold HEPES buffer (Feelisch *et al.*, 1996) and subsequent reduction with excess sodium dithionate (0.958 mg). The solution immediately changed from brownish red (mixture of oxyHb and metHb) to a dark red (deoxyhemoglobin) colour after the reductant was added. Oxygenation was carried out by blowing 100 % oxygen over the surface while the solution was gently swirled for 15 minutes. The

gradual colour change from dark red to bright red was indicative of the oxygenation of hemoglobin. Desalting and purification was performed by passing the resulting oxyHb solution through a Sephadex G-25 column. The oxyHb is eluted as a single bright-red band. The front and back edges were discarded.

The concentration of oxyHb was calculated by methods described by Feelisch *et al.*, 1996; Hevel *et al.*, 1991. 10 µl of the oxyHb stock solution was added to 2990 µl of HEPES buffer in a cuvette and the absolute absorbance was determined in triplicate at 415 nm against a blank buffer. The concentration of oxyHb (C_{oxyHb}) was calculated with the following equation (5.2) using a molar extinction coefficient $E_{414(oxyHb)}$ of 131.0 mM^{-1} cm^{-1}.

$$CoxyHb = \frac{A_{415nm} \times 300 \text{ (dilution factor)}}{E_{415(oxyHb)}} \quad (5.2)$$

Using the above equation, the final calculated oxyHb concentration was found to be 0.76 mM. The stock solution was then aliquoted in 200 µl units, snapped freezed with liquid N_2 and stored at -70 °C.

Calcium chloride solution ($CaCl_2$; 12.5 mM), L-arginine (1 mM) and NADPH (5 mM) was prepared in HEPES buffer.

The test compounds were dissolved in HEPES buffer, methanol, tetrahydrofuran or DMSO, the concentration of the organic solvents should not exceed 2 % of the final incubation concentrations because it can't be tolerated in the assay. This gave a series of concentrations in the micro molar range. 7-Nitroindazole was dissolved in methanol and aminoguanidine was dissolved in the HEPES buffer, these two compounds were used as the reference compounds in final concentrations ranging from 10 µM to 10 mM.

Oxyhemoglobin, $CaCl_2$, L-arginine and the test compound was then diluted in the HEPES buffer to give final concentrations 250 µM $CaCl_2$ and 1 mM L-arginine.

The reaction mixture was prewarmed for three minutes to the required assay temperature of 37 °C and the reaction was started by the addition of NADPH and the tissue extract (100 µl) (in the form of rat brain homogenate) with a final NADPH concentration of 100 µM. After establishing the baseline, continuous scans with a scan rate of 600 nm/min

every 10 seconds were recorded between 390 nm and 430 nm. The conversion of oxyHb to metHb was monitored over a period of 10 minutes (figure 4.5).

4.1.5 RESULTS AND DISCUSSION

From the continuous spectrophotometric scans, the slope value of the different spectra between 401 nm and 421 nm were calculated and used as an index to determine NOS activity. Two of the recorded spectra of compound **7** are depicted in figure 4.5 and figure 4.6 and represents the control and 31.25 μM incubations respectively. At 411 nm one can observe the isosbestic point and a gradual increase in absorption at 401 nm with a subsequent decrease at 421 nm. The change in absorption difference between 401 and 421 nm was used as an indication of NOS activity of compound **7**.

A decrease in absorbance at 401 nm is indicative of a decrease in metHb formation and thus a decrease in enzyme activity. Enzyme activity is expressed as the rate at which NO (or metHb) is generated. The resulting slope value of the change in absorbance between two specific wavelengths (e.g. 401 nm and 421 nm) over time is representative of this conversion rate.

From the spectra depicted in figures 4.5 and 4.6, the difference in the change of absorbance (ΔA) between 401 nm and 421 nm versus time was calculated by plotting the ΔA of the respective wavelengths against time (figures 4.7 and 4.8). In order to determine the amount of NO formed, the change in absorbance difference between 401 and 421 nm is measured during the initial linear phase of the reaction. If the change in absorbance at 401 nm is plotted against time and the change in absorbance over time at 421 nm is substracted, the slope of this resulting curve is an indication of the increase in molar amount of metHb, and is identical to the molar amount of NO generated. A decrease in enzyme activity is observed when the slope value of the control was compared to that of the 31.25 μM inhibitor concentration. The slope values of the curves are linear over the first four minutes and can also be used as an indication of NO formation.

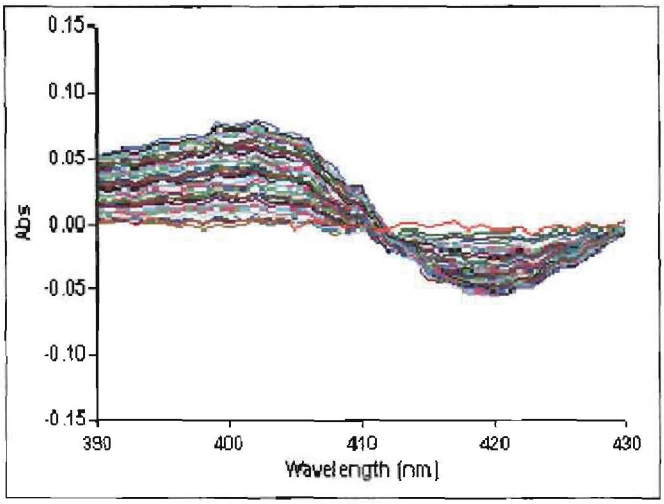

Figure 4.5: This figure is a typical spectrophotometric recording of the control incubation (0 mM inhibitor). Continious scans between 390 nm and 430 nm were performed as the oxyHb was converted to metHb. At 411 nmn one can observe the isosbestic point and a gradual increase in absorption (ΔA) over time at 401 nm with a subsequent decrease at 421 nm.

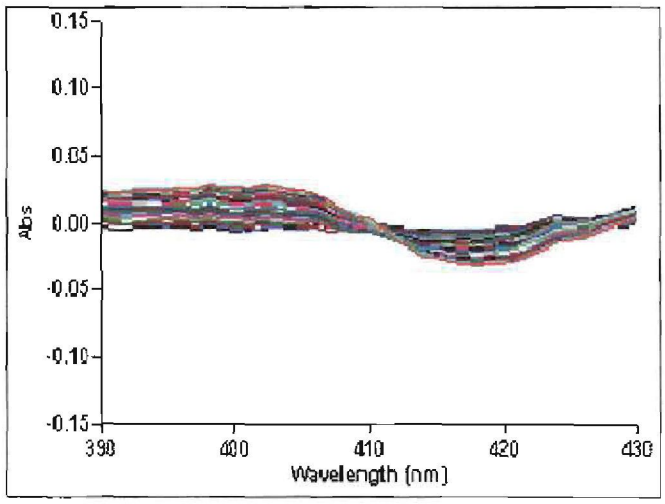

Figure 4.6: Absorbance difference between 401 and 421 nm of compound 7 (31.25 μM final test compound concentration) over a period of 10 minutes. (ΔA = absorbance over time). When compared to the spectra at 0 mM inhibitor (figure 4.5).

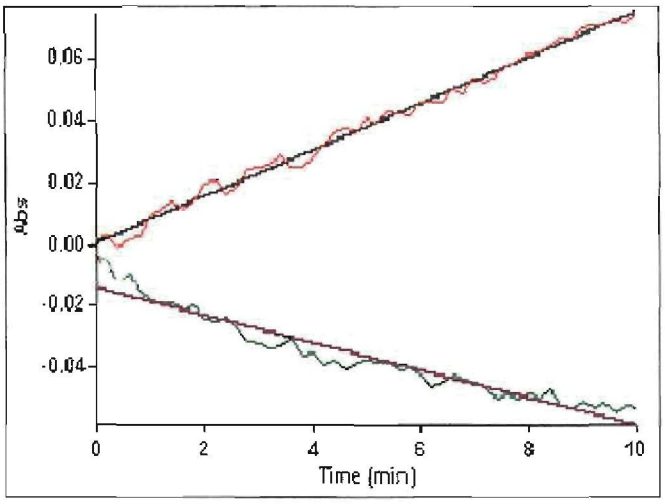

Figure 4.7: Determination of the change in absorbance of the control incubation. (0 mM inhibitor; figure 4.5). The change in absorbance at 401 nm and 421 nm versus time was calculated and the difference of the respective slope values $[(m_{\Delta A(401\ nm)}) - (m_{\Delta A(421\ nm)})]$ gives an indication of enzyme activity.

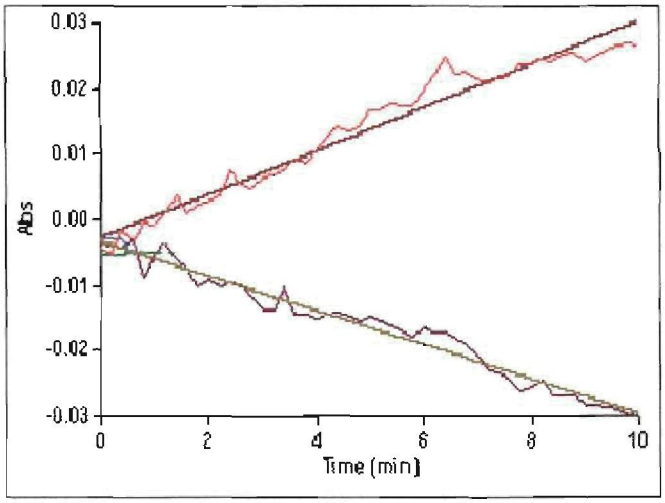

Figure 4.8: Determination of the change in absorbance with compound 7 (31.25 µM inhibitor; figure 4.7). The difference in slope values $[(m_{\Delta A(401\ nm)}) - (m_{\Delta A(421\ nm)})]$ is representative of enzyme activity and in comparison with the control (figure 4.6), indicates a decrease in enzyme activity with the addition of the novel inhibitor.

The inhibition data of a series of concentrations were then plotted on a graph to determine the IC_{50} value. The dose response curve was calculated as an average of two experiments. Each experiment was done in triplicate and data points are the mean values ± the standard error of the mean. In order to compare the NOS activity of the new compounds, all synthesised compounds were tested in this identical procedure. Compounds **1**, **4**, **7**, **8** and

9 showed meaningful IC_{50} values and NOS activity. Compounds **2**, **5** and **6** showed low or no inhibition and compound **3** was not evaluated.

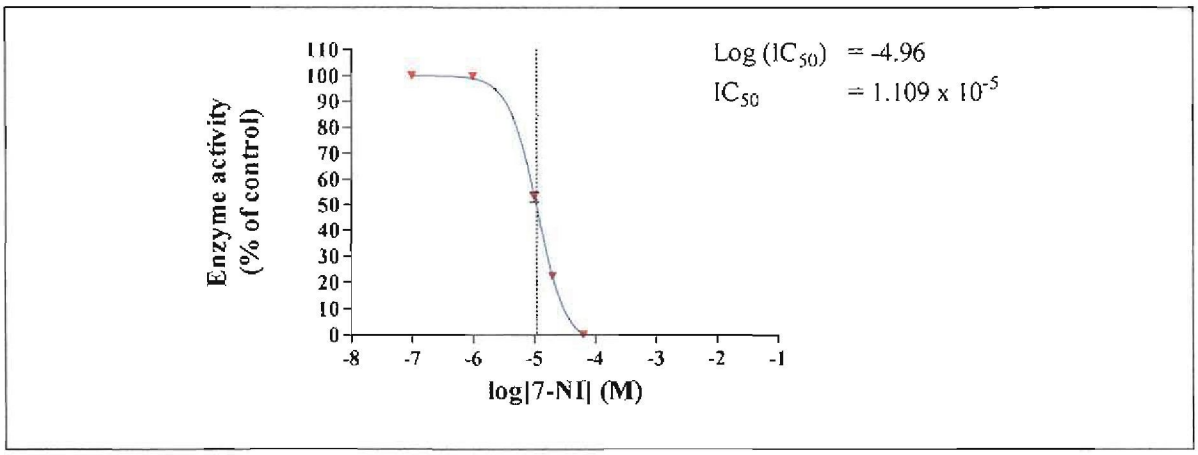

Figure 4.9: Inhibition curve of 7-NI on NOS activity.

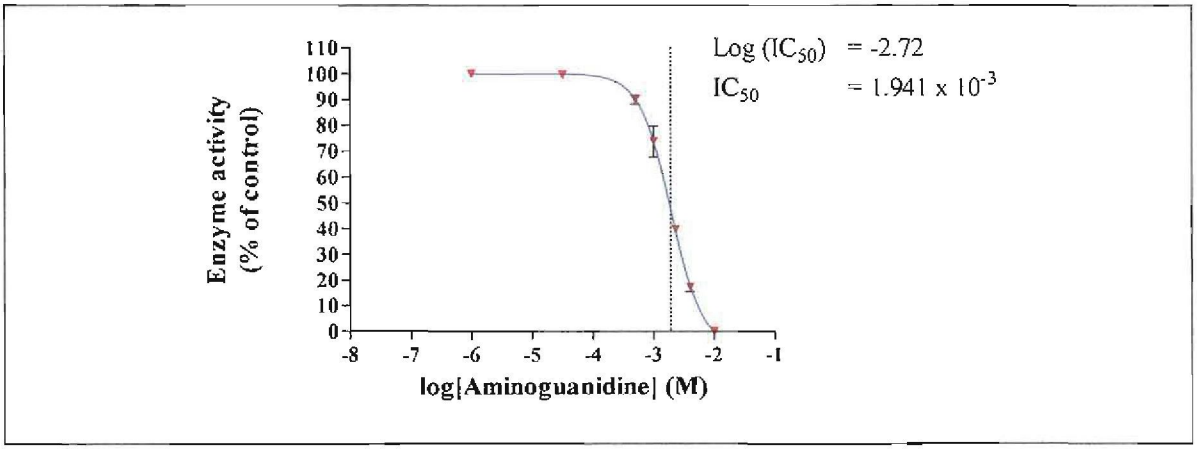

Figure 4.10: Inhibition curve of aminoguanidine on NOS activity.

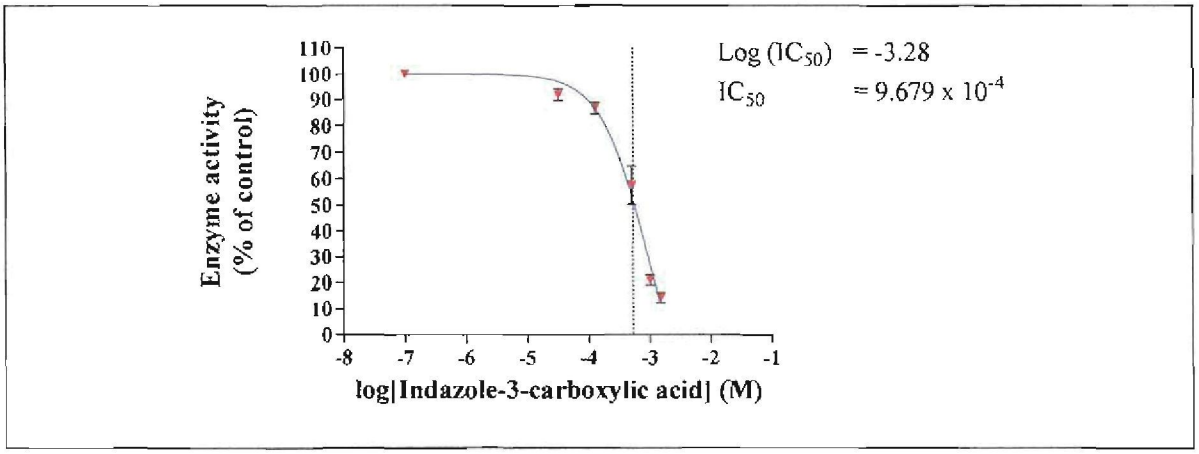

Figure 4.10: Inhibition curve of indazole-3-carboxylic acid on NOS activity.

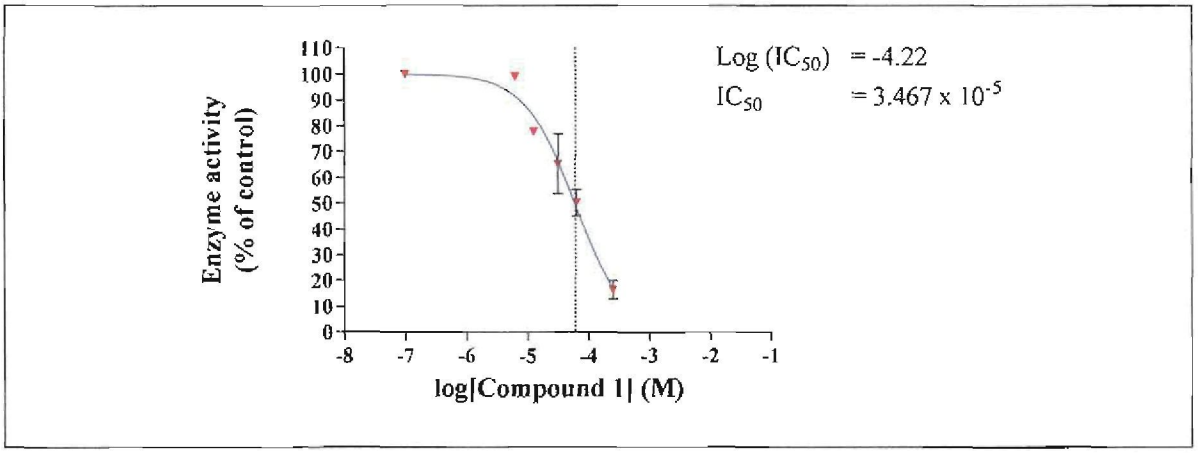

Figure 4.11: Inhibition curve of compound **1** on NOS activity.

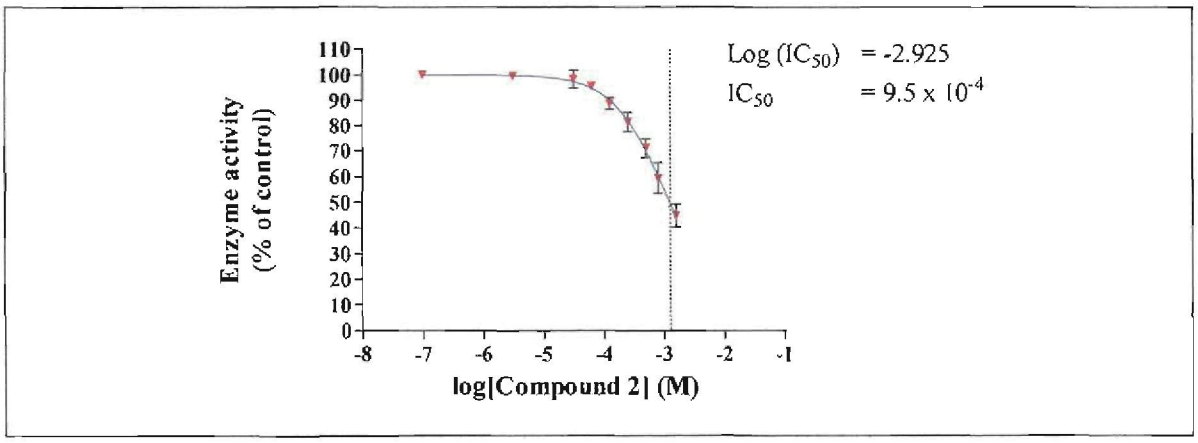

Figure 4.12: Inhibition curve of compound **2** on NOS activity.

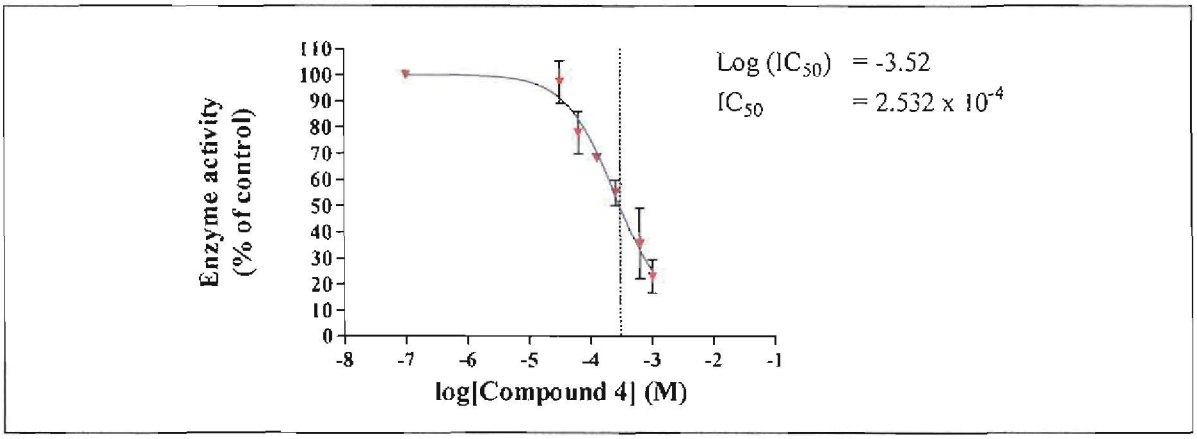

Figure 4.13: Inhibition curve of compound 4 on NOS activity.

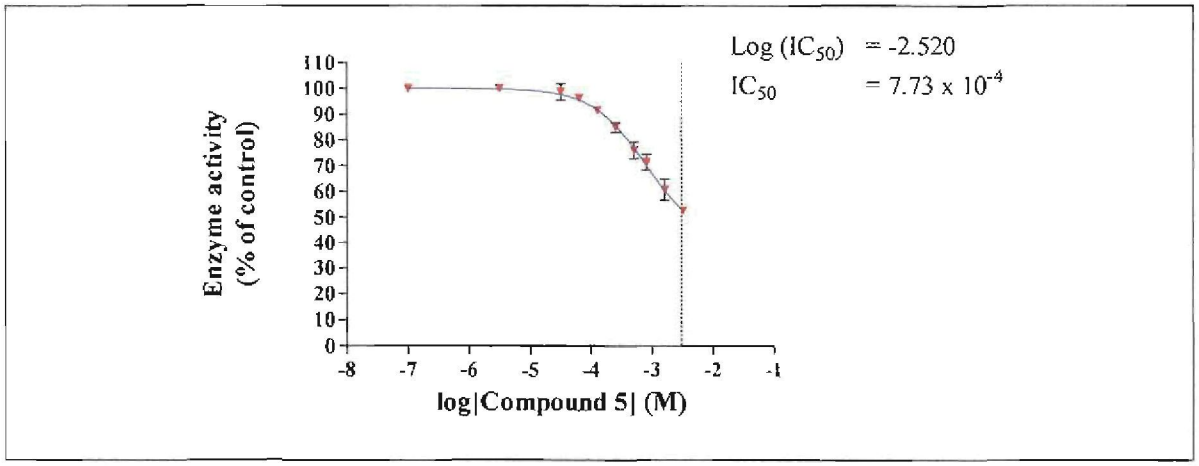

Figure 4.15: Inhibition curve of compound 5 on NOS activity.

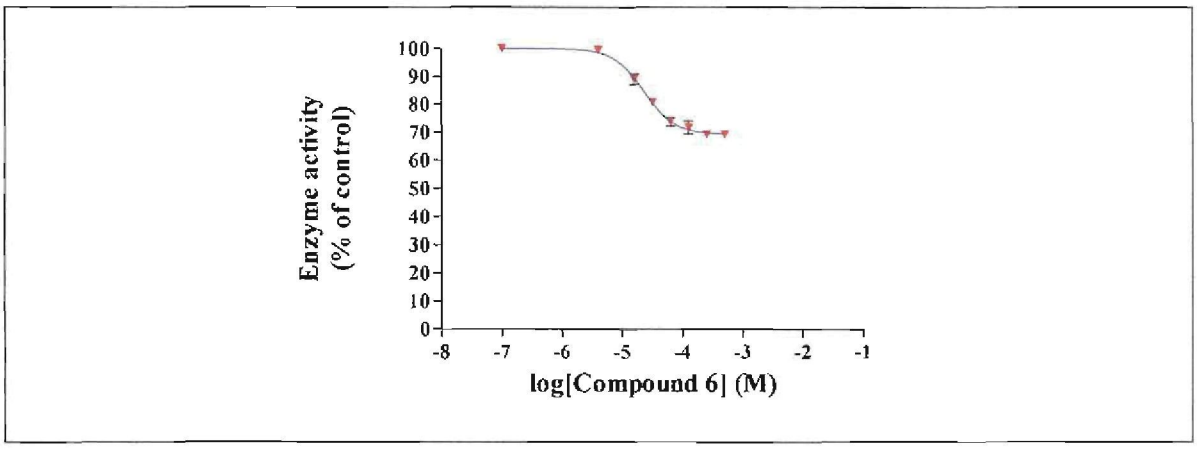

Figure 4.16: Inhibition curve of compound 6 on NOS activity. No IC_{50} values were calculated as the compound only showed 30.64 % inhibition, before solubility problems occurred.

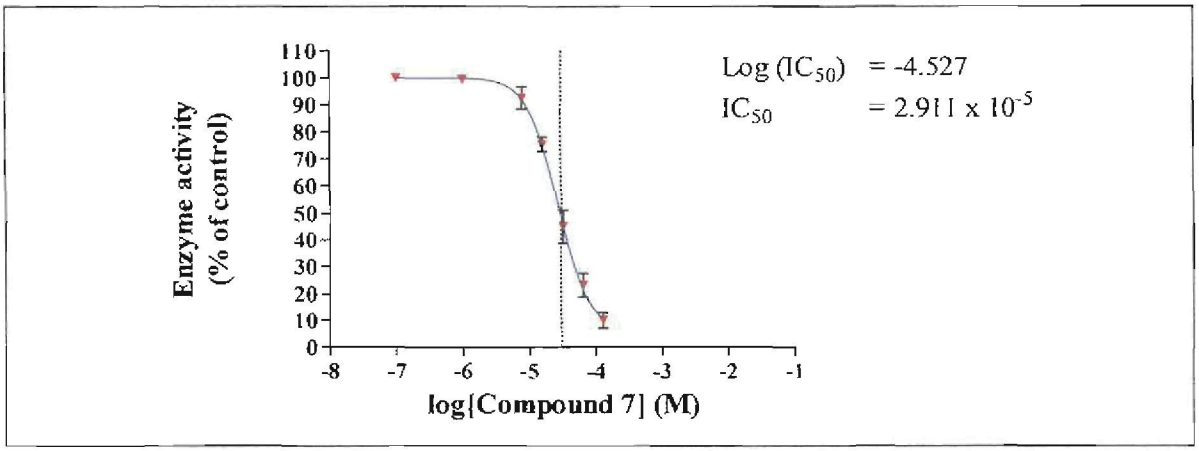

Figure 4.17: Inhibition curve of compound 7 on NOS activity.

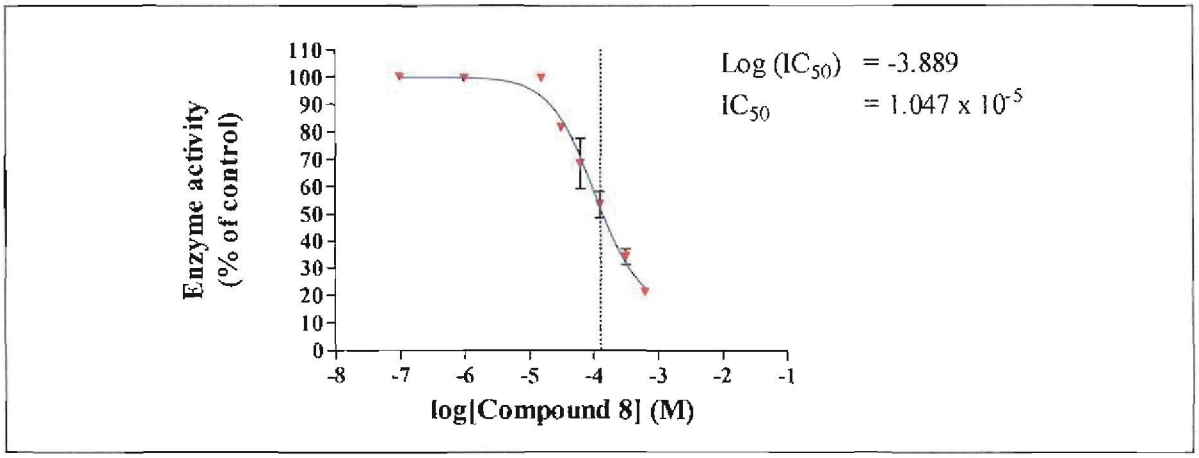

Figure 4.18: Inhibition curve of compound **8** on NOS activity.

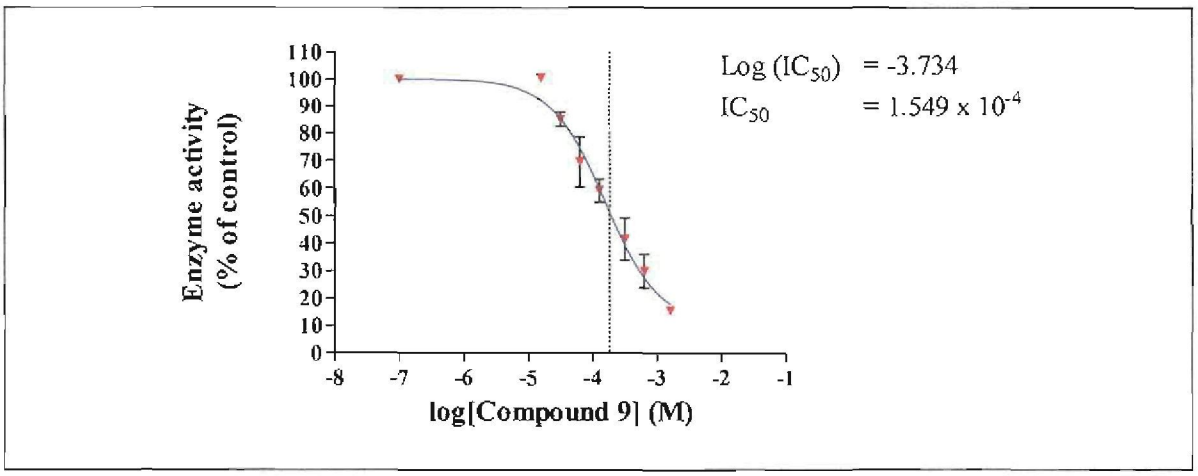

Figure 4.19: Inhibition curve of compound **9** on NOS activity.

The inhibition curves of the selected compounds were then superimposed in a single graph and the calculated IC_{50} values and percentage NOS inhibition were compared (table 5.1 and table 5.2). From the calculated IC_{50} values and percentage NOS inhibition; compounds **1**, **4**, **7**, **8** and **9** revealed promising results as possible NOS inhibitors.

When these compounds are compared to 7-NI (figure 4.20), one can clearly see that none of the structures showed as high activity as 7-NI.

All the compounds however showed more potent inhibitory activity than aminoguanidine (figure 4.20). Aminoguanidine is a selective iNOS inhibitor, and the lower activity observed could, to a certain degree, be attributed to this fact. For future biological evaluations it is thus recommended that the compounds with high inhibitory activities be tested for their isoform selectivity.

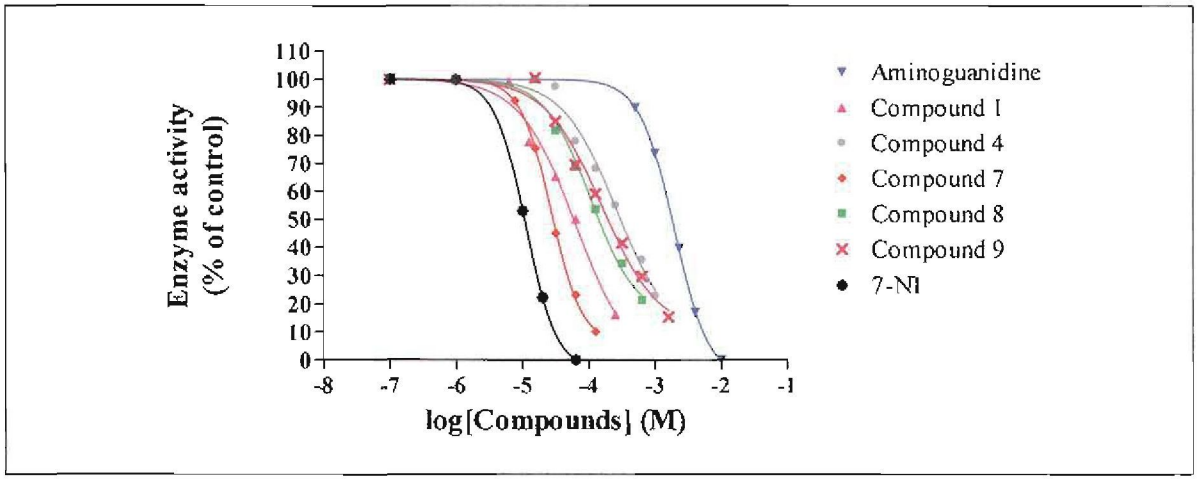

Figure 4.20: Inhibition curves of compounds with meaningful activities are superimposed to compare their IC_{50} values.

Compounds **2**, **5** and **6** showed low or no inhibition of the NOS enzyme when compared to 7-NI and aminoguanidine (figure 4.22). This lower activity may be attributed to the less structural similarity that these compounds have towards 7-NI.

100 % inhibition of NOS could not be obtained for the novel synthesised fluorescent structures as solubility becomes a limiting factor at higher concentrations. Because of these solubility problems the percentage NOS inhibitory activity of the test compounds at various concentrations, are also included in table 4.2.

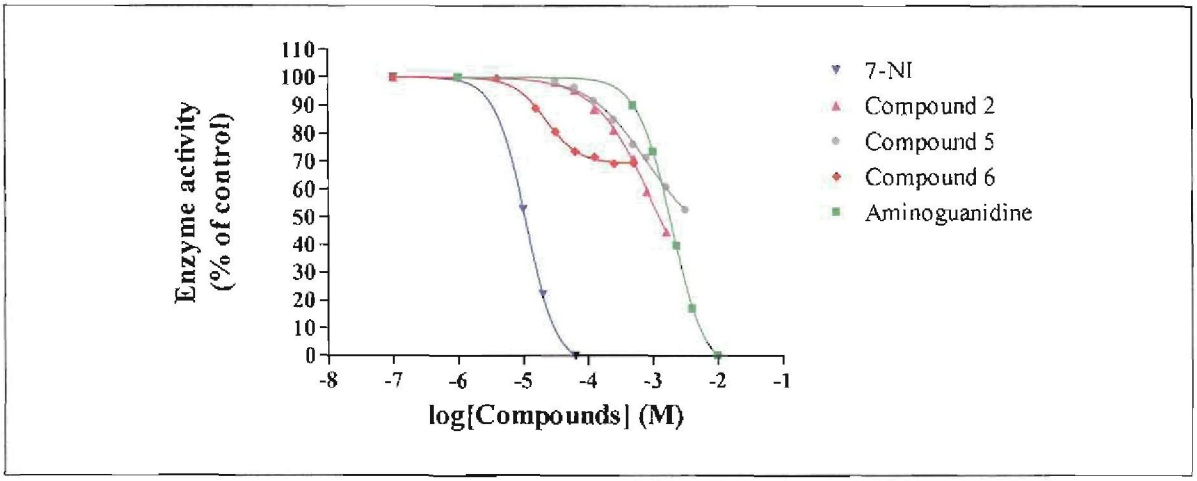

Figure 4.22: Superimposed inhibitory curves of test compounds with low NOS inhibitory activity, with amninoguanidine and 7-NI as reference compounds.

The indazole structures, compounds **1** and **4** showed significant NOS activity compared to aminoguanidine and to 7-NI. Compound **1** has a higher activity than compound **4**, and both of these compounds exhibit better inhibition of the enzyme than the indazole-3-carboxylic acid structure (figure 4.23). This confirms that both the "cage" and the adamantane compounds increase the activity of the indazole structures. As compound **1** has a higher activity, it can be deducted that the "cage" moiety increases the affinity for the NOS enzyme more than the adamatane moiety. The increased activity of the compounds conjugated to the polycyclic structures could be because of the higher lipophilicity and membrane permeability of these compounds.

The 1-cyanoisoindole adamantane compound (7) showed a ten fold increase in activity when compared to the 1-tiocyanoisoindole adamantane and 1-nitrocyanoisoindole adamantane compounds (**8** and **9**) (figure 2.24). It will however be interesting to test these compounds for their isoform selectivity, to determine which functional group on position one would show the best selectivity on the various NOS isoforms.

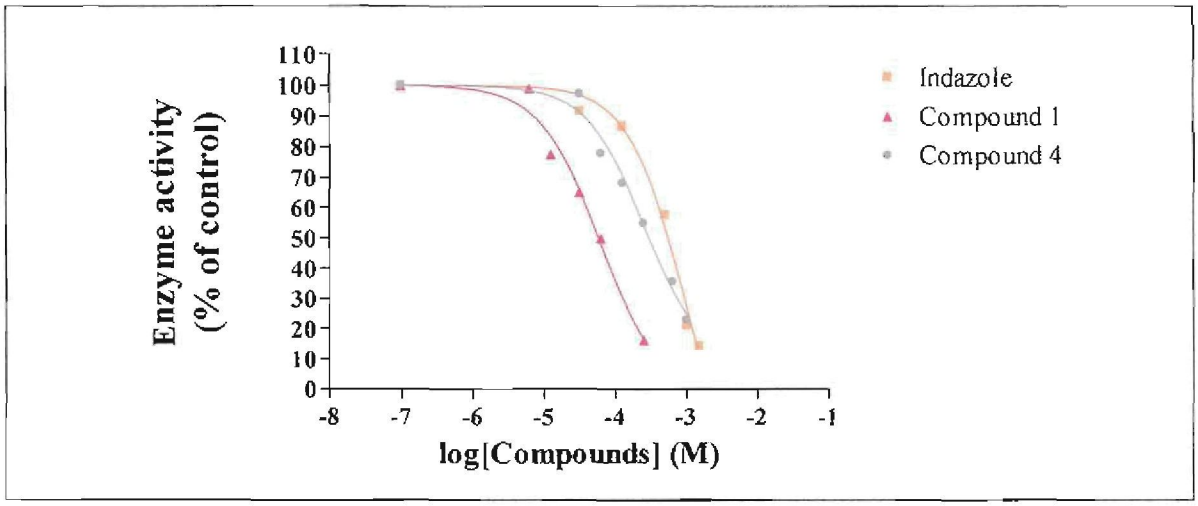

Figure 4.23: Superimposed inhibitory curves of the indazole test compounds, showing the increased activities of the compounds conjugated with the "cage" (**1**) and adamantane (**4**), towards the unconjugated indazole-3-carboxylic acid.

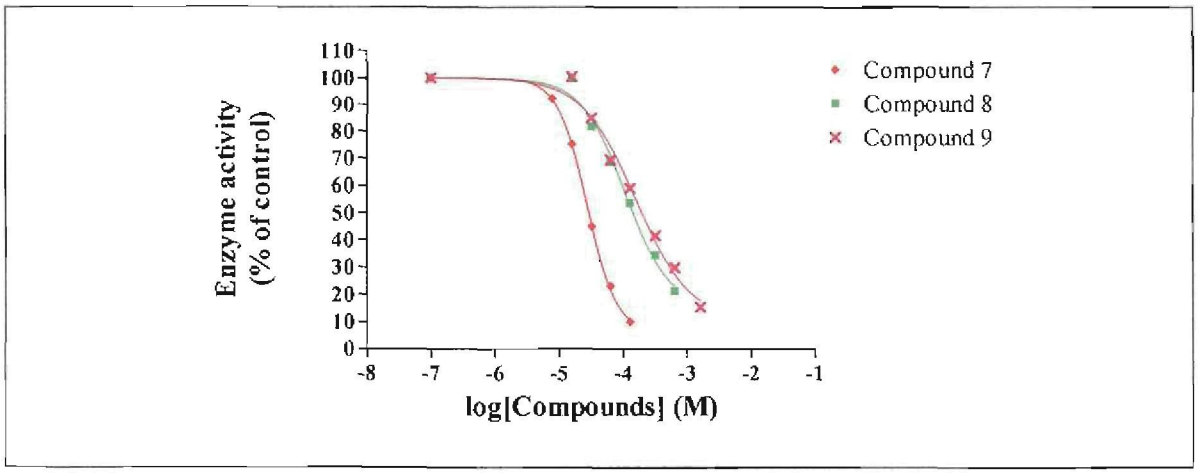

Figure 4.24: Inhibition curves of the isoindole adamantane test compounds, showing the effect of the different functional groups on position 1. The 1-cyanoisoindole structure (**7**) showed a ten fold increase in activity when compared to the 1-tiocyano- and 1-nitrocyanoisoindole compounds (**8** and **9**)

Table 4.1: Test compounds with their IC_{50} values and maximum percentage NOS inhibition.

Structure	Log(IC_{50})	IC_{50}(M)	Maximum % NOS inhibition
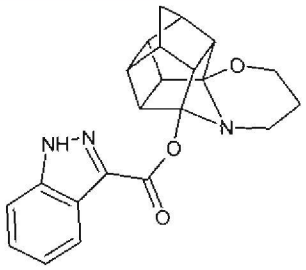 (1)	-4.22	3.467×10^{-5}	83.73% at 250 μM
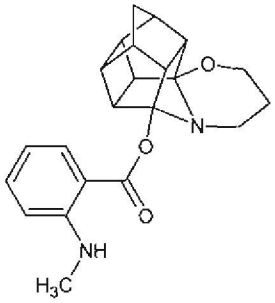 (2)	-2.925	9.5×10^{-4}	55.11 % at 1.15 mM
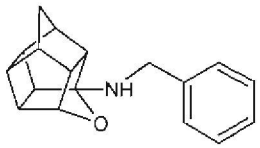 (3)	Not tested	Not tested	Not tested
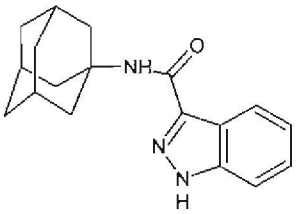 (4)	-3.52	2.532×10^{-4}	77.1 % at 300 μM
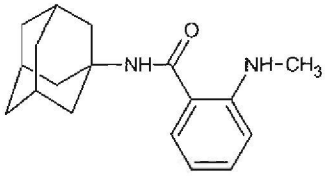 (5)	-2.52	7.73×10^{-4}	47.36 % at 3 mM

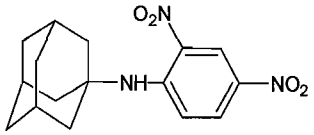 **(6)**	Solubility problems and less potent compound.		30.64 % at 250 µM
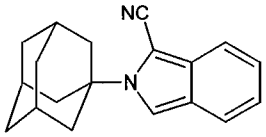 **(7)**	-4.527	2.911×10^{-5}	89.9 % at 125 µM
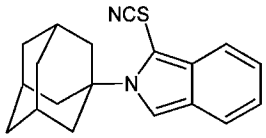 **(8)**	-3.889	1.049×10^{-5}	78.8 % at 750 µM
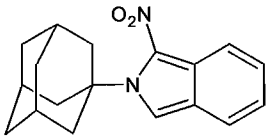 **(9)**	-3.734	1.549×10^{-4}	84.5 % at 1.15 mM
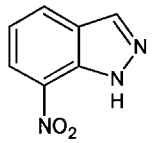 **(10)**	-4.96	1.109×10^{-5}	100 % at 62.5 µM
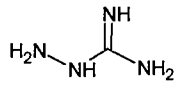 **(11)**	-2.72	1.941×10^{-3}	100 % at 10 mM
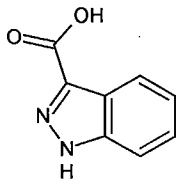 **(12)**	-3.28	9.649×10^{-4}	85.61 % at 1.15 mM

Table 4.2: Test compounds with their percentage inhibition at specific concentrations.

Compound	500 µM	250 µM	125 µM	61.5 µM	31.3 µM	15.6 µM
1.	NA*	83.7 %	73 %	47.5 %	37.8 %	15 %
2.	28.9 %	18.6 %	11.3 %	5.5 %	1.7 %	0 %
3.	NA	NA	NA	NA	NA	NA
4.	63 %	45.1 %	31.9 %	22.2 %	2.65 %	0 %
5.	24 %	15.2 %	8.6 %	3.7 %	1.3 %	0 %
6.	30.6 %	30.6 %	28.3 %	26.2 %	19.2 %	5 %
7.	NA	89.9 %	46.5 %	31.5 %	16.5 %	0 %
8.	78.7 %	65.3 %	46.2 %	31.4 %	18.4 %	0 %
9.	70.2 %	58.2 %	40.9 %	30.5 %	15 %	0 %
7-NI	100 %	100 %	100 %	100 %	90 %	50 %
Amino-guanidine	10 %	6.96 %	0 %	0 %	0 %	0 %
Indazole-3-carboxylic acid	42.3 %	27 %	13.3 %	10 %	8.3 %	0 %

*NA = not available

4.2 CONCLUSION

From the results it is clear that in the series of compounds evaluated, only the compounds containing the indazole and isoindole moiety, **1**, **4**, **7**, **8** and **9** show promising NOS inhibition. Comparison of the IC_{50} and percentage inhibition values of the test compounds

and 7-NI and aminoguanidine revealed that although the novel compounds are less potent than 7-NI, it showed promising results as NOS inhibitors with sub millimolar potency. The solubility problems could be addressed by synthesising the salts of the compound or by employing a different assay procedure. For future biological evaluations it is thus recommended that the compounds with high inhibitory activities be tested for their NOS isoform selectivity.

The polycyclic structures that were applied as carrier molecules, thus not only serve as pharmacokinetic enhancer but also to improve pharmacodynamics. With the described calcium activity of the polycyclic structures and taking the above aspects into account these novel compounds may find application as multipotent drugs in neurodegeneration. The polycyclic cage thus appears to be a useful scaffold to explore in order to design potential pharmacological active compounds in the field of neurodegeneration.

CHAPTER 5
SUMMARY AND CONCLUSION

Nitric oxide's (NO) role in neurodegenerative diseases is well known and although not the sole entity responsible for the aetiology of these diseases, it forms an integral part of the mechanisms involved in neurodegeneration. Understanding this process and finding effective inhibitors for it formed the rational of this study. To reach the study objective a series of novel fluorescent compounds were synthesised and evaluated *in vitro* for nitric oxide synthase (NOS) inhibition. The pentacyclic "cage" and amantadine structures were incorporated onto the novel fluorescent moieties with structural similarities to 7-NI, a known NOS inhibitor. These structures revealed promising *in vitro* activity and this study and further investigations of the novel inhibitors will contribute to the better understanding of the mechanisms involved in neurodegeneration and contribute to potential therapeutic compounds in this field.

5.1 INTRODUCTION

Neurodegenerative disorders are debilitating age-related disorders. Currently these disorders are treated only symptomatically with no drugs available that are used clinically to prevent neurodegenerative diseases. We therefore decided to synthesise a series of fluorescent NOS inhibitors by employing pentacyclic structures as scaffold for the substitution of the respective fluorophores. The primary aim of the current study was thus to design novel structures with increased neuroprotective activity, by means of a dual mechanism of action, owing to the fluorescent structures inhibitory effect on NOS and secondly, due to the documented antagonistic action of the cage amines on N-methyl-D-aspartate (NMDA) receptors.

Synthesis and NOS assay of the novel compounds were performed to determine their potential as fluorescent polycyclic ligands for neuroprotection.

5.2 SYNTHESIS AND CHARACTERISATION

Synthesis of the pentacyclo[5.4.0.0^{2,6}.0^{3,10}.0^{5,9}]undecane-8,11-dione resulted in a yield of 80.76 % and was used as the basis for further substitutions. Various linkers were to be applied between the cage structure and the fluorescent moieties to reduce steric hindrance, but because of multiple reactions and spontaneous rearrangement of the cage structure the idea was rejected and a new strategy applied. This new strategy entailed the conjugation of the fluorescent moieties to the rearranged polycyclic structure 3-hydroxy-4-aza-8-oxoheptacyclo[9.4.1.0^{2,10}.0^{3,14}.0^{4,9}.0^{9,13}.0^{12,15}]tetradecane and the polycyclic amine, amantadine. The fluorescent moieties were conjugated to the polycyclic structures by esterfication, amination and amide formation. Nine novel fluorescent polycyclic compounds were synthesised with percentage yields varying between 16 % and 50 %. Flash column chromatography and recrystallisation were mostly used in the purification of the compounds. Purification of some of the structures proved to be a challenge due to the formation of various unidentified impurities. This complicated the extraction, purification and recrystallisation processes and contributed to the low yields of some of the compounds. NMR and IR spectra showed the characteristic signals and MS confirmed the molecular masses of the compounds.

The ^{1}H-NMR spectra (spectrum 1) of the tetradecane compound shows the characteristic AB system of H-12 at δ_H 1.80:1.52 and the broad singulet of the hydroxyl group (H-17) at δ_H 4.97-3.94. The two multiplets between δ_H 3.85-3.67 represents H-14 and H-16 while H-15 is observed as a multiplet between δ_H 1.75-1.55. In the ^{13}C-NMR (spectrum 2), the overlapping singulets of C-3 and C-5 are seen at δ_c 101.30 while carbons 14, 16, 15 and 12 are observed as triplet signals at δ_c 62.69, 42.41, 41.67 and 24.33, respectively. The IR spectrum (spectrum 4) of the tetradecane compound exhibits a strong broad absorption at 3446 cm^{-1} confirming the free hydroxyl group and a strong absorption at 1125 cm^{-1}, which may be attributed to the ether group on C-5. This data correlates to that attained earlier in our laboratories.

Table 5.1: Compounds synthesised and characterised

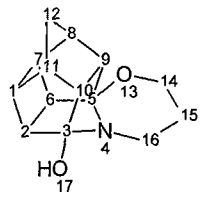 **Tetradecane**	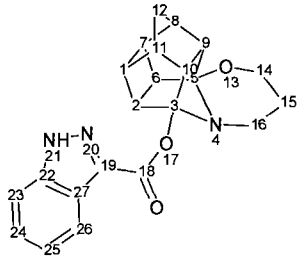 **(1)**	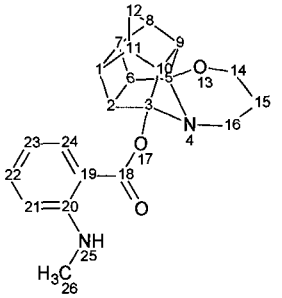 **(2)**
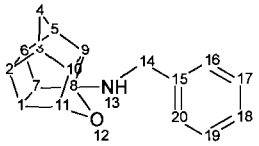 **(3)**	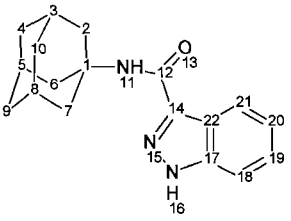 **(4)**	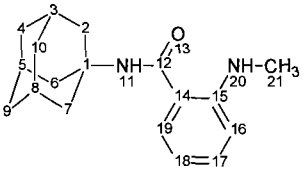 **(5)**
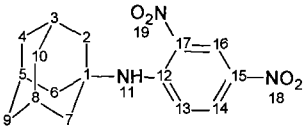 **(6)**	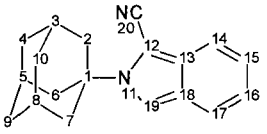 **(7)**	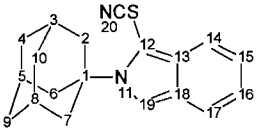 **(8)**
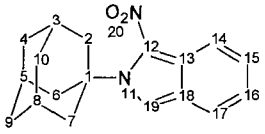 **(9)**		

The characteristic signals of the tetradecane structure are also observed in the ^{1}H-NMR spectra (spectrum 5) of **1**. Aromatic signals indicative of the indazole moiety are observed between δ_H 8.14-7.67. In the ^{13}C-NMR (spectrum 6), the carbonyl carbon (C-18) of the ester is observed at δ_c 163 and the mass spectrum (spectrum 7) indicates a molecular ion at m/z 375, confirming the calculated mass. The IR spectrum (spectrum 8) of **1** exhibits a medium absorption at 3277 cm^{-1} which can be attributed to the N-H stretch vibration and the strong vibration at 1625 cm^{-1} confirms the carbonyl carbon (C-18).

The ^{1}H-NMR spectra (spectrum 9) of **2** shows al the characteristic signals of the tetradecane structure and a strong doublet signal at δ_H 2.88, representing the methyl group (H-26). The two doublet of doublets observed at δ_H 7.91 and δ_H 6.64 are indicative of H-24 and H-21. H-22 and H-23 are observed at δ_H 7.38 and δ_H 6.57. The ^{13}C-NMR (spectrum 10) has a signal at δ_c 109.74 indicating the two singulets of C-3 and C-5. Carbons 14, 16, 15 and 12 indicates the triplet signals of the tetradecane structure at δ_c 63.05, 43.91, 43.88 and 24.00, respectively. The singulets at δ_c 29.63 and δ_c 166.6 are indicative of the methyl group of C-21 and the carbonyl carbon (C-18) of the ester. The mass spectrum (spectrum 11) shows a molecular ion at m/z 276, confirming the calculated mass. The IR spectrum (spectrum 12) of **2** exhibits a medium absorption at 3377cm^{-1}, attributed to a N-H stretch vibration and the strong vibration at 1667 cm^{-1} for the carbonyl carbon (C-18).

The spectral data of **3** was identical to that described in literature (Zah *et al.*, 2003).

The characteristic signals of the adamantane structure are observed in the ^{1}H-NMR spectra (spectrum 17) of **4.** A singulet at δ_H 2.10 indicating H-3, 5 and 7, a doublet at δ_H 2.01 for H-2, 8 and 9 and a multiplet at δ_H 1.70-1.65 for H-4, 6 and 10 is observed. The ^{1}H-NMR spectral data of the indazole structure correlates with that of compound **1.** The ^{13}C-NMR (spectrum 18) shows the singulet of C-1 at δ_c 51.59 and the characteristic signals of amantadine are observed at 48.27, 34.74 and 27.23. The mass spectrum (spectrum 19) indicates a molecular ion at m/z 295 confirming the calculated mass of the compound. The IR spectrum (spectrum 20) of **4** exhibits a medium absorption at 3459 cm^{-1}, which is attributed to the N-H stretch vibration and the strong vibration at 1672 cm^{-1} represents the amide carbonyl carbon (C-18).

^{1}H-NMR spectra (spectrum 21) of **5** shows al the characteristic signals of the adamantane structure and the spectral data of the anthranilic moiety correlates with that of compound **2** at the low field of the spectrum. In the ^{13}C-NMR (spectrum 22), the singulet of C-1 at δ_c 54.28 and the characteristic signals of amantadine are observed at δ_c 40.49, 35.65 and 28.99. The singulet at δ_c 29.63 confirms the methyl group of C-21. The mass spectrum (spectrum 23) indicates a molecular ion at m/z 284 confirming the calculated mass of the compound. The IR spectrum (spectrum 24) of **5** confirms the presence of the amide bond.

The characteristic signals of the adamantane structure and a broad singulet at δ_H 1.55 for the N-H proton are observed in the ^{1}H-NMR spectra (spectrum 25) of **6**. Low field signals corresponding to the 1, 2, 5-substituted aromatic ring confirms the presence of the structure. The mass spectrum (spectrum 27) indicates a molecular ion at m/z 317 confirming the calculated mass of the compound. The IR spectrum (spectrum 28) exhibits a medium absorption at 3439 cm^{-1} attributed to the N-H stretch vibration of the compound and the strong absorption at 1541 cm^{-1} indicative of the NO_2 groups.

The spectra of all three isoindole structures (**7**, **8** and **9**) show the characteristic ^{1}H-NMR and ^{13}C-NMR signals of the adamantane-isoindole conjugate (spectrums 29, 33 and 37). The isoindole signals correlated to that of literature (Di Montigny *et al.*, 1993 & Malan *et* al., 2004). The IR spectrums (spectrums 36 and 40) of **7** and **8** showed the signal of the cyano group at 2190.7 cm^{-1} and 2190.4 cm^{-1}, respectively. These signals are indicative for the formation of the cyano-isoindole structure and gave conformation of these compounds.

5.3 BIOLOGICAL EVALUATION

An *in vitro* oxyhemoglobin (oxyHb) assay was employed to determine the activity of the novel compounds at an enzymatic level of NOS. This assay is principally based on the reaction of nitric oxide (NO) with oxyHb and the formation of methemoglobin (metHb) (Hevel *et al.*, 1991 & Feelisch *et al.*, 1996). OxyHb, $CaCl_2$ and L-Arginine was prewarmed in the assay buffer to 37°C. The reaction was started by the addition of NADPH and tissue extract (in the form of rat brain homogenate). In order to determine the amount of NO formed, the change in absorbance difference between 401 and 421 nm was measured during the initial linear phase of the reaction. The change in absorbance at 401 nm was plotted against time and the change in absorbance over time at 421 nm was subtracted. The slope of this resulting curve gave an indication of the increase in molar amount of metHb, and is identical to the molar amount of NO generated. From this inhibition data the IC_{50} values were calculated and compared.

Of the newly synthesised compounds, structures **1**, **4**, **7**, **8** and **9** demonstrated meaningful NOS inhibition in the micromolar range. This confirmed that the presence of the indazole and isoindole moieties are important pharmacophores for effective NOS inhibition

(Ferrante *et al.*, 1999 & Przedborski *et al.*, 1996). Solubility problems were observed during the biological evaluation and 100 % inhibition could not be obtained with the novel structures. Synthesis of the salts of the test compounds could provide a simple solution for this and will be evaluated in further studies.

The indazole and isoindole structures were compared to aminoguanidine and 7-nitroindazole and exhibited activity which ranged between these two known NOS inhibitors.

5.4 CONCLUSION

The urgent need of selective nNOS inhibitors are of great importance in the treatment of neurodegenerative disorders. Considering that NOS is primarily activated by the NMDA receptor, the combination of inhibition properties (calcium channel blocking and selective NOS inhibition) makes the selected novel structures excellent drug candidates for possible treatment of neurodegenerative disorders.

A series of novel structures incorporated, the polycyclic moieties and fluorophores with structural similarity to 7-NI were successfully synthesised. These compounds showed increased potency when compared to the fluorophores and micromolar activities were obtained. Although the assay employed in the biological evaluation did not differentiate between the respective NOS isoforms, the results show that the test compounds have promising activity as NOS inhibitors and could be of potential value in the further study of neurological disorders.

We have identified a series of fluorescent structures with moderately high affinity for the NOS enzyme, which may be utilised for further *in vitro* and *in vivo* studies using modern imaging techniques (e.g. confocal laser scanning microscopy, flow cytometry or multiphoton microscopy) and these compounds could thus have potential as useful pharmacological tools to investigate enzyme-ligand interactions in the quest for effective neuroprotective strategies. This could lead to a greater insight into the neuroprotective mechanism and a possible cure/treatment for neurodegenerative disorders. The results obtained in this study clearly indicate the potential of these novel isoindole and indazole fluorescent polycyclic structures as novel NOS inhibitors. With the documented calcium

channel activity of the cage structures and taking the above aspects into account, these novel compounds may find application as multipotent drugs in neuroprotection.

In order to more accurately determine the selectivity of the novel inhibitors, inhibition studies with individual NOS isoforms along with a larger series of derivatives needs to be conducted. Additional assays on the NMDA receptor, Ca^{2+} channel activity, MAO-B receptor and blood brain barrier permeability will furthermore elaborate on these compounds potential value. The application of computer assisted molecular modelling will aid in this regard and may be of value for the further exploration of other novel neuroprotective structures.

REFERENCES

ABDULATIF, Y., HANAD, J.P., WICKSTED, G.S., DIXON, S. & deROCHEMONT, L.P. Laser-induced transient and permanent gratings in Eu^{3+}-doped dual alkaline earth silicate glasses. 1998. *Journal of Non-Crystalline Solids*, 241:59-70.

ALDERTON, W.K., COOPER, C.E. & KNOWLES, R.G. 2001. Nitric oxide synthases: structure function and inhibition. *Biochemistry Journal*, 357: 593-615.

ALEXI, T., BORLONGAN, C.V., FAULL, R.L.M., WILLIAMS, C.E., CLARK, R.G., GLUCKMAN, P.D. & HUGES, P.E. 2000. Neuroprotective strategies for basal ganglia degeneration: Parkinson's and Huntington's disease. *Progress in Neurobiology*, 60:409-470.

AXZELROD, D., HERMAN, B., CENTONZA FROHLICH, V.E., MURPHY, D.B., PISTON, D.W., HARDEE, C., KINOSHITA, R., WAKEFIELD, T., JOHNSON, J., ERDOGAN, T., ABRAMOWITZ, M., FESTER, K.W., KAWANO, Y., ENDERS, R.G., SPRING, K.R., PARRY-HILL, M.J., FELLERS, T.J., CLAXTON, N.S. & DAVIDSON, M.W. 2005. Fluorescence Microscopy. [Web] http://icecube.berkeley.edu/-bramall/work/astrobiology/fluorescence .html. [Date of use: 26 Feb 2006].

BADDEDGE, P., BLAND-WARD, P.A., HART, S.L. & MOORE, P.K. 1993. Inhibition of rat cerebellar nitric oxide synthase by 7-nitroindazole and related substituted indazoles. *British Journal of Pharmacology*, 110:225-228.

BARLAS, M., DENLI, O., GONUL, N., HASCICEK, C., OZADAMAR, SUKRU., CEDDEN, F. & ELHAN, A. The effect of continuous release of methelene blue form

a drug delivery system on the intestine: an experimental study in chick embryo gastroschisis model. *Journal of Ankara medical school*, 24:159-164.

BERKLEY, P. 2005. Fluorescence. [Web] http://icecube.berkeley.edu/-bramall/work /astrobiology/fluorescence .html. [Date of use: 27 Feb 2006].

CASTAGNOLI, K., PALMER, S., ANDERSON, A., BUETERS, T. & CASTAGNOLI, N. 1998. The neuronal nitric oxide synthase inhibitor 7-nitroindazole also inhibits the monoamine oxidase-B-catalyzed oxidation of 1-methyl- 4-phenyl-1,2,3,6-tetrahydropyridine. *Chemical Research in Toxicology*, 11:716-717.

CASTAGNOLI, P.K., STEYN, J.S., PETZER, J.P., VAN DER SCHYF, C.J. & CASTAGNOLI, N. 2000. Neuroprotection in the MPTP parkinsonian C57BL/6 mouse model by a compound isolated from tobacco. *American Chemical Society*, 14:523-527.

CLEETER, M.W., COOPER, J.M., & SCHAPIRA, A.H.V. 1992. Irreversible inhibition of mitochondrial complex 1 by MPTP: Evidence for free radical involvement. *Journal of Neurochemistry*, 58:786-789.

COOKSEN, R.C., GRUNDWELL, E., HUDEC, J. 1958. Synthesis of cage-like molecules by irradiation of Diels-Alder adducts. *Chemistry and Industry*. 39:1003-1004.

COOKSON, R.C., GRUNDWELL, E., HILL, R.R. & HUDEC, J. 1964. Photochemical cyclisation of Diels-Alder adducts. *Journal of the Chemical Society*, 3062-3075.

DACRES, H. & NARAYANASWA, R. 2005. Sensitive optical NO sensor based on bis[(2,9-dimethyl-1,10-phenanthroline)] copper(II) complex. *Sensors and Actuators*, 107:14-23.

DANYSZ, W., PARSONS, W.G., KORNHUBER, J., SCHMIDT, W.J., QUACK, G. 1997. Aminoamantadines as NMDA receptor antagonists and anti-parkinsonian agents. *Neuroscience and Biobehavioural Reviews*, 21:455-468.

DAWSON, T.M., DAWSON, V.L. & SNYDER, S.H. 1992. A novel neuronal messenger molecule in brain: The free radical nitric oxide. *Annals of Neurology*, 32:297– 311.

DAWSON, V.L., DAWSON, T.M., LOMDON, E.D., BREDT, D.S. & SNYDER, S.H. 1991. Nitric oxide mediates glutamate neurotoxicicty in primary cortical cultures. *Proceedings of the National Acadamy of Sciences of the United states of America*, 88:6368-6371.

DAWSON, J. & KNOWLES, R.G. 1999. A microtiter-plate assay of nitric oxide synthase activity. *Molecular Biotechnology*. 12:275-278.

DE MONTIGNY, P., STOBAUGH, J.F., GIVENS, R.S., CARLSON, R.G., SRINIVASACHAR, K., STENSON, L.A. & HIGUCHI, T. 1993. Naphthalene-2,3-dicarboxyaldehyde/cyanide ion: a rationally designed fluorogenic reagent for primary amines. *Analytical Chemistry*, 59:1096 – 1101.

DI MONTE, D.A., ROYLAND, J.E., ANDERSON A., CASRAGNOLI, K. & LANGSTON, J.W. 1997. Inhibition of monoamine oxidase contributes to the protective effect of 7-nitroindazole against MPTP neurotoxicity. *Journal of Neurochemistry*, 69:1771-1773.

DIFIGLIA, M. & VONSATTEL, J.P.G. 1998. Huntington disease. *Journal of Neuropathology & Experimental Neurology*, 57:369-38.

DOBRUCKI, J. 2003. Fluorescence and confocal microscopy. [Web] http://helios.mol.uj.edu.pl/conf_c/moun.html. [Date of access: 22 Mrt 2006].

DOBRUCKI, J. 2003. Fluorescence and confocal microscopy. [Web] http://helios.mol.uj.edu.pl/conf_c/moun.html. [Date of access: 22 Mrt].

EVANKO, D. 2005. Focus on fluorescence imaging: Principles and practice of microscope techniques. *Nature Methods*, 12:901.

FEARNLEY, J.M. & LEES, A.J. 1999. Ageing and Parkinson's disease. *Proceedings of the National Academy of Sciences of the United States of America*, 93:4565-4571.

FEELISCH, M., & NOACK, E.A. 1987. Correlation between nitric oxide formation during degradation of orgzanic nitrates and activation of guamylate cyclase. *European Journal of Pharmacology*, 193:9-30.

FEELISH, M., KUBITZEK, D. & WERRINGLOER, J. 1996. The oxyhemoglobin assay. (*In* Feelish, M. & Stamler, J.S., eds. Methods in nitric oxide research. Londen: Wiley & Sons Ltd. P. 455-478).

FEELISH, M., KUBITZEK, D., WERRINGLOER, J. 1996. The oxyhemoglobin assay. (*In* Feelish, M. & Stamler, J.S., eds. Methods in nitric oxide research. Londen: Wiley & Sons Ltd. P. 455-478).

FERRANTE, R.J., HANTRAYE, P., BROUILLET, E. & BEAL, M.F. 1999. Increased nitrotyrosine immunoreactivity in substantia nigra neurons in MPTP treated baboons is blocked by inhibition of neuronal nitric oxide synthase. *Brain research*, 823:177-182.

FOISSNER, I., WENDEHENNE, D., LANGEBARTELS, C., DURNER, J. & PLANT, J. 2000. In vivo imaging of an elicitor-induced nitric oxide burst in tobacco. *The Plant Journal*, 23:817-824.

FORNO, L. 1996. The Lewy Body in Parkinson's disease. *Advances in Neurology*, 45:35-43.

GIBB, W.R.G. 1999. The significance of the Lewy body in the diagnosis of idiopathic Parkinson's disease. *Applied Neurobiology*, 15:27-44.

GREENE, J.G. & GREENAMYRE, J.T. 1996. Bioenergetics and glutamate excitotoxicity. *Progress in Neurobiology,* 48:613-634.

GRIFFITH, O.W. & KILBOURN, R.G. 1996. Nitric oxide synthase inhibitors: amino acids. *Methods in Enzymology*, 268: 375-392.

GU, M.T., TANNOUS, T. & SHEPPARD, C.J.R. 1994. Improved axial resolution in confocal fluorescence microscopy using annular pupils. *Optics Communications*, 110:533-539.

GUNSEKERA, T.S., VEAL, D.A., & ATTFIELD, P.V. 2003. Potential for broad applications of flow cytometry and fluorescence techniques in microbiological and somatic cell analyses of milk. *International Journal of Food Microbiology*, 85:269-279.

HANDY, R.L.C., WALLACE, P., GAFFEN, Z.A., WHITEHEAD, K.J. & MOORE, P.K. 1995. The antinociceptive effect of 1-(2 trifluoromethylphenyl)imidazole (TRIM), a potent inhibitor of neuronal nitric oxide synthase in vitro, in the mouse, *British Journal of Pharmacology*, 116:2349–2350.

HANTRAYE, P., BROUILLET, E., FERRANTE, R., DOLAN, R., MATTHEWS R.T. & BEAL, M.F. 1996. Inhibition of neuronal nitric oxide synthase prevents MPTP-induced parkinsonism in baboons. *Nature Medicine*, 64:936-939.

HASEGAWA, E., THAKESHIGE, K., OISHI, T., MURAI, Y., & MINIKAMI, S. 1990. 1-Methyl-4-phenylpyridinium induces NADH-dependent superoxide formation and enhances NADH-dependent lipid peroxidation in bovine heart submitochondrial particles. *Biochemistry & Biophysical Research Community*, 170:2049-1055.

HAUGLAND, J.G., GREGORY, J., SPENCE, M.T.Z., JOHNSON, I. & MILLER, E. 2002. Handbook of fluorescent probes and research products. Chapter 1: Introduction to fluorescent techniques. USA: Molecular probes. p1-7.

HEVEL, J.M., WHITE, K.A. & MARLETTA, M.A. 1991. Purification of the inducuble murine macrophage nitric oxide synthase. Identification as a flavoprotein. *Journal of Biological Chemistry*, 266:22789-22791.

HOFFMAN, BB. & TAYLOR, P. 2001. Goodman and Gilman's. The pharmacological basis of therapeutics. Chapter 6: Neurotransmission. New York: McGraw-Hill. 148p.

HUANG, H., MARTASEK, P., ROMAN, L.J., MASTERS, B.S.S. & SILVERMAN, R.B. 1999. Potent and highly selective inhibitors of neuronal nitric oxide synthase. *Journal of Medicinal Chemistry*, 42:3147–3153.

ISCHIROPOULOS, H., ZHU, L., CHEN, J., TSAI, M., MARTIN, J.C., SMITH, C.D. & BECKMAN, J.S. 1992. Peroxynitrite-mediated tyrosine nitration catalyzed by superoxide dismutase. *Archives of Biochemistry and Biophysics*, 298:431-437.

JARDIM, L.B., M.L. PEREIRA, L., SILVEIRA, A., FERRO, J., SEQUEIROS, J. & GUILIANI, R. 2001. Machado-Joseph disease in South Brazil: clinical and molecular characterization of kindreds. *Journal of Neurology*, 104:224–231.

JELLINGER, K. 1997. Overview of morphological changes in Parkinson's disease. *Advances in neurology*, 45:1-18.

KAWAGUCHI, T., OKAMOTO, M., TANIWAKI, M., AIZAWA, M., INOUE, M. & KATAYAMA, S. 1994. CAG expansions in a novel gene for Machado-Joseph disease at chromosome 14q32. *Nature Genetics*, 8:221–228.

KELM, M., DAHMANN, R., WINK, D. FEELISCH, M. 1997. The nitric Oxide/Superoxide assay. *The Journal of Biological Chemistry*, 272:9922-9932.

KERWIN, J.F., LANCASTER, J.R. & FELDMAN, P.L. 1995. Nitric Oxide: A new paradigm for second messengers. *Journal of Medicinal Chemistry*, 38:4342-4362.

KNEUBEUHLER, S., THULL, U., ALTOMARE, C., CARTA, V., GAILLARD, P., CARRUPT, P.A., CAROTTI, A. & TESTA, B. 1995. Inhibition of monoamine oxidase-B by 5H-Indeno[1,2-c]pyridazines. Biological activities, quantitative structure-activity relationships (QSARs) and 3D QSARs. *Journal of medicinal chemistry*, 38:3974-3883.

KNOWLES, R.G. & MONCADA, S. 1994. Nitric oxide synthase in mammals. *Journal of Biochemistry*, 12:275-279.

KOJIMA, H., NAKATSUBO, N., KIKUCHI, K., KAWAHARA, S., KIRINO, Y., NAGOSHI, H., HIRATA, Y. & NAGANO, T. 1998. Detection and imaging of nitric oxide with novel fluorescent indicators: Diaminofluoresceins. *Analytical Chemistry*, 70:2446-2453.

LANGSTON, J.W., IRWIN, I., LANGSTON, E.B. & FORNO, L.S. 1994. Pargyline prevents MPTP-induced parkinsonism in primates. *Journal of Science*, 225:1480-1482.

LI, L., KRACHT, J., PENG, S., BERNJARDT, G. & BUSCHAUER, A. 2003. Synthesis and Pharmacological Activity of Fluorescent Histamine Receptor Antagonists Related to Mepyramine. *Bioorganic & Medicinal Chemistry Letters*, 13:1245-1248.

LOPEZ-FIGUEROA, M.O., DAY, H.E., LEE, S., RIVIER, C., AKIL, H. & WATSON, S.J. 2000. Temporal and anatomical distribution of nitric oxide synthase mRNA expression and nitric oxide production during central nervous system inflammation. *Research Community*, 852:239-246.

MALAN, S.F., VAN MARLE, A., MENGE, W.M., ZULIANA, V., HOFFMAN, M., TIMMERMAN, H. & LEURS, R. 2004. Fluorescent ligands for the histamine H_2 receptor: synthesis and preliminary characterization. *Bioorganic & Medicinal Chemistry Letters*, 12:6495-6503.

MARSDEN, C.D. 1990. Parkinson's disease. *The Lancet*, 335:948-925.

MARTIN, I.N., WOODWARD, J.J. WINTER, M.B., WILLIAM, T.B. & MARLETTA, M.A. 2007. Design and synthesis of C5 Methylated L-arginine analogues as active site probes for nitric oxide synthase. *Journal of the American Chemical Society*, 129:12563 -12570.

MATTHEWS, R.T., YANG, L. & BEAL. 1997. S-methylthiocitrulline, a neuronal nitric oxide synthase inhibitor protects against malonate and MPTP neurotoxicity. *Journal of Neurology*, 143:282-286.

MIZOGUCI, K., YOKOO, H., YOSHIDA, M., TANAKA. K., TANAKA, M. 1994. Amantadine increases the extracellular dopamine levels in the striatum by re-uptake inhibition and by NMDA antagonism. *Brain research*, 662:255-258.

MONCADA, S., PALMER, R.M.J. & HIGGS, E.A. 1991. Nitric oxide: Physiology, pathophysiology, and pharmacology. *Pharmacological Reviews*, 43:109–142.

MOORE , P.K., WALLACE, P., GAFFEN, Z., HART, S.L. & BADDEBEGE, R.C. 1993. Characterization of the novel nitric oxide synthase inhibitor 7-nitro indazole and related indazoles: Antinociceptive and cardiovascular effects. *British Journal of pharmacology*, 110:219–224.

MUSCARA, M.N. & WALLACE, J.L. 1999. Nitric Oxide V. Therapeutic potential of nitric oxide donors and inhibitors. *American journal of Physiology*, 276:1313-1316.

NAKATSUKA, M., NAKASUTA, K. & OSAWA, Y. 1998. Metabolism-based inactivation of penile nitric oxide synthase activity by guanabenz. *Drug Metabolism and Disposition: The Biological Fate of Chemicals*, 26: 497-501.

NISHIHIRA, J. 2000. Macrophage migration inhibitory factor (MIF): Its essential role in the immune system and cell growth. *Journal of Interferon and Cytokin research*, 9:751-762.

NYIREDY, S.Z., ERDELMEIER, C.A.J., MEIER, B. & STICHER. O. 1985. "Prisma": ein modell zur optimierung der mobilen phase für die Dünnschichtchromatographie, vorgestellt anhand verschiedener naturstofftrennungen. *Planta Medica,* 241–246.

OGDEN, J.E. & MOORE, P.K. 1995. Inhibition of nitric oxide synthase-potential for a novel class of therapeutic agent. *Trends in Biotechnology*, 13: 70-78.

OKABE, N., IKEDA, K. & KOHYAMA, Y. 1994. N-Nitro-L-arginine methyl ester hydrochloride. *ACTA Crystallographica*, 50:2088-2089.

OLIVER, D.W., DEKKER, T.G., & SNYCKERS, F.O., 1991. Pentacyclo[5.4.$0^{2,6}$.$0^{3,10}$.$0^{5,9}$]undecylamines. Synthesis and pharmacology. *European Journal of Medicinal Chemistry*. 26:375-379.

OOMS, F., NORBERG, B., ISIN, E.M., CASTAGNOLI, N., VAN DER SCHYF, C.J. & WOUTERS, J. 2000. 7-nitroindazole. *ACTA Crystallographica*, 56:474-475.

PADDOCK, S. 2002. Optical Sectioning-Slices of Life. *Science*, 295:1319-1321.

PALMER, R. M. J., FERRIGE, A.G. & MONCADA, S. 1987. Nitric oxide release accounts for the biological activity of the endothelium-derived factor. *Nature*, 327:524–526.

PARSONS, C.G, DANYSZ, W, QUACK, G. Memantine is a clinnically well tolerated *N*-methyl-D-aspartate antagonism (NMDA) receptor antagonist – Review of preclinical data *Neuropharmacology*, 38:735- 767.

PRIVAT, C., LANTOINE, F., BEDIOUI, F., MILLANVOYE van BRUSSEL, E., DEVNYNCK, J. & DEVYNCK, M.A. 1997. Nitric oxide production by endothelial cells: comparison of three methods of quantification. *Life Sciences*, 61:1193-1202.

PRZEDBORSKI, S., JACKSON-LEWIS, V., YOKOYAMA, R., SHIBATA, T., DAWSON, V.L. & DAWSON, T.M. 1996 Role of neuronal nitric oxide in 1-methyl-4-phenyl-1,2,3,6-tetrahydropyridine (MPTP)-induced dopaminergic neurotoxicity. *Proceedings of the National Academy of Sciences of the United States of America*, 93:4565-4571.

REIF, A., FROHLICH, L.G., KOTSONIS, P., FREY, A., BOMMEL, H.M., WINK, D.A., PFLEIDERER, W. & SCHMIDT, H.H.H.W. 1999. Tetrahydrobiopterin inhibits monomerization and is consumed during catalysis in neuronal NO synthase. *Journal of Biological Chemistry*, 274:24921–24929.

ROBINSON, J.P. 2005. The Principles of Confocal Microscopy: Components of the Microscope. [Web] http://www.cyto.purdue.edu/flowcyt/educate/pptslide.html. [Date of use: 14 Feb 2006].

ROMAN, L.J., MATTASEK, P. & MASTERS, B.S.S. 2002. Intrinsic and extrinsic modulation of nitric oxide synthase activity. *Chemical Reviews*, 102:1179-1189.

ROSENBERG, R.N. Machado-Joseph disease: an autosomal dominant motor system degeneration. *Movement disorders*, 7:193–203.

ROYLAND, J.E., DELFANI, K., LANGSTON, J.W., JANSON, A.M. & DI MONTE, D.A. 1999. 7-nitroindazole prevents 1-methyl-4-phenyl-1,2,3,6-

tetrahydropyridine-induced ATP loss in the mouse striatum. *Brain research*, 839:41-48.

SALTER, M. & KNOWLES, R.G. 1989. Assay of NOS activity by the measurement of conversion of oxyhemoglobin to methemoglobin by NO. (*In* Titheradge, M.A., ed. Methods in molecular biology, vol. 100. Nitric oxide protocols.) Totowa, New Jersey: Humana press. p. 61-65.

SAMIL, A., NUTT, J.G. & RANSOM, B.R. 2004. Parkinson's disease. *The Lancet*, 363:1783-1790.

SCHULZ, J.B., MATTHEW, R.T., MUQIT, M.M., BROWN, S.E. & BEAL, M.F. 1995. Inhibition of neuronal nitric oxide synthase by 7-nitroindazole protects against MPTP-induced neurotoxicity in mice. *Journal of Neurochemistry*, 64:936-939.

SEQUEIROS, J. & COUTINHO, P. 1993. Epidemiology and clinical aspects of Machado-Joseph disease. *Advances in Neurology*, 61:139–153.

SMEYNE, R.J. & JACKSON-LEWIS., V. 2004. The MPTP model of Parkinson's disease. *Mollecular Brain Research*, 134:57-66.

SPECIALE, S.G. 2002. Insights into parkinsonian neurodegeneration. *Neurotoxicology and Teratology*, 24:607-620.

STANDAERT, D.G. & YOUNG, A.B. 2000. Treatment of central nervous system degenerative disorders. (In Gardnman, J.G., Limbird, L.E., ed. Goodman & Gillman's Pharmacological basis of therapeutics. Tenth Edition. New York : McGraw-Hill. P. 549-568.)

STEVANIN, L.B., DURR, A. & BRICE, A. 2000. Clinical and molecular advances in autosomal dominat cerebellar ataxias: from genotype to phenotype and physiopathology. *European Journal of Human Genetics*, 8:14–18.

STUEHR, D.J. 1999. Mammalian nitric oxide synthase. *Biochimica et Biophysica ACTA/General Subjects*, 1411:217–230.

TAKIYAMA, Y., NISHIZAWA, M., TANAKA, H., KAWASHIMA, H., SAKAMOTO, H. & KARUBE, Y. 1993. The gene for Machado-Joseph disease maps to human chromosome 14q, *Nature Genetics*, 4:300–303.

WELLS, S. 2004. Choice of Fluorescent Probes. [Web:] http://www.micro.magnet.fsu.edu/primer/techniques/fluorescence/fluorochrome.html [Date of use: 9 Feb 2006].

WINK, D.A., NIMS, RW., DARBYSHIRE, J.F., CHRISTODOULOU, D., HANBAUER, I., COX, G.W., LAVAL, F., LAVAL, J., COOK, J.A., KRISHNA, M.C., DeGRAFF, W.G., MITCHELL, J.B. 1994. Reaction kinetics for nitrosation of cysteine and glutathione in aerobic nitric oxide solutions at neutral Intermediates generated in the NO/02 reaction pH. Insights into the fate and physiological effects of intermediates generated in the NO/02 reaction. *Chemical research in toxicology,* 7:519-525.

ZAH, J., TERRE'BLANCHE, G., ERASMUS, E. & MALAN, S.F. 2003. Physicochemical prediction of a brain-blood distribution profile in polycyclic amines. *Bioorganic & medicinal chemistry,* 11:3569-3578.

ANNEXURE A

SPECTRAL DATA

^{1}H-NMR, ^{13}C-NMR, MS AND IR

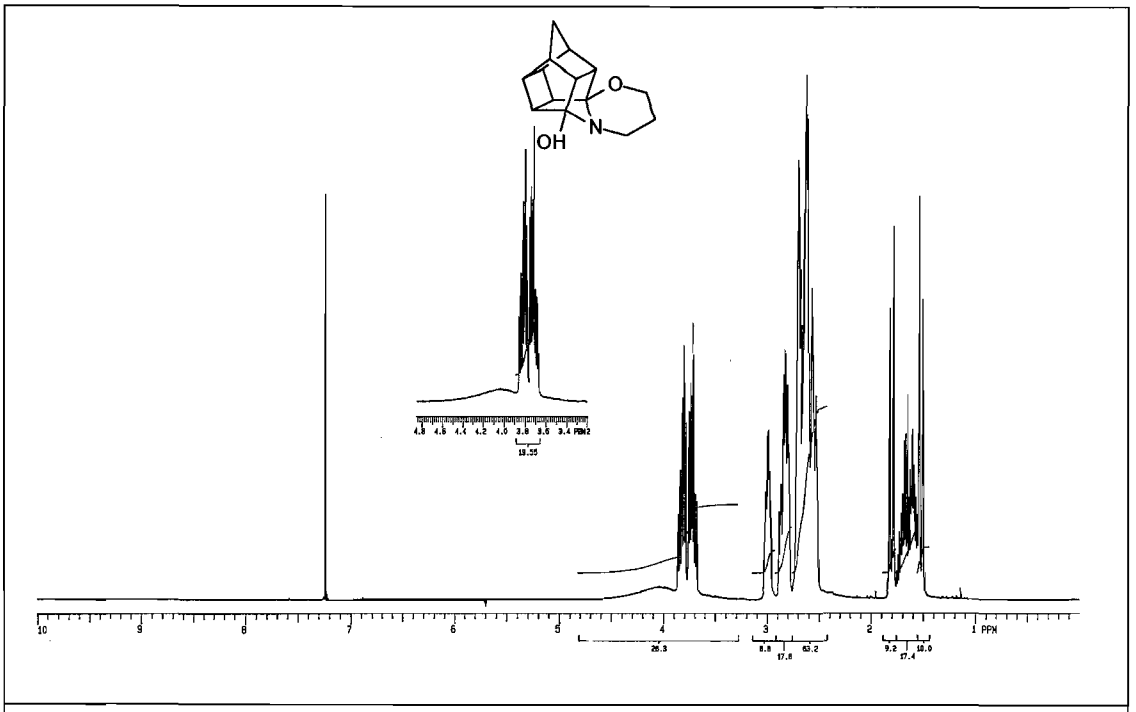

Spectrum 1.

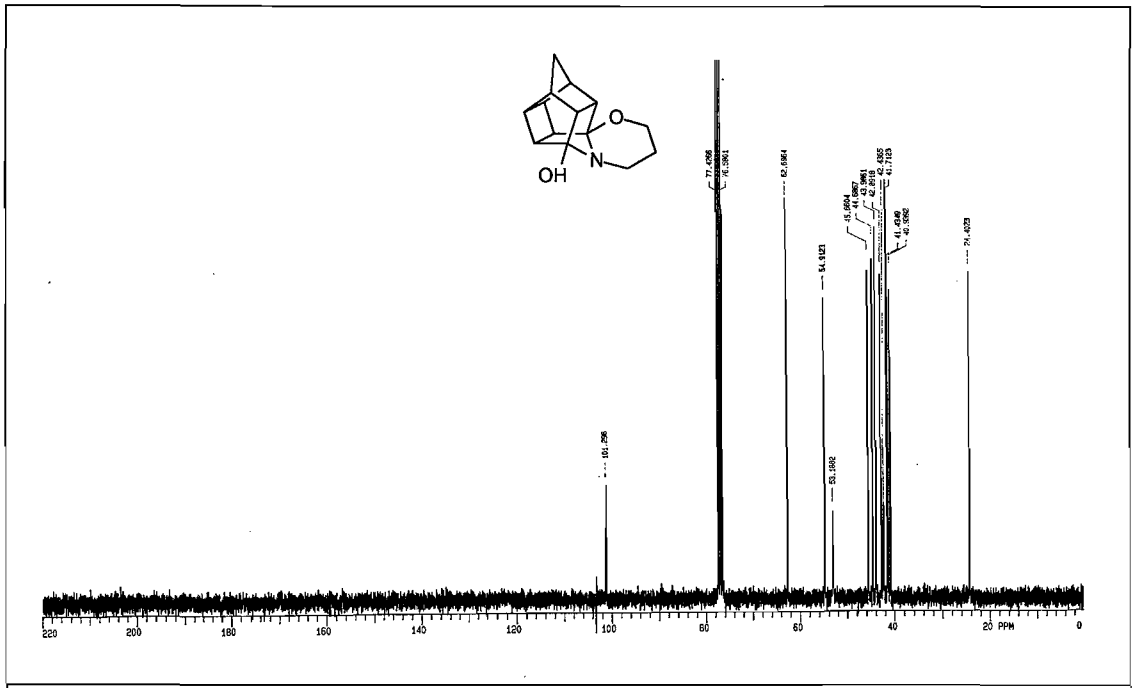

Spectrum 2.

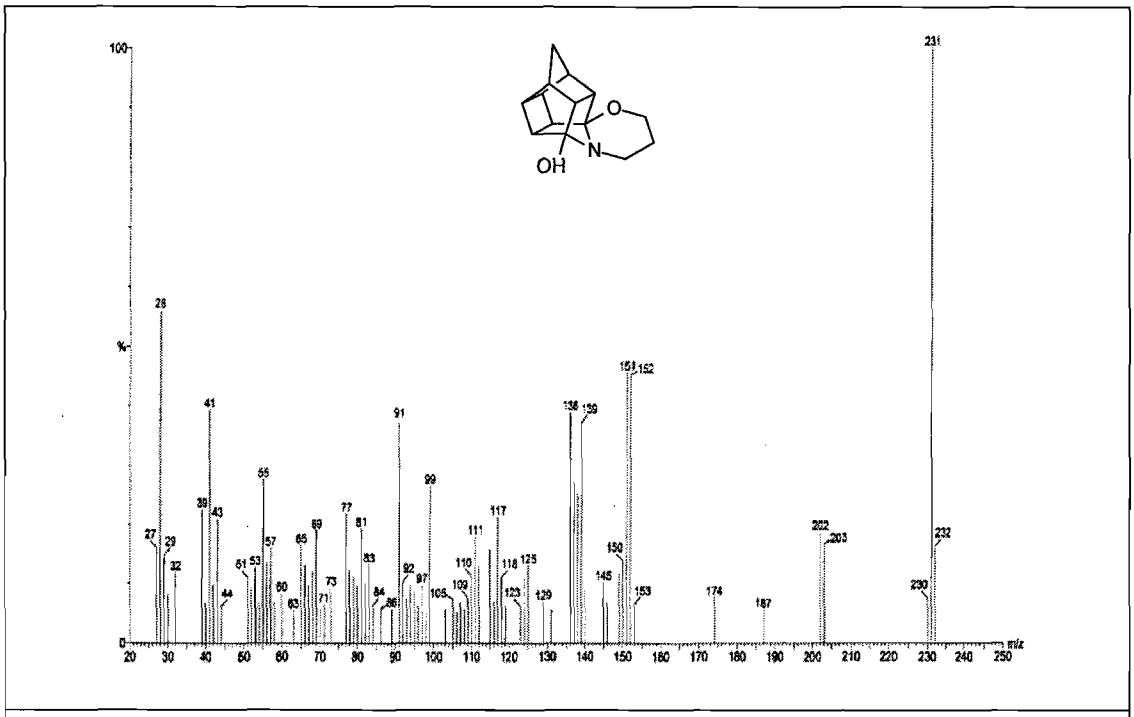

Spectrum 3.

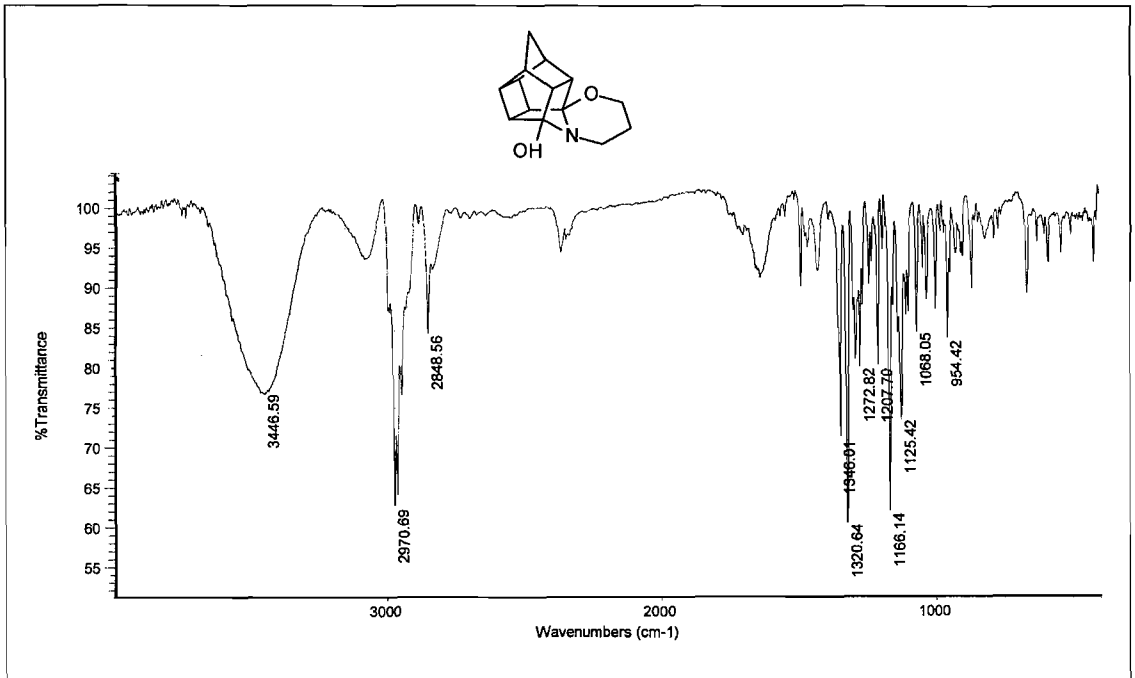

Spectrum 4.

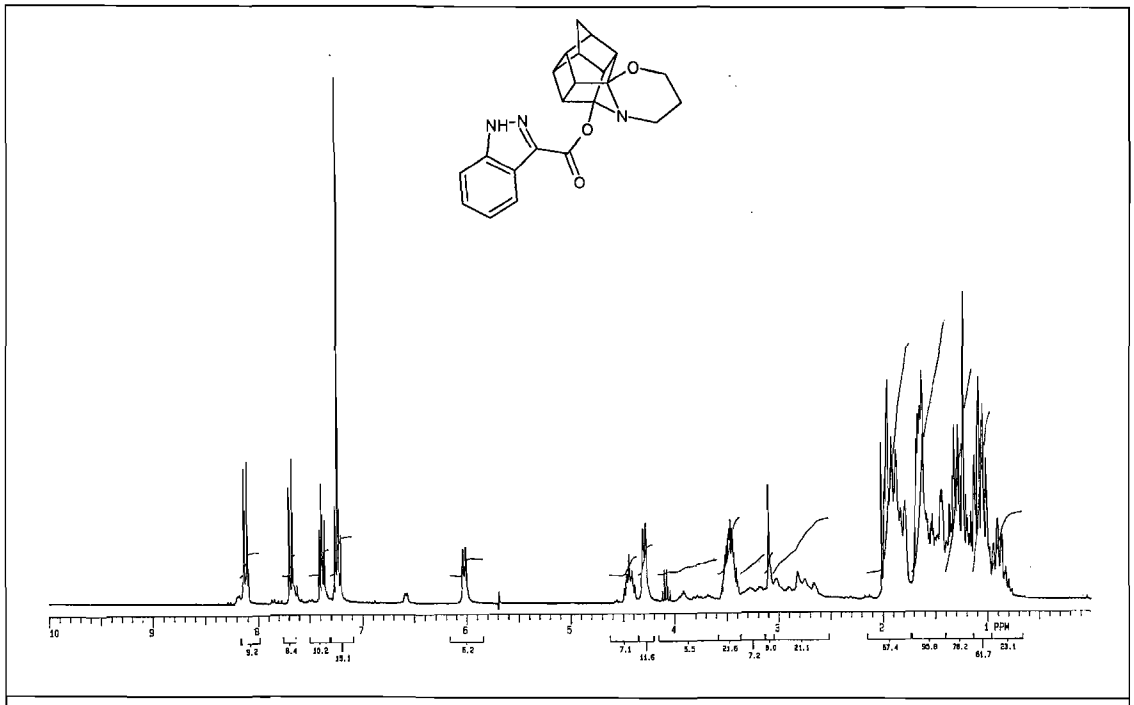

Spectrum 5 .

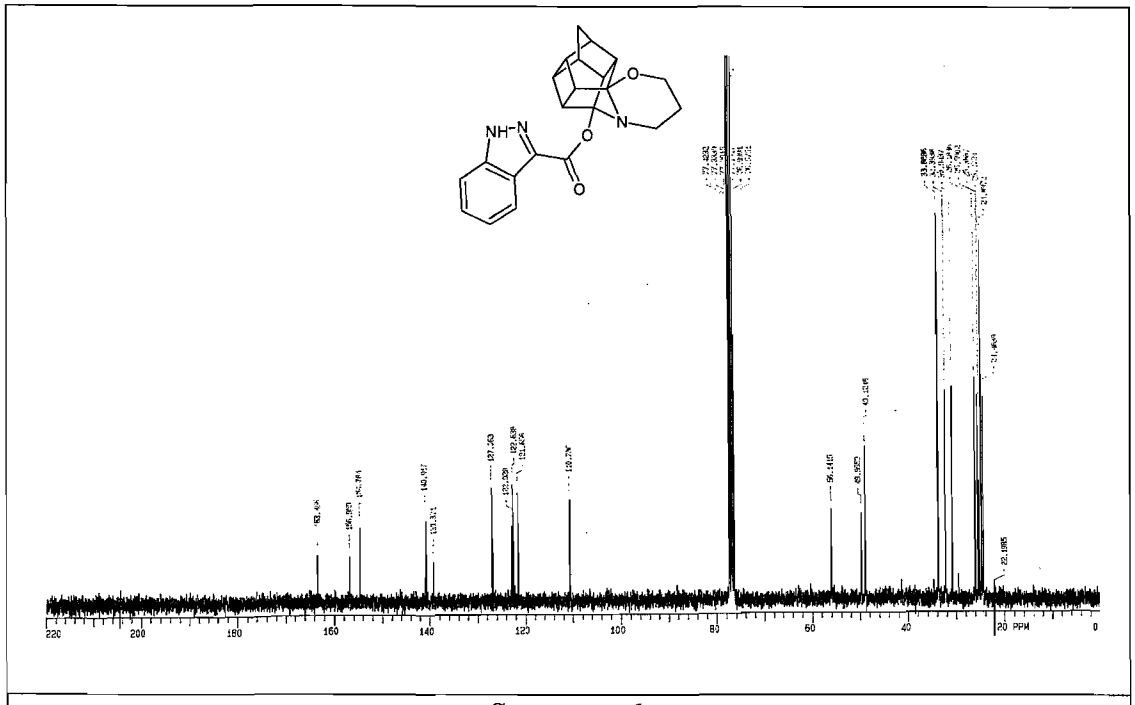

Spectrum 6.

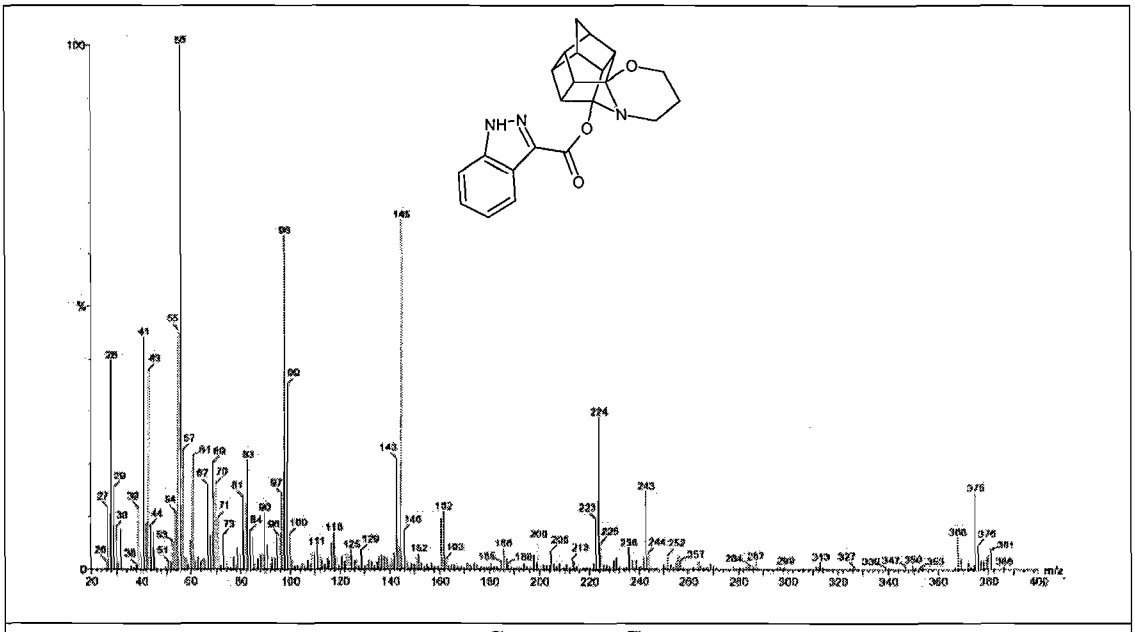

Spectrum 7.

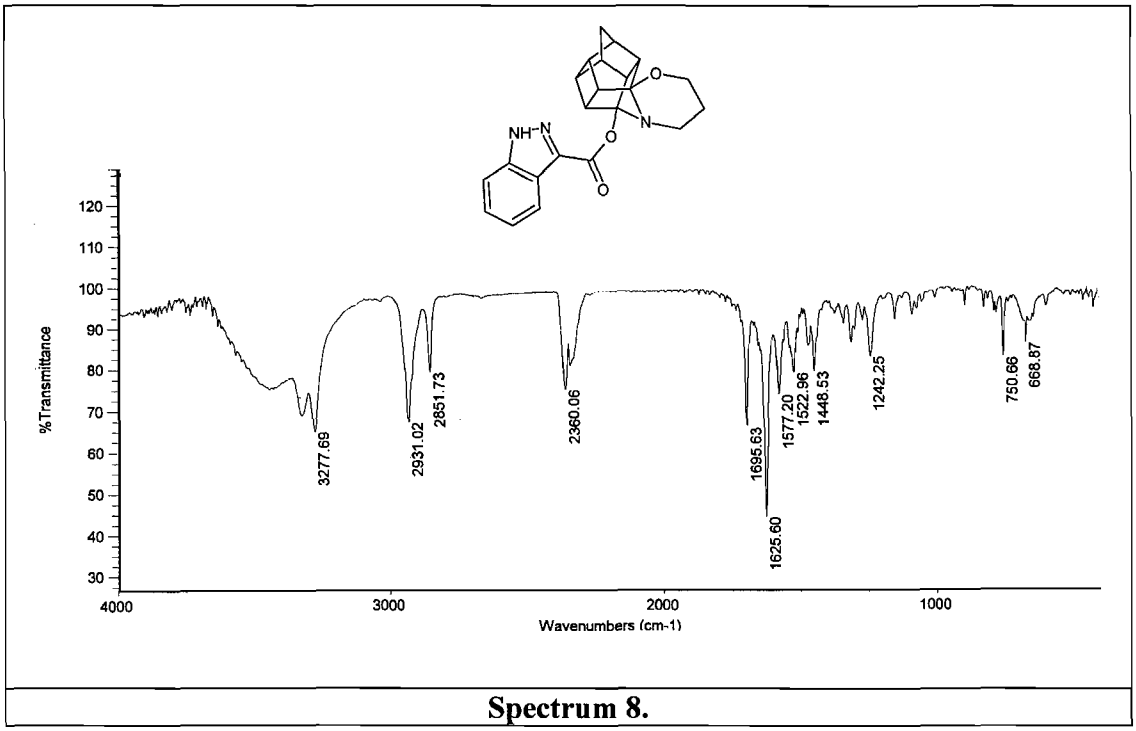

Spectrum 8.

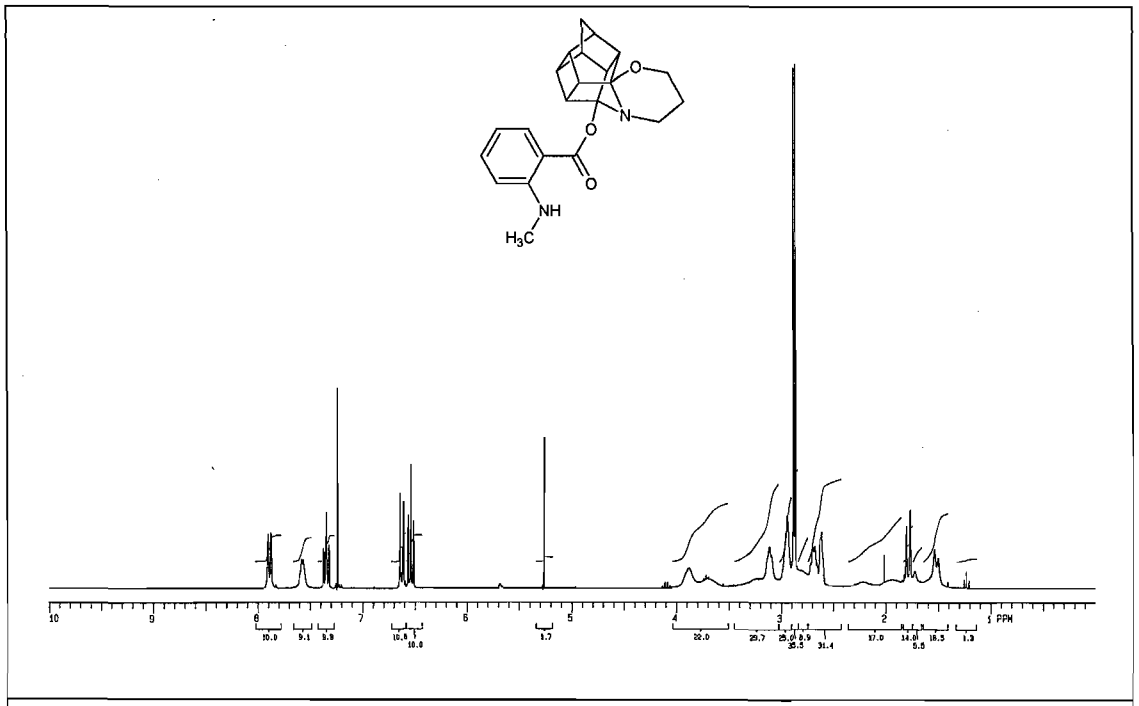

Spectrum 9.

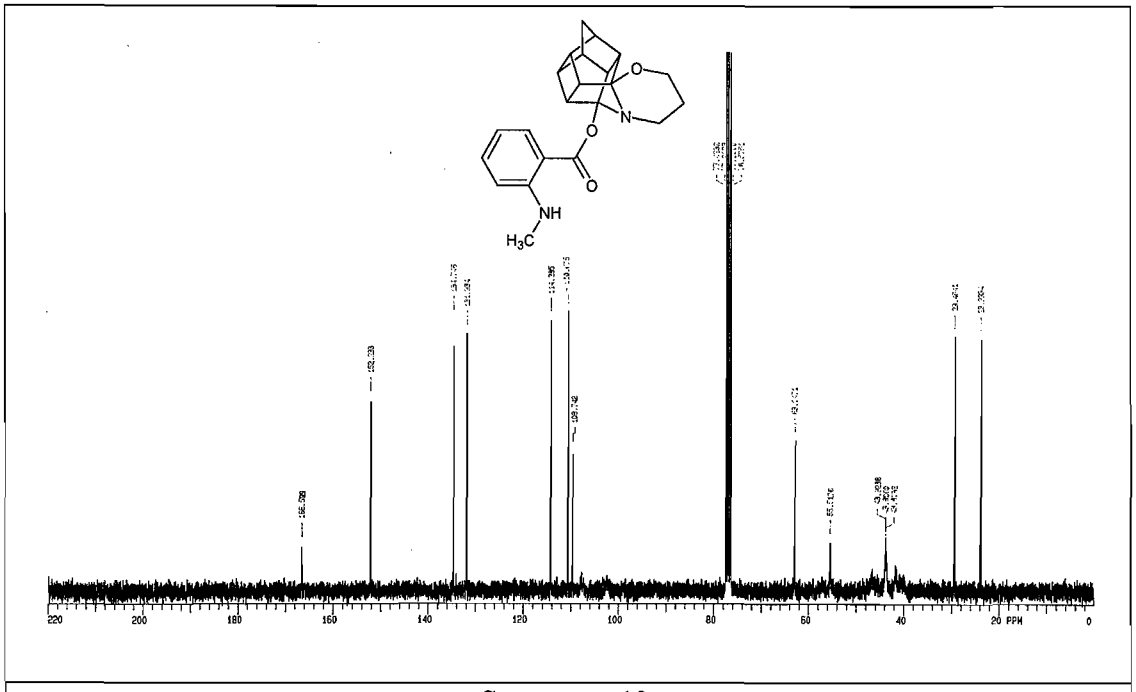

Spectrum 10.

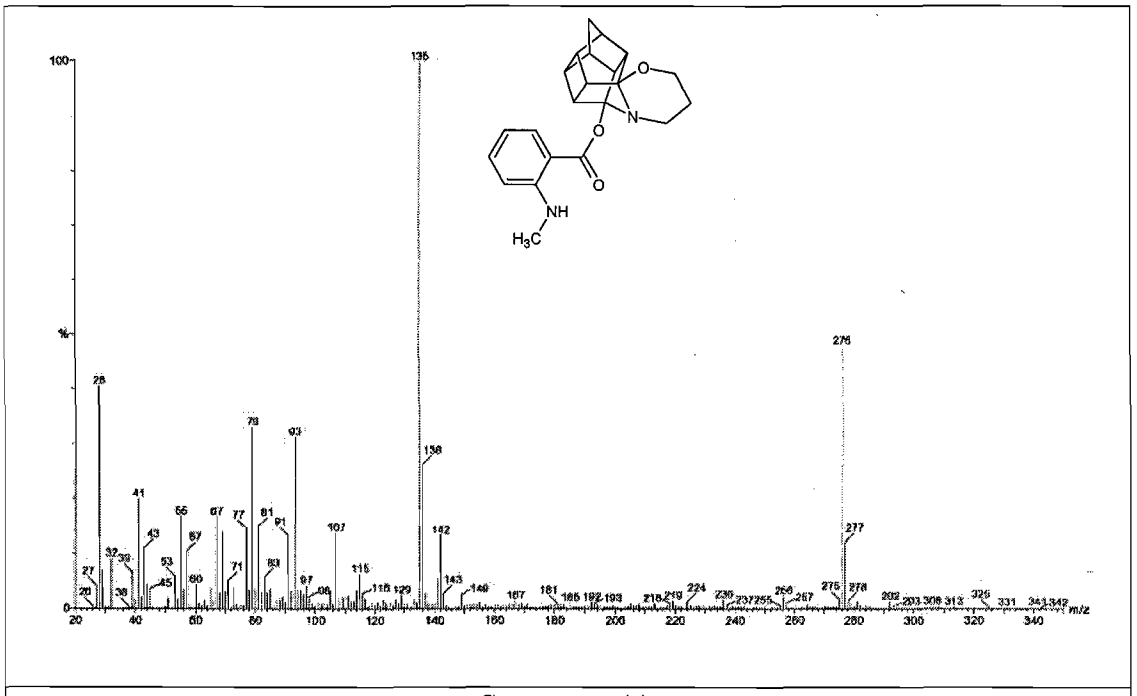

Spectrum 11.

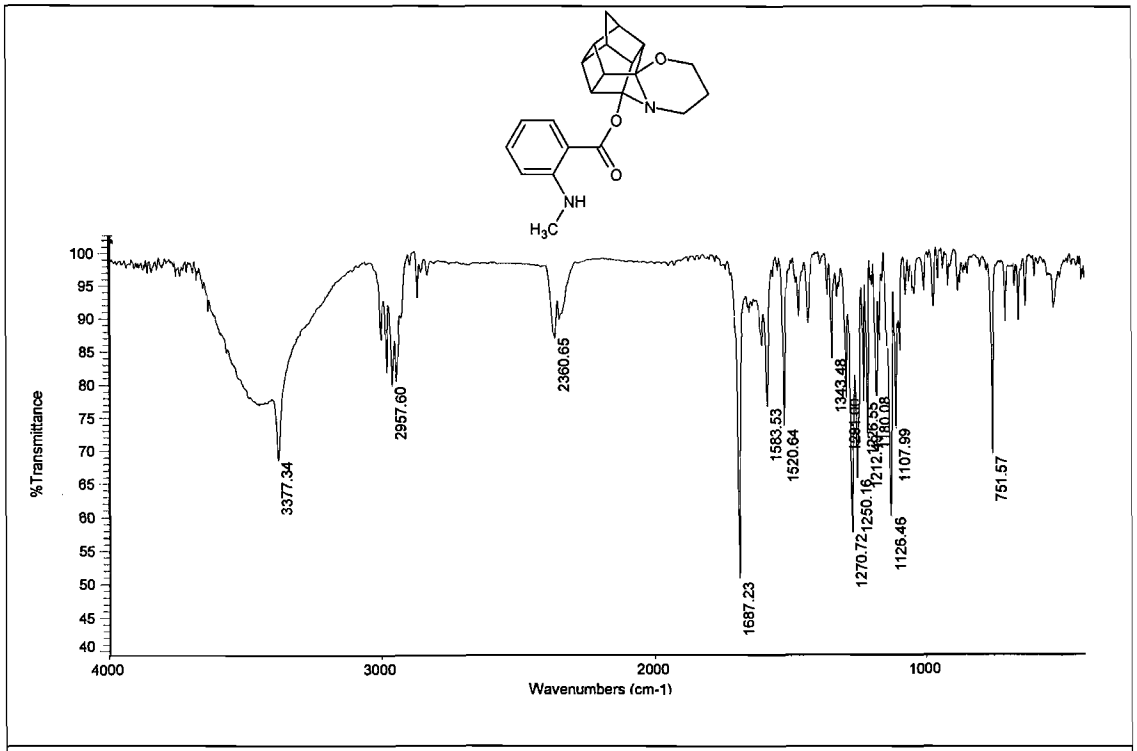

Spectrum 12.

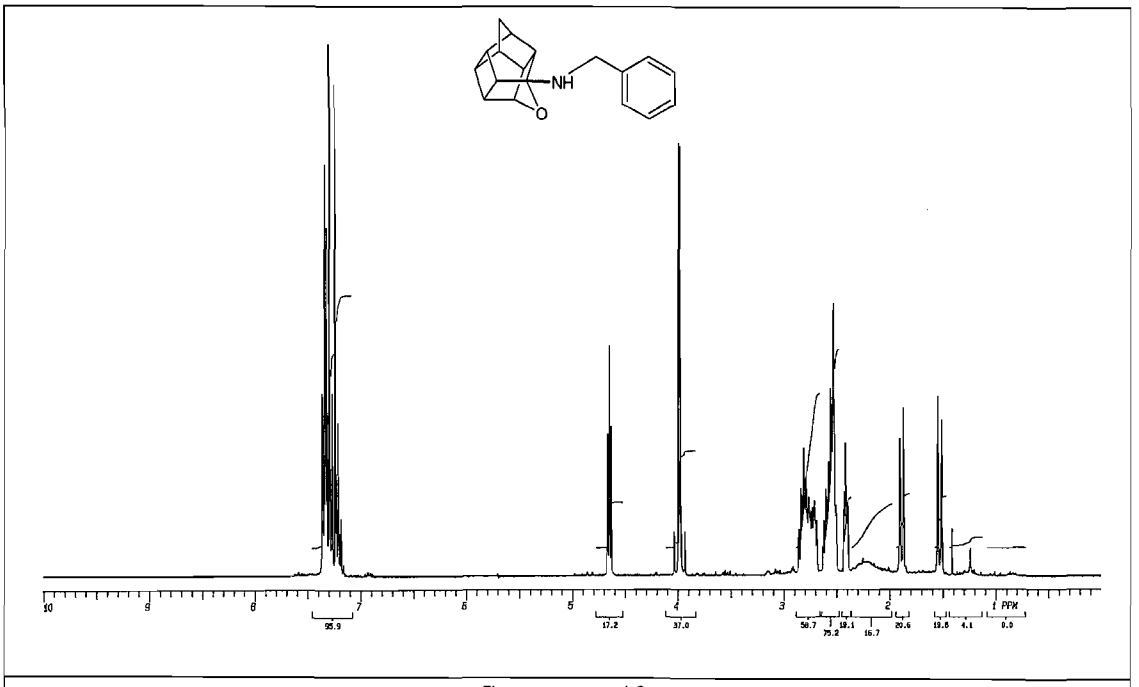

Spectrum 13.

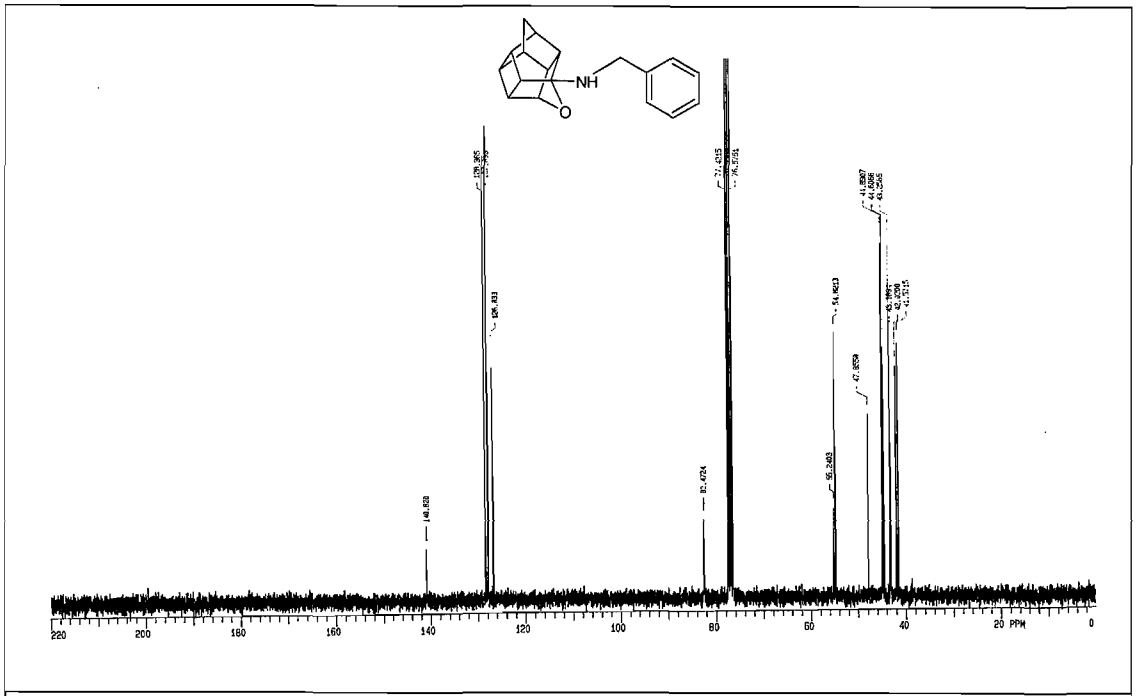

Spectrum 14.

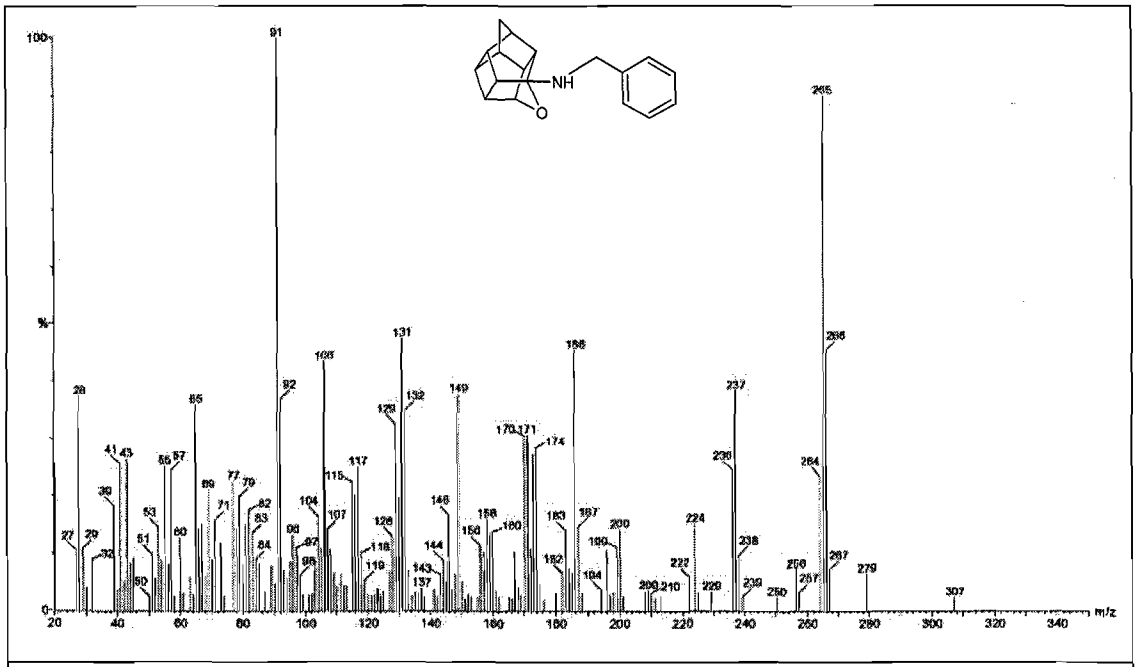

Spectrum 15.

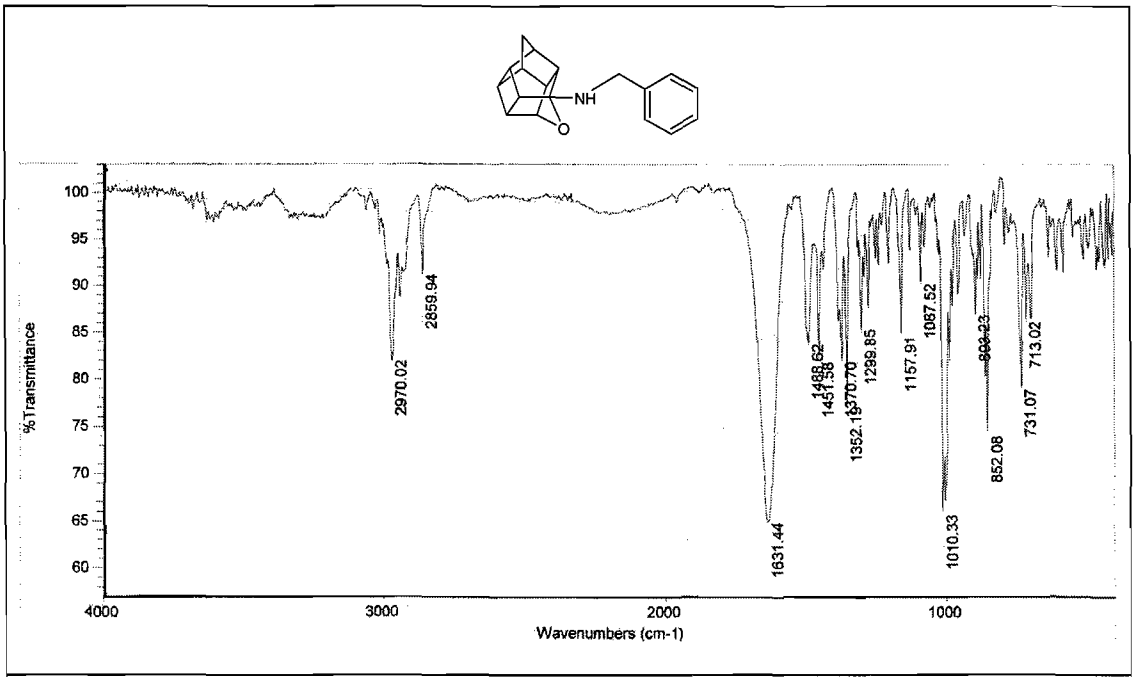

Spectrum 16.

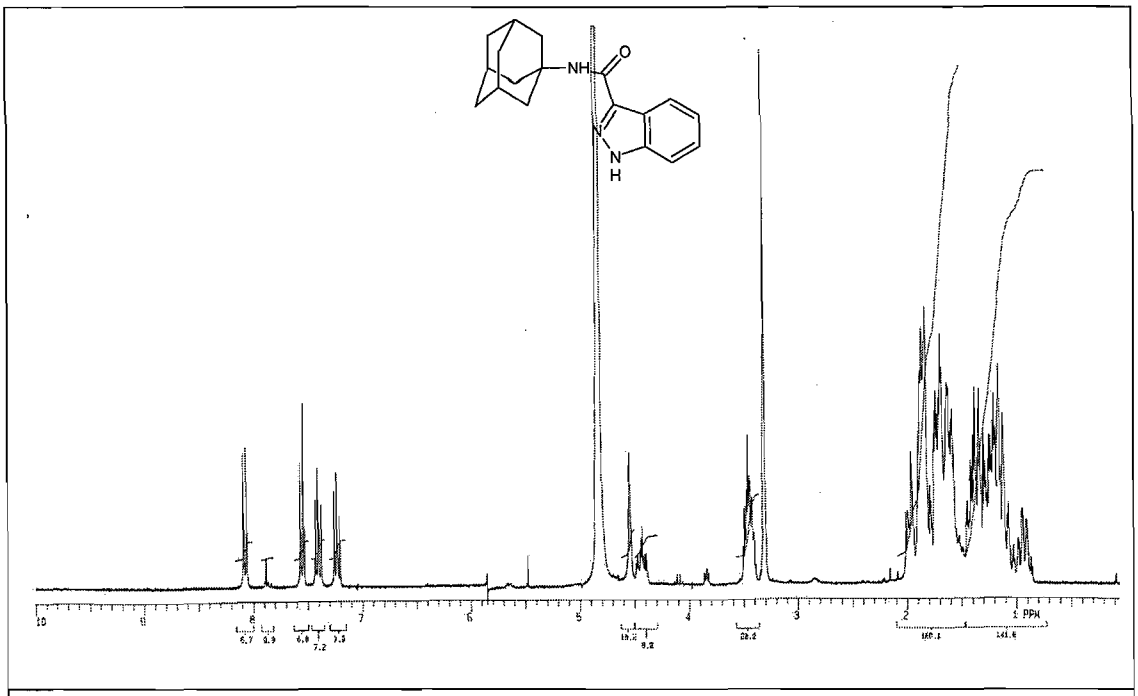

Spectrum 17.

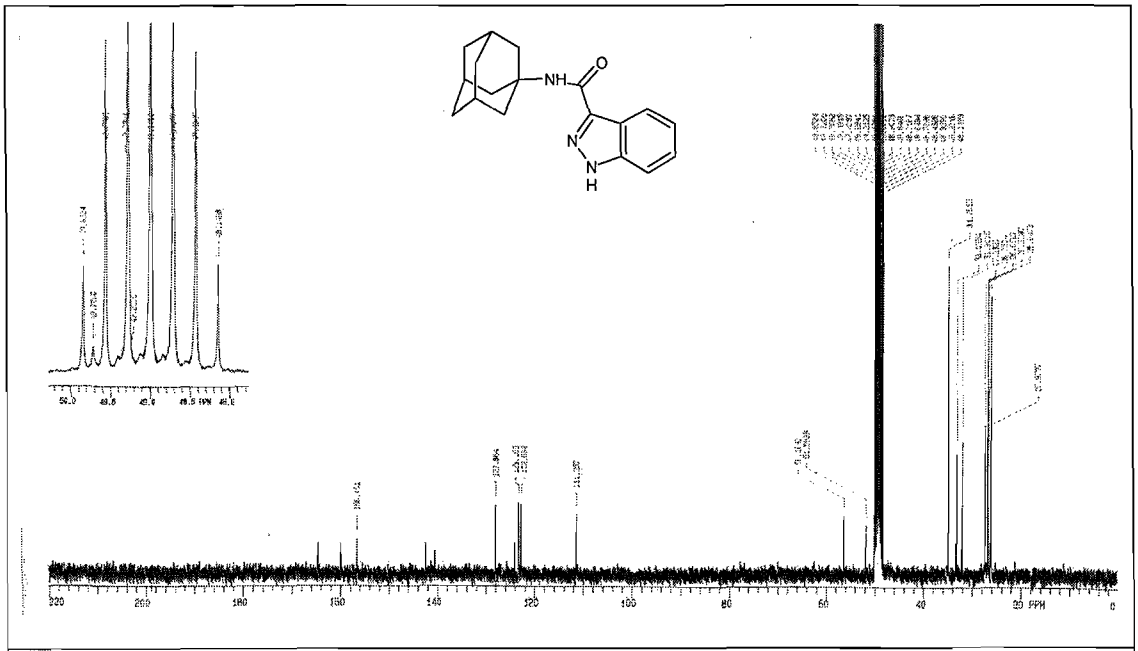

Spectrum 18.

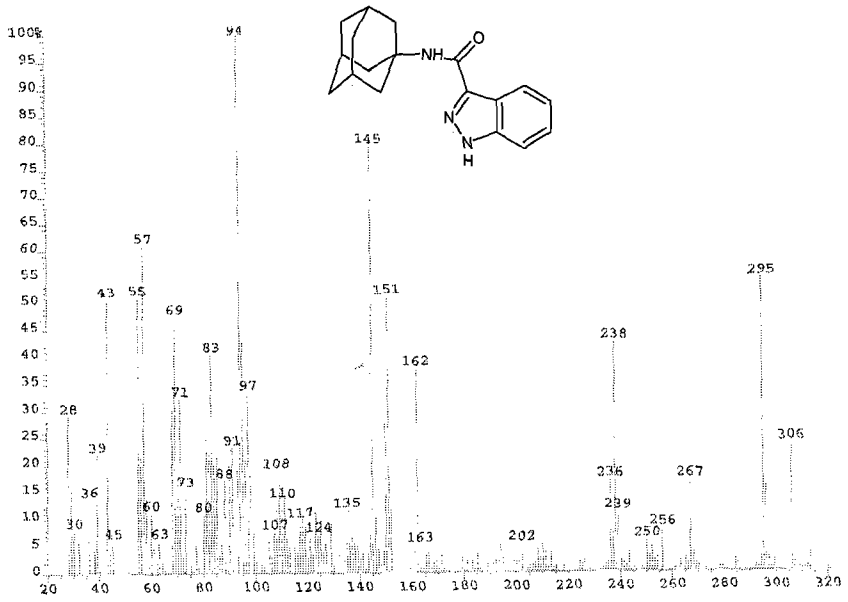

Spectrum 19.

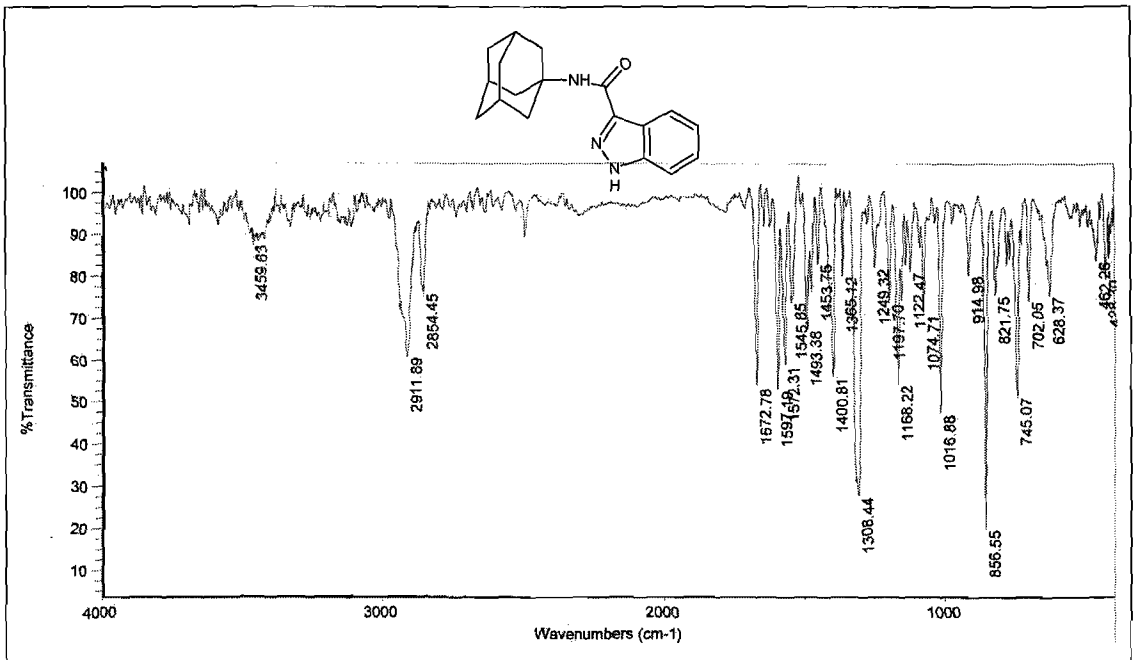

Spectrum 20.

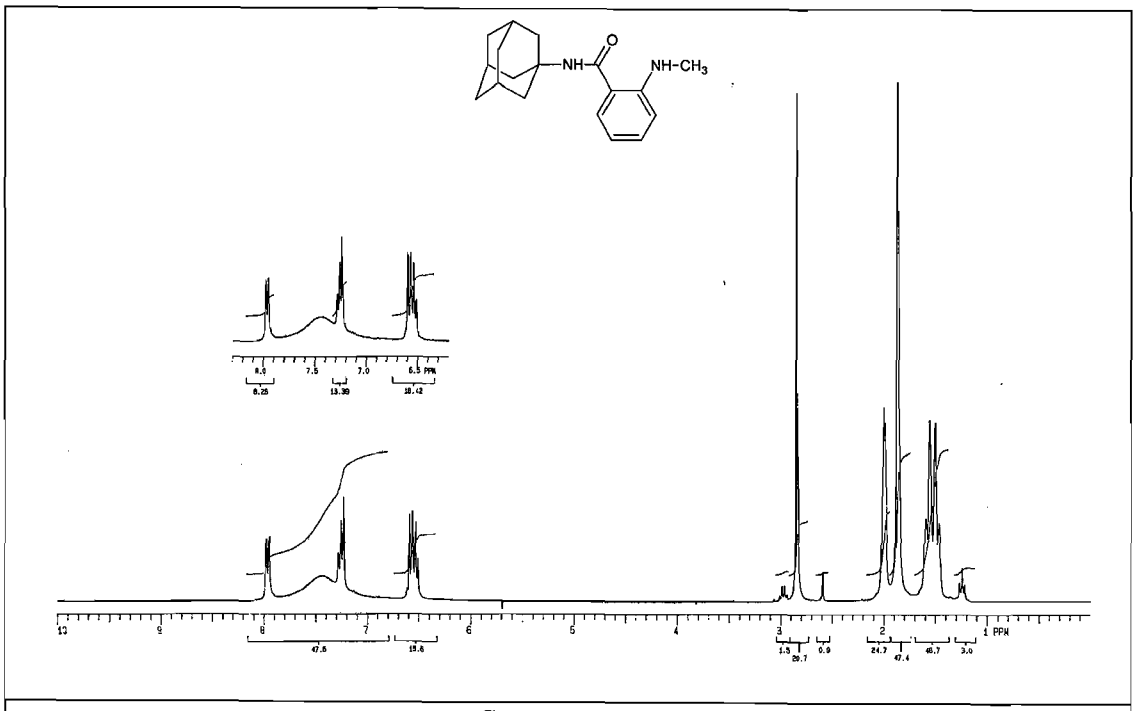

Spectrum 21.

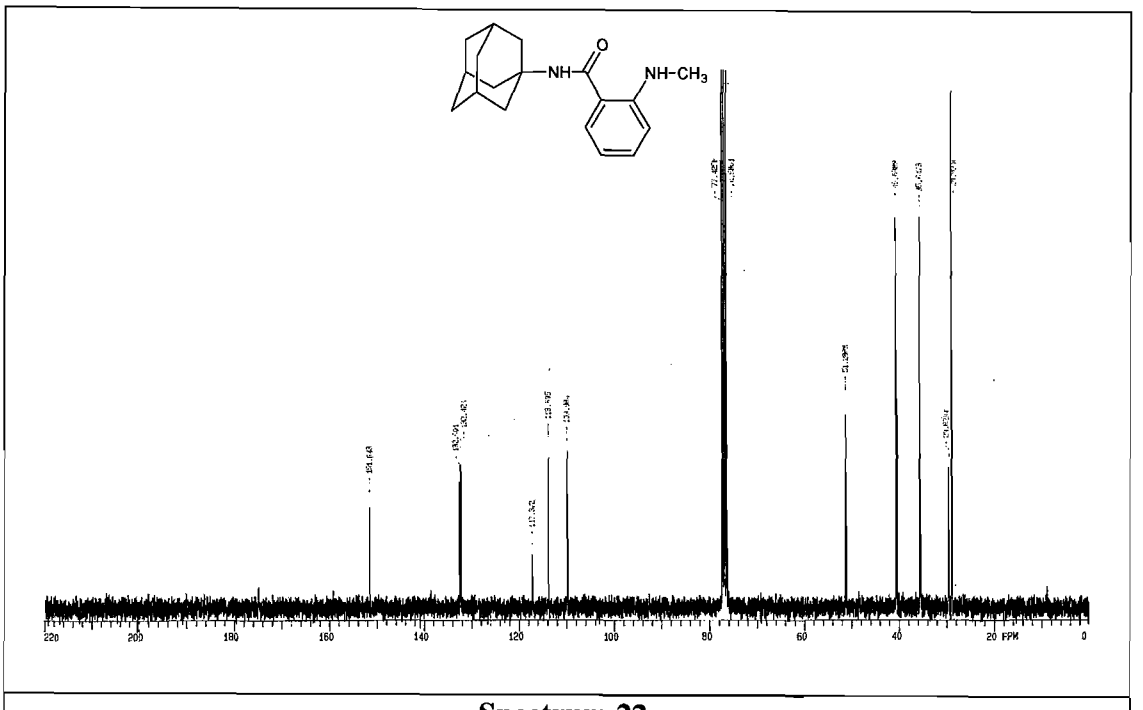

Spectrum 22.

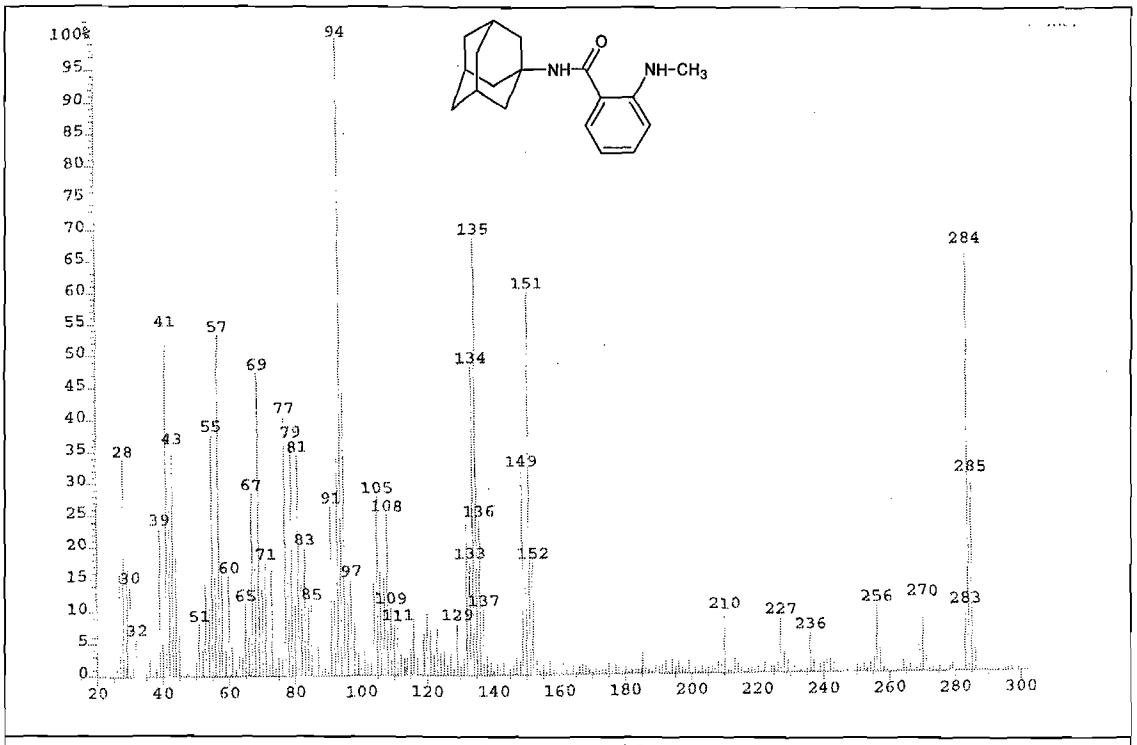

Spectrum 23.

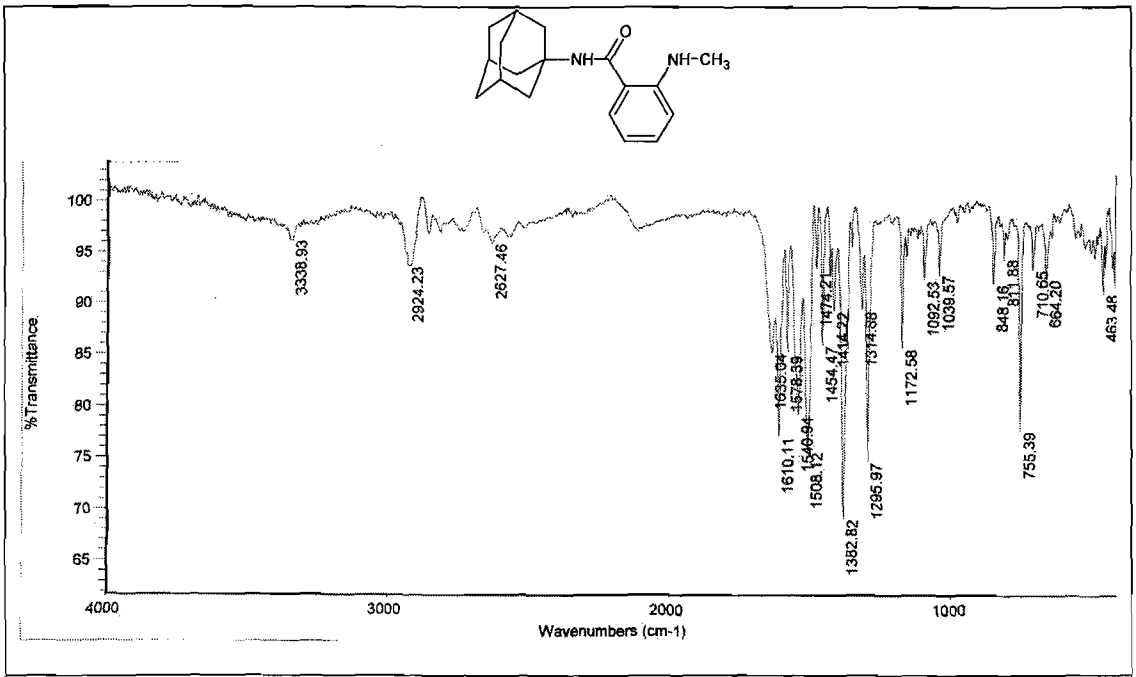

Spectrum 24.

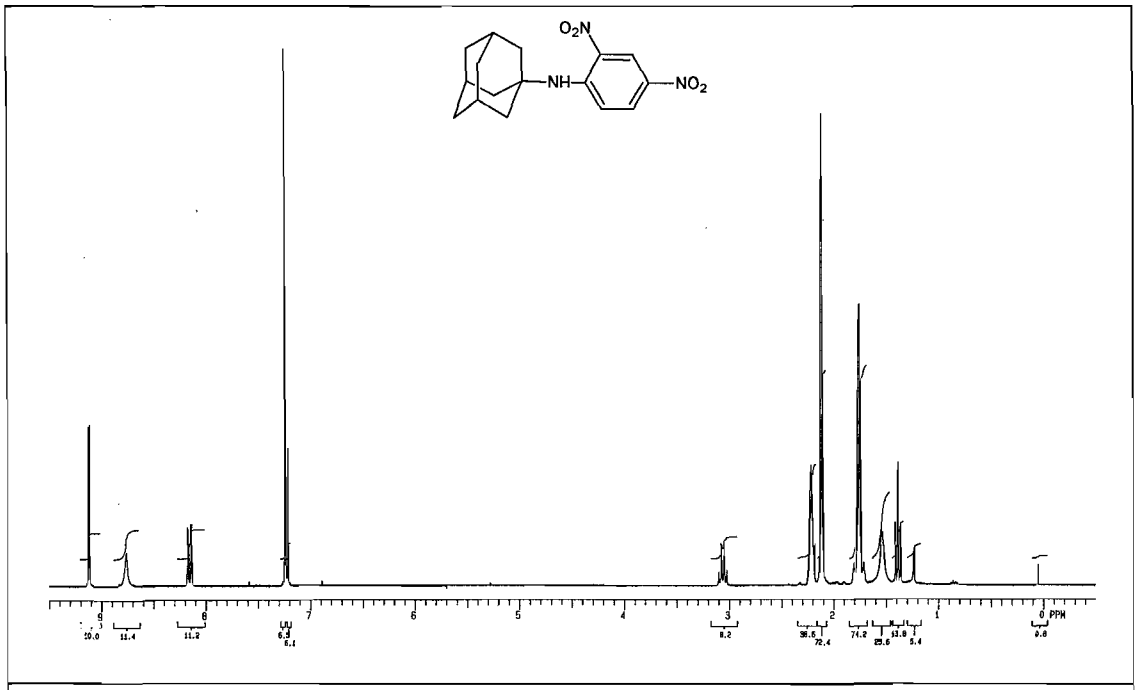

Spectrum 25.

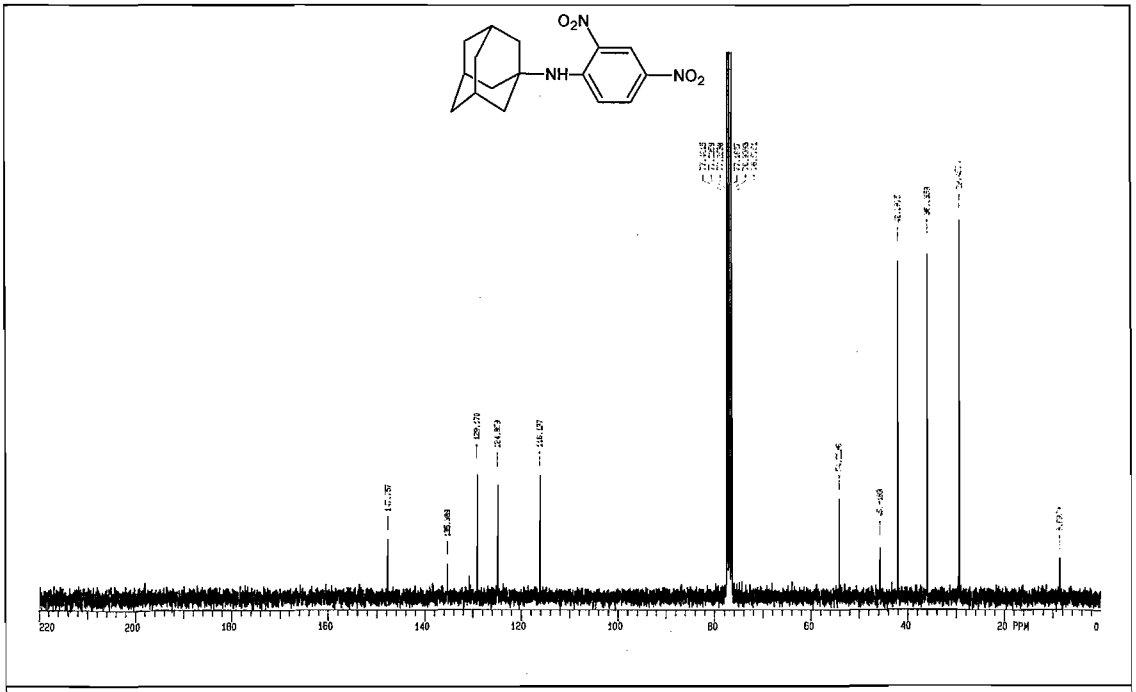

Spectrum 26.

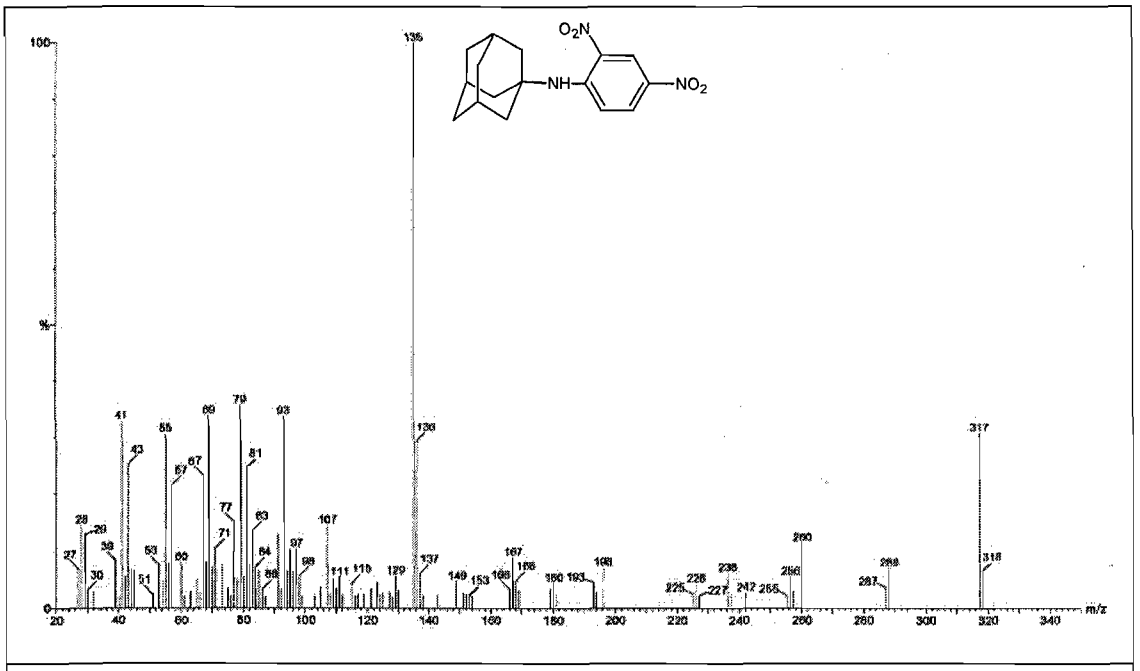

Spectrum 27.

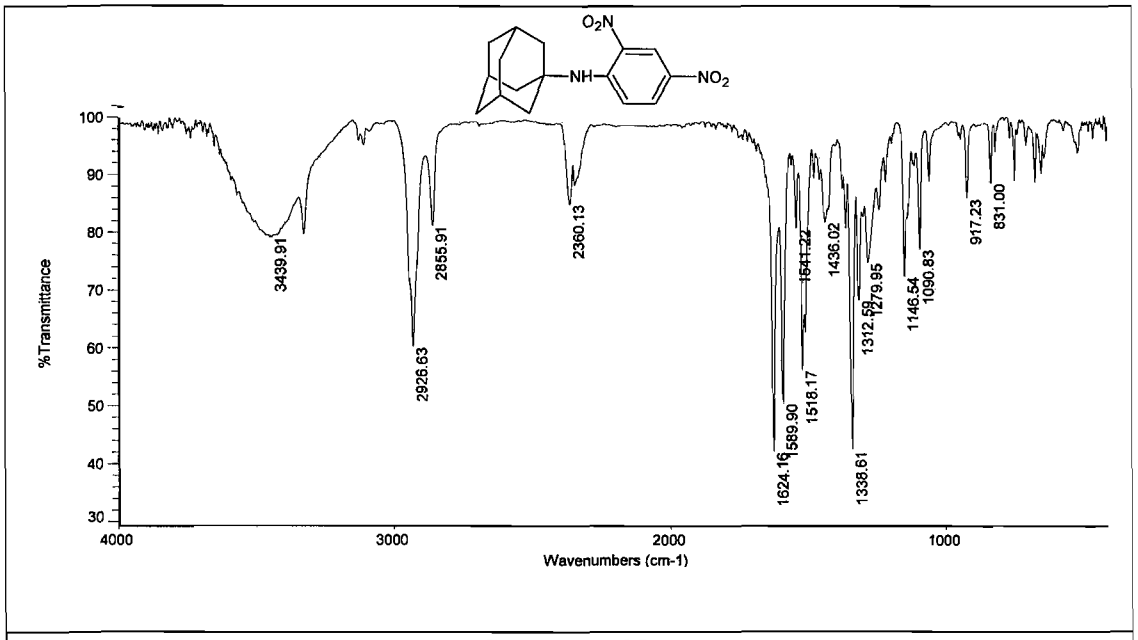

Spectrum 28.

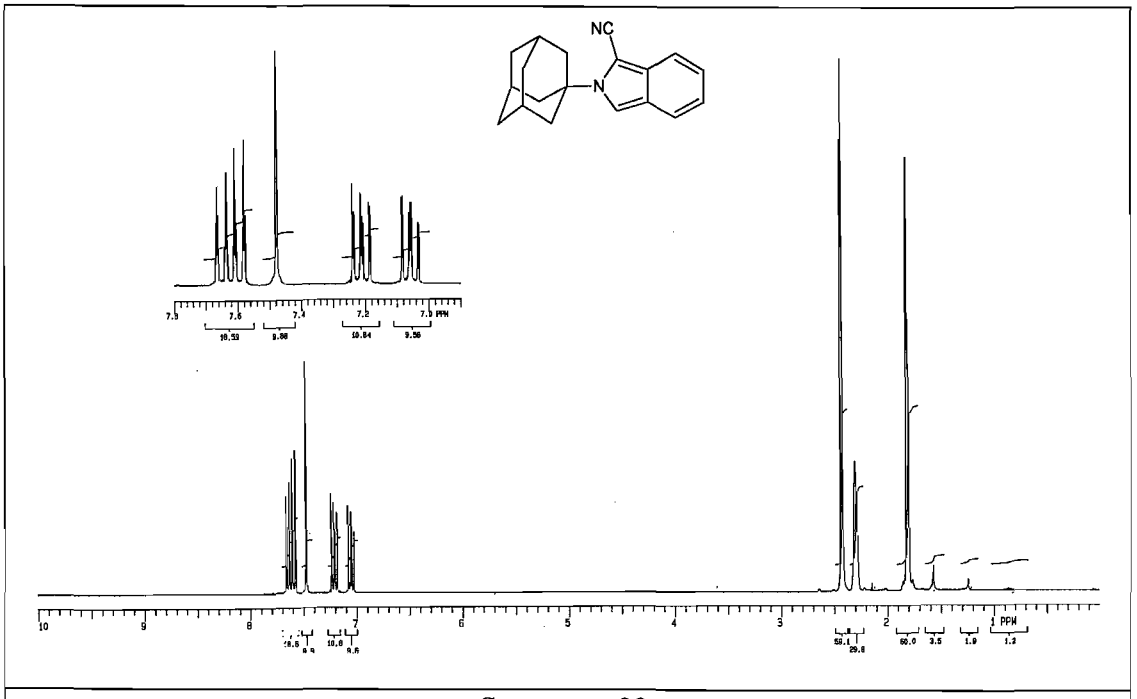

Spectrum 29.

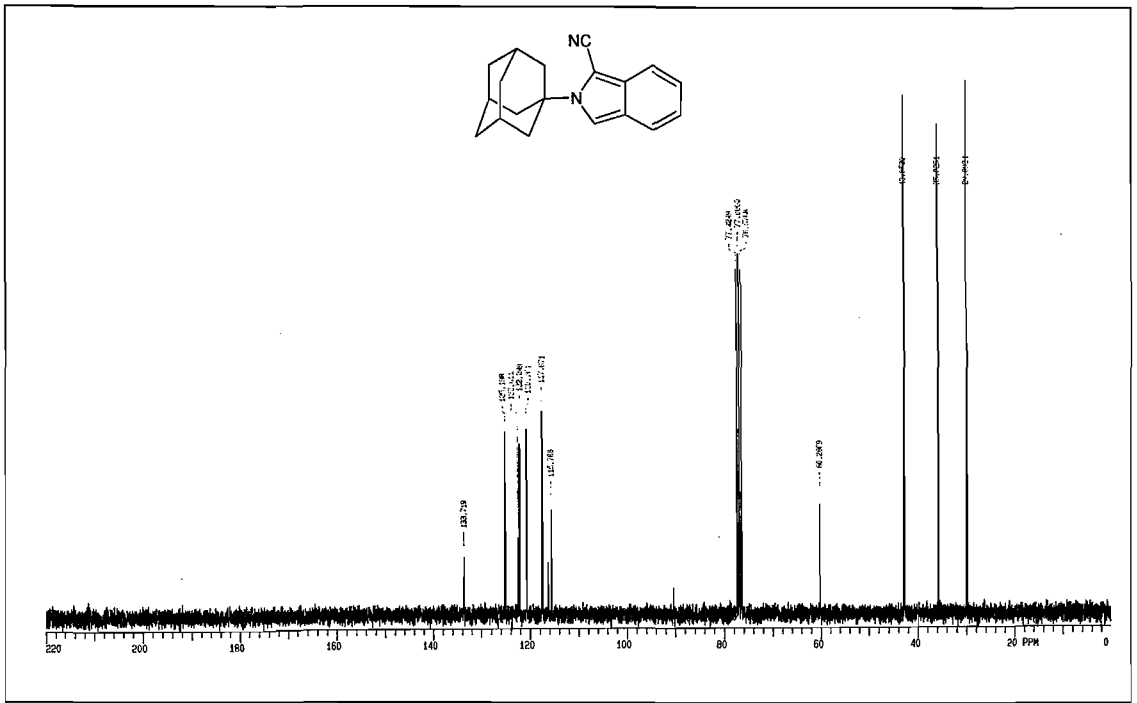

Spectrum 30.

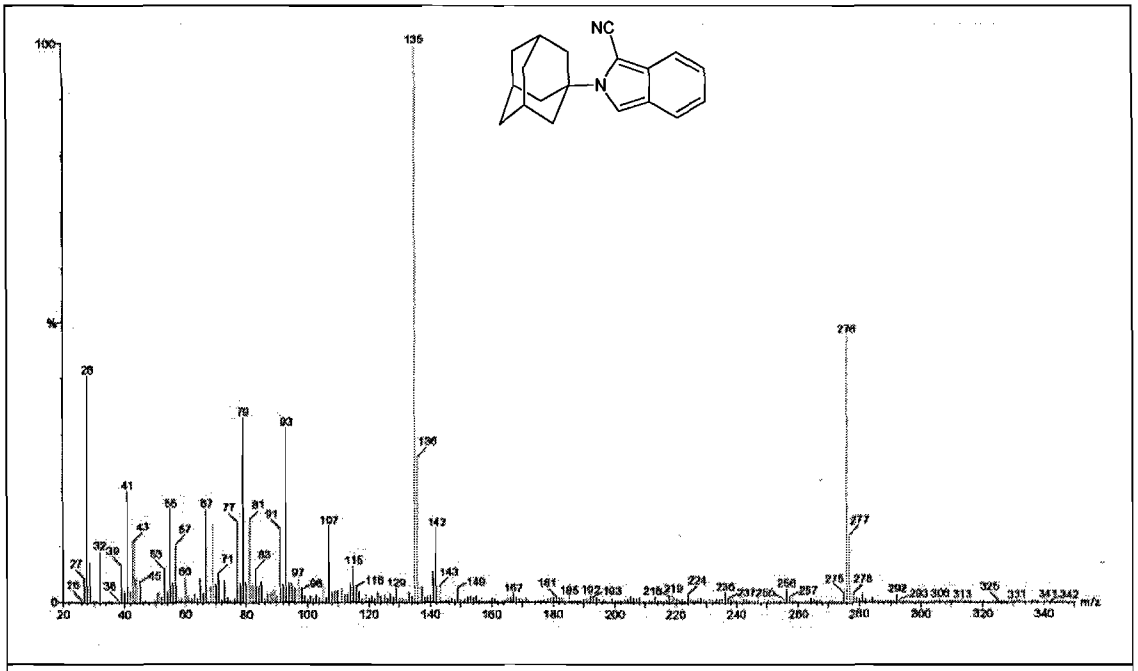

Spectrum 31.

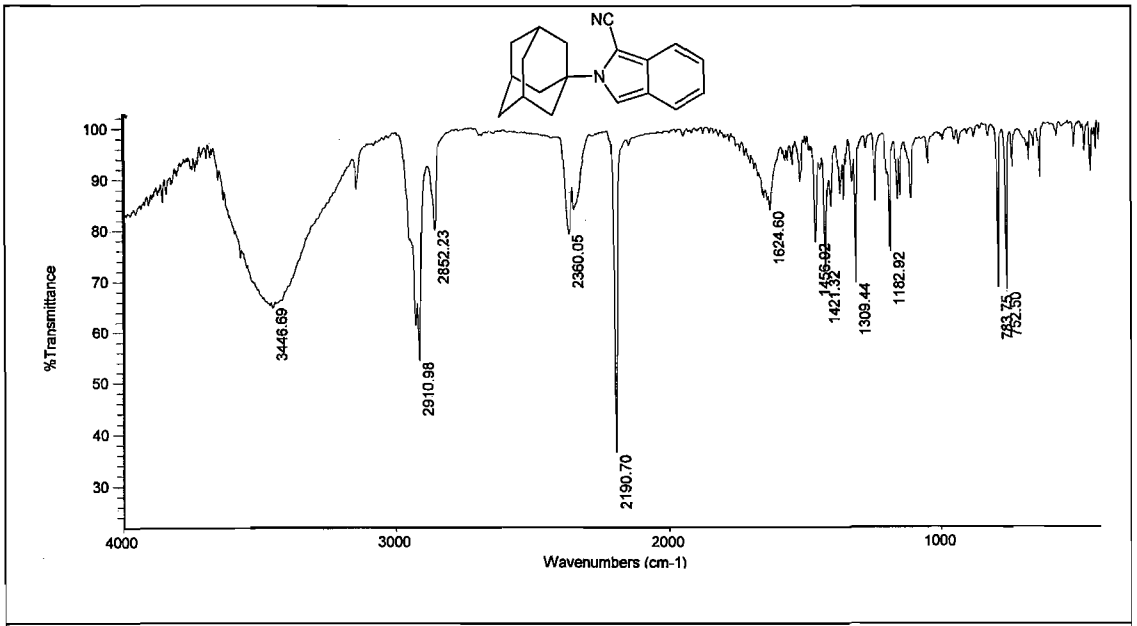

Spectrum 32.

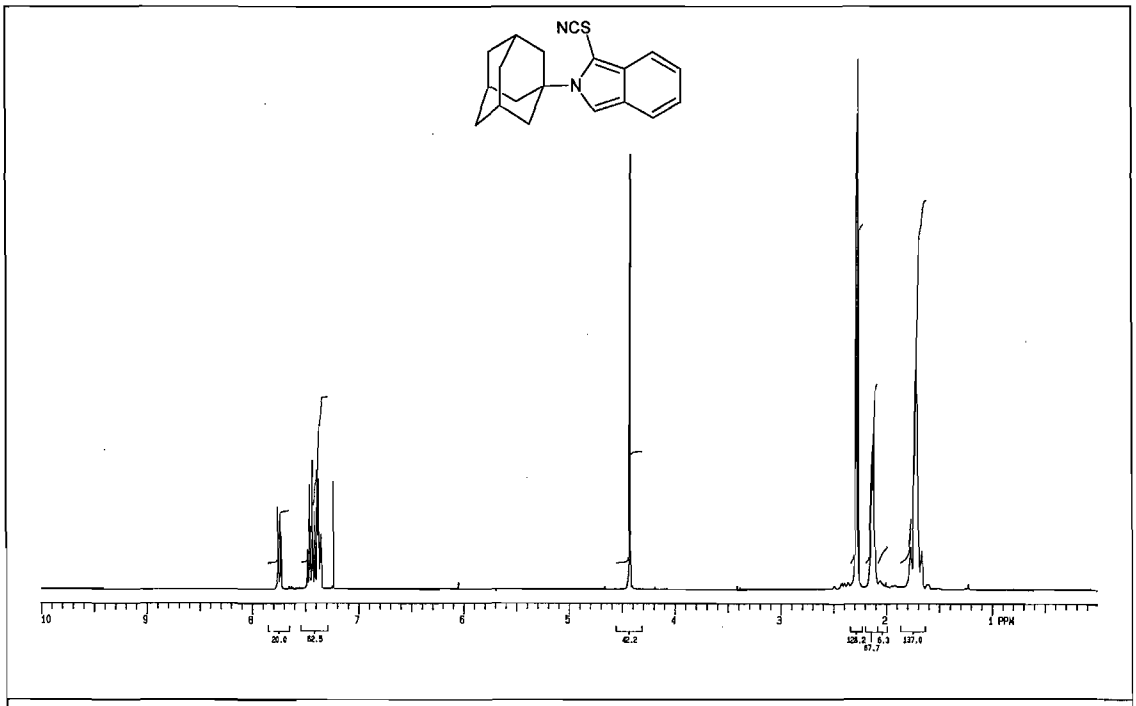

Spectrum 33.

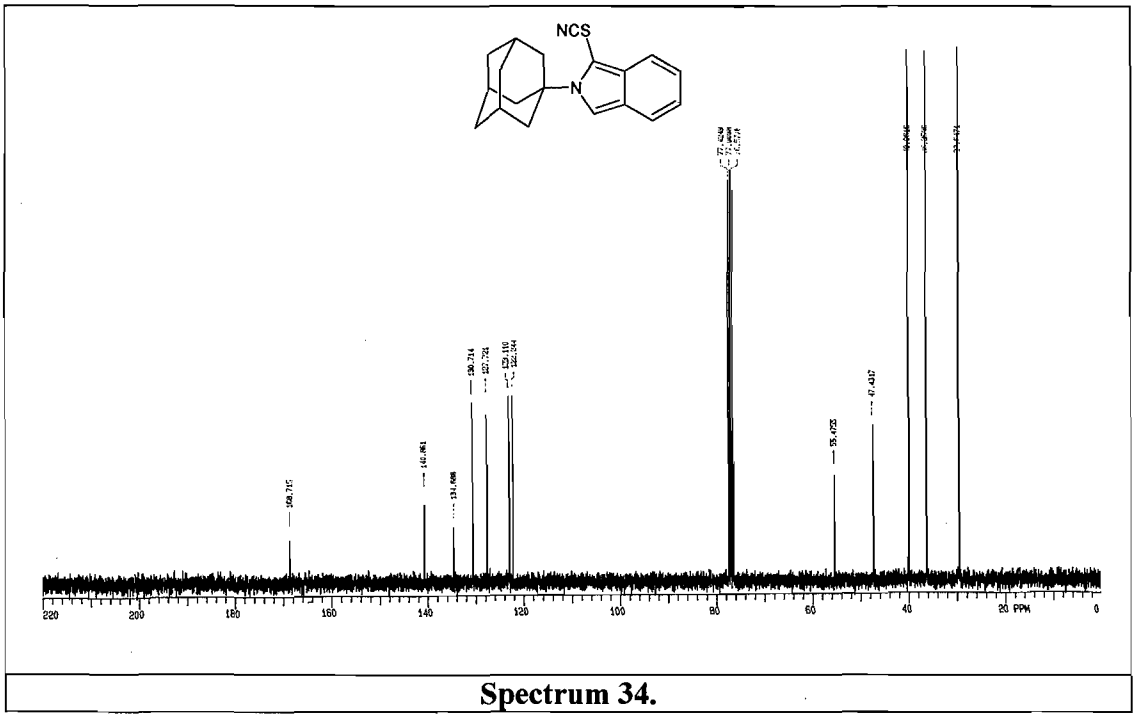

Spectrum 34.

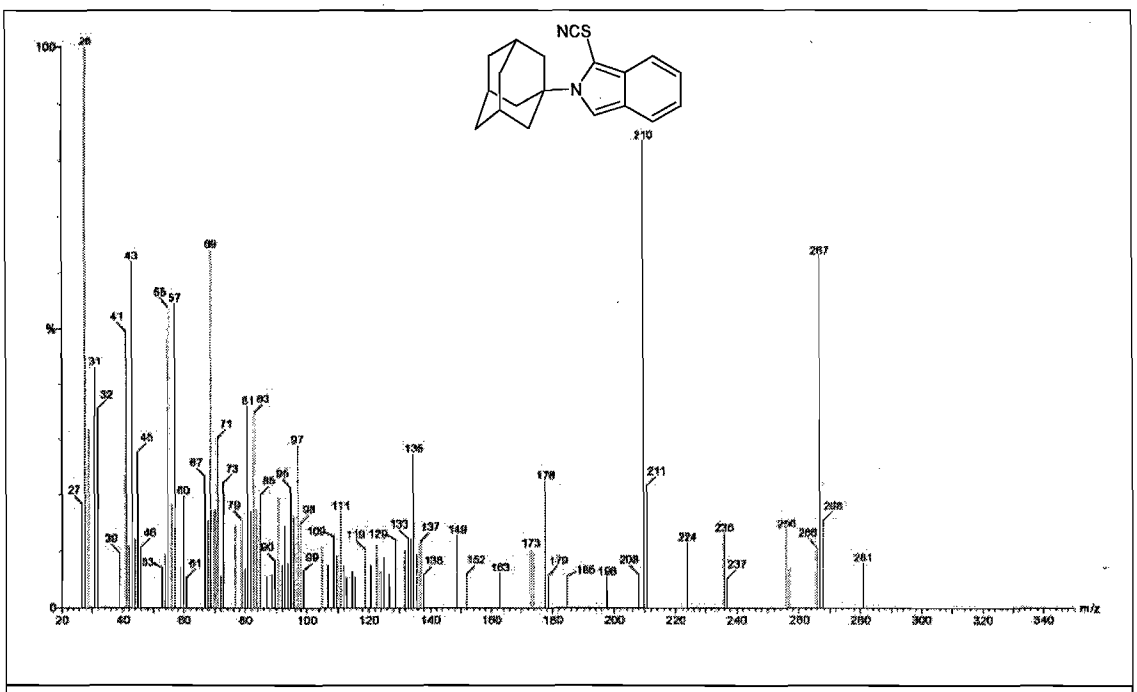

Spectrum 35.

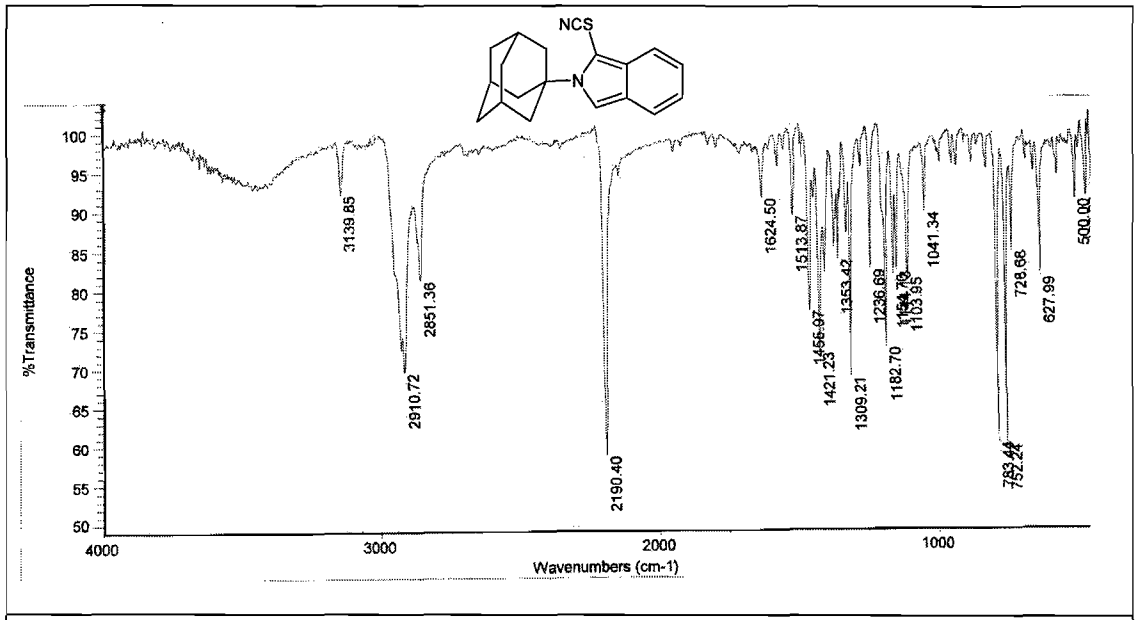

Spectrum 36.

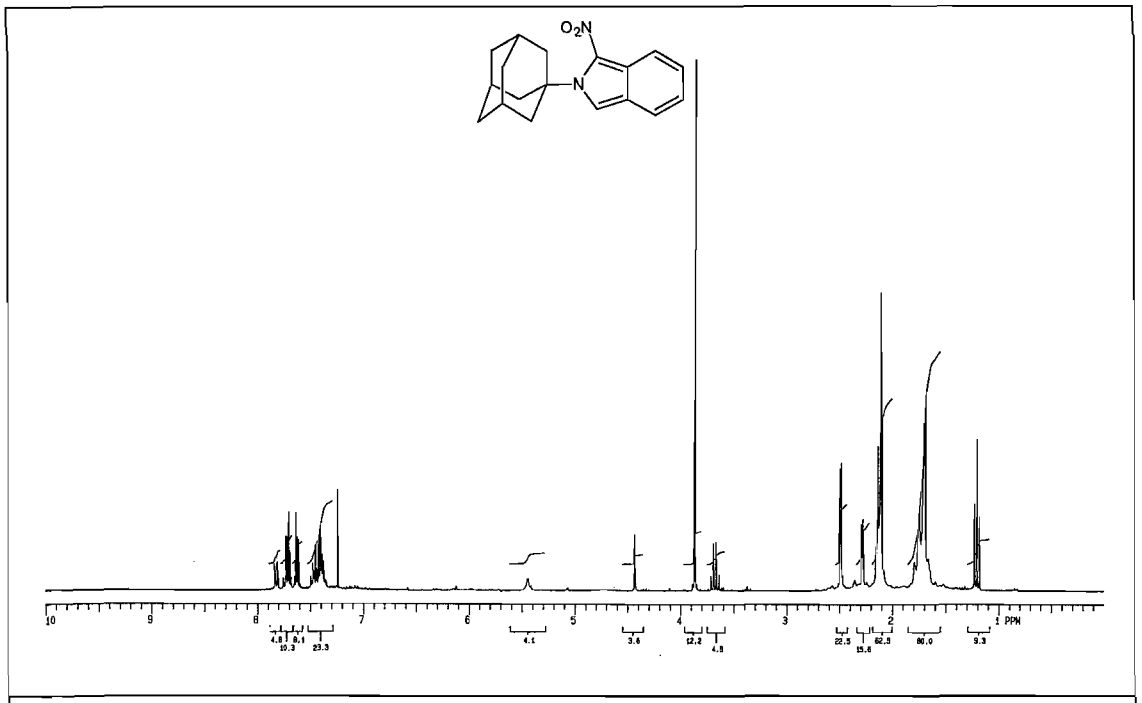

Spectrum 37.

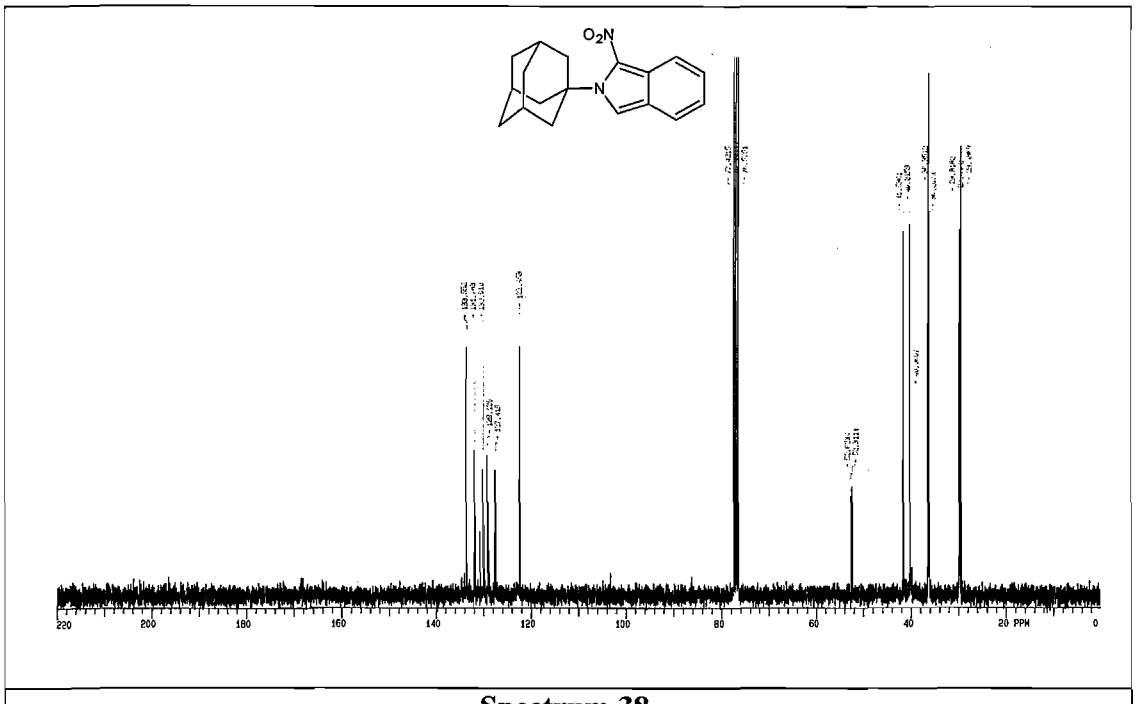

Spectrum 38.

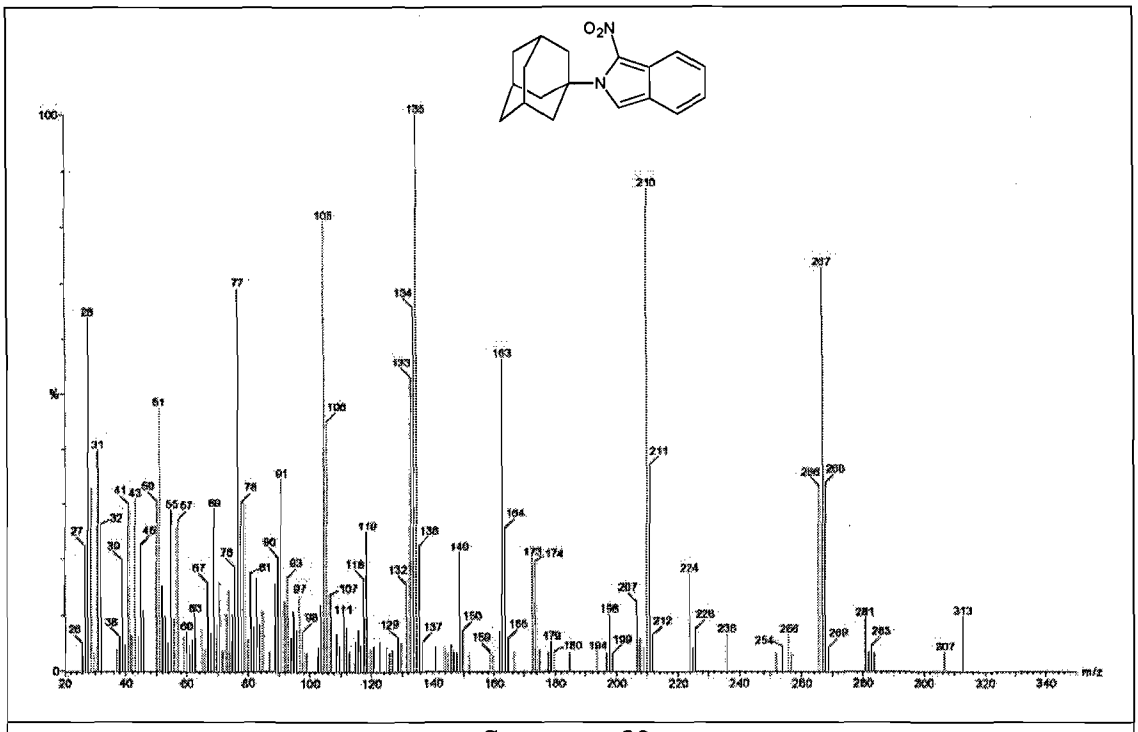

Spectrum 39.

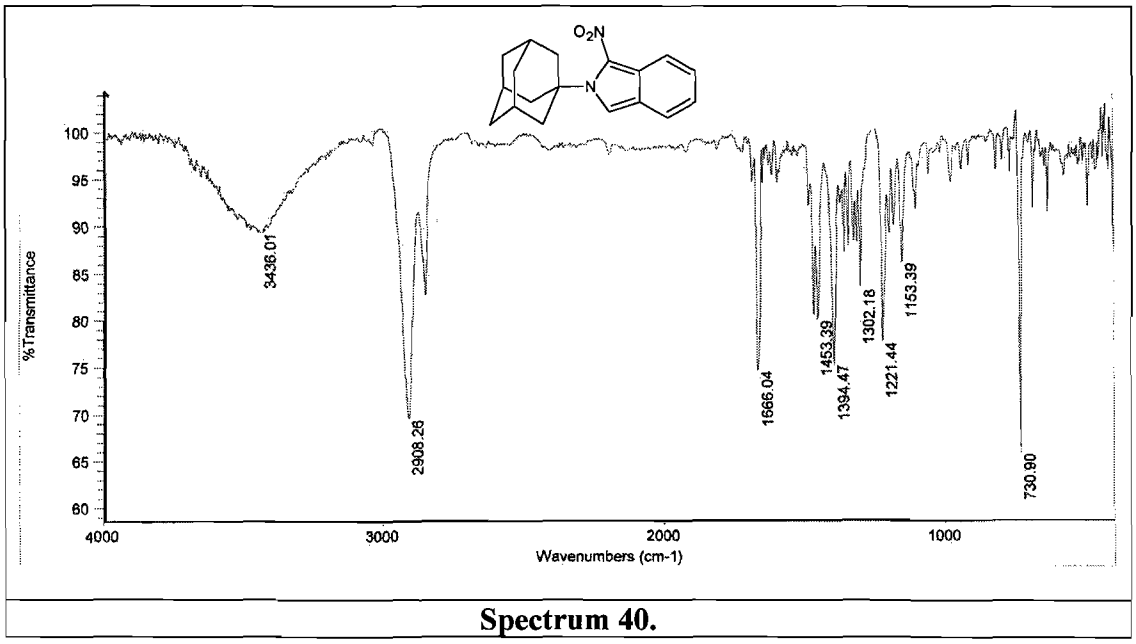

Spectrum 40.

ACKNOWLEDGEMENTS

I would like to express my sincere gratitude to my parents, Andre and Lina Joubert for allowing me the opportunity to further my studies as well as their unwavering support and love – Thank you for always believing in me, I love you.

I would also like to express my gratitude to the following people for their assistance and contributions.

- Prof. Sarel Malan
- Dr. Sandra van Dyk
- Mev. Nellie Scheepers
- Leandri Joubert
- Bennie Repsold
- Benno van Niekerk and Leani Potgieter
- Dennis Wilkes
- Mr. A. Joubert and Dr. J Jordaan.
- CENQAM
- Kagiso Sempe
- The staff at Pharmaceutical Chemistry
- The National Research Foundation (NRF)

This study was funded by the National Research Foundation (South Africa). Opinions expressed and conclusions arrived at, are those of the author and not necessarily to be attributed to the NRF